Sede Amministrativa: Università degli Studi di Padova
Sede Consorziata: Università degli Studi di Bologna

Dipartimento di Tecnica e Gestione dei Sistemi Industriali, DTG Vicenza
Dipartimento di Ingegneria Industriale, DIN Bologna

CORSO DI DOTTORATO DI RICERCA IN INGEGNERIA MECCATRONICA E DELL'INNOVAZIONE MECCANICA DEL PRODOTTO

CICLO XXXII

Accelerated life testing in mechanical design

Test accelerati nella progettazione meccanica

Coordinatore: Chiar.ma Prof.ssa Daria Battini

Supervisore: Ing. Massimiliano De Agostinis
Co-Supervisore: Ing. Giorgio Olmi

Dottorando: Ing. Francesco Robusto

SOMMARIO

L'introduzione di nuovi prodotti sul mercato è un processo di lunga durata, che comprende tipicamente sia fasi di progettazione che di sperimentazione. Sovente, la fase di validazione sperimentale condiziona notevolmente i tempi complessivi del processo. Infatti, in molti settori industriali, la procedura di sviluppo prodotto è basata su metodologie di tipo trial and error. Prove di validazione intermedie vengono eseguite su prototipi fisici in scala reale, ed in base all'esito di queste il design viene rielaborato (in caso di esito negativo) o validato (se l'esito è positivo). L'efficienza di tale metodo sotto il profilo temporale è, notoriamente, sub-ottimale.

Per migliorare l'efficienza di tale processo è, ad esempio, possibile sfruttare metodologie di prova accelerate, che consistono nel sottoporre il prodotto ad una condizione di prova più gravosa rispetto alle normali condizioni di lavoro. In tale modo, si può conseguire una riduzione del numero di cicli necessari a portare a rottura il componente, con evidenti ricadute vantaggiose sull'efficienza del processo. Un'ulteriore modalità di accelerazione della prova consiste nel passare da prova sull'assieme globale a prova sui sottoassiemi o singoli componenti.

È tuttavia obbligatorio, affinché i risultati ottenuti mediante tali metodologie di prova siano utili per la progettazione, adottare opportune precauzioni. Ad esempio, è fondamentale preservare la modalità di rottura originaria del componente. Per fare ciò, si rende necessario, fra le altre cose, conoscere la relazione tra le condizioni al contorno dell'intero assieme e le sollecitazioni dei singoli componenti. Nel presente elaborato, la metodologia sopra descritta viene illustrata facendo riferimento alla sua applicazione a componenti del settore serraturiero (dimostratore).

Sono stati effettuati numerosi test sperimentali, per caratterizzare la vita a fatica e la resistenza all'usura dei materiali coinvolti nella costruzione del dimostratore.

Sono inoltre stati sviluppati modelli numerici FEM per determinare le sollecitazioni dei sottoassiemi e componenti del dimostratore durante la fase di test.

Combinando i risultati sperimentali con quelli numerici, è stato possibile sviluppare un modello analitico in grado di stimare con buona approssimazione la vita effettiva del dimostratore, quando sottoposto a prove accelerate.

I principi alla base di questa procedura possono essere applicati, senza perdita di generalità, a numerosi settori dell'industria.

ABSTRACT

The introduction of new products on the market is a time-consuming process, which typically includes both design and testing phases. Often, the experimental validation phase significantly affects the overall process time. Indeed, in many industrial sectors, the product development procedure is based on trial and error methodologies. Intermediate validation tests are performed on full-scale physical prototypes and, based on their outcome, the design is updated (in the case of a negative result) or validated (if the result is positive). The efficiency of this method in terms of time-resources is notoriously sub-optimal.

To improve the efficiency of this process it is, for example, possible to exploit accelerated test methodologies, which consist in subjecting the product to test conditions that exceed its actual working conditions. In this way, a reduction in the number of cycles necessary to bring the component to final failure can be achieved, with obvious beneficial effects on the efficiency of the process. Another way to accelerate the test is to switch from testing the top-level assembly to performing tests on subassemblies or individual components.

It is however mandatory, to ensure that the results obtained with these test methods are useful for the design, to take appropriate precautions. For example, it is essential to preserve the original failure mode of the component. To do this, it is necessary, among other things, to know the relationship between the boundary conditions of the entire assembly and the stresses of the individual components. In the present paper, the methodology described above is illustrated with reference to its application to locking industry components (demonstrator).

Several experimental tests have been carried out, in order to characterize the fatigue life and wear resistance of the materials involved in the construction of the demonstrator.

Numerical FEM models were also developed to determine the stresses of the sub-assemblies and components of the demonstrator during the test phase.

Combining the experimental results with the numerical ones, it was possible to develop an analytical model. Such model allows estimating the endurance of the demonstrator when subjected to accelerated tests. The model has shown a good correlation with experimental results.

The principles underlying this procedure can be applied, without any loss in terms of generality, to many sectors of the industry.

TABLE OF CONTENTS

1. GENERAL CONSDERATION ABOUT ACCELERATED LIFE TESTING

1.1 Introduction

Product reliability contributes strongly to the quality of the product and to the competitiveness of the company in the market: for this reason, companies invest millions of euros in the study of the reliability of their products. The engineers' efforts are aimed at assessing reliability based on product design, use, the type of material used, production technologies and again depending on the fault and the main cause that triggered the fault. The decisions related to the development of the component are taken as a function of the results of the reliability tests carried out: they are generally carried out on a few units due to the high costs of making the prototypes (or specimens) and due to the extended times to perform a single complete test on the entire useful life of each test unit [1].

Although the designer's considerations and the tests on the prototype indicate that the product have a certain useful life, it is still necessary to validate these statements in order to demonstrate and quantify the actual life of the product. This demonstration can be complex, especially as regards the cases in which a useful life of years is expected. In these cases, indeed, it is not at all practical and economical to implement a reliability test at the nominal working conditions. It can be fundamental to overload the product and make the boundary conditions of the test more burdensome. So, accelerated life test can be derived in order to quickly extrapolate the information and data needed to quantify the actual expected life [2].

Accelerated life tests can therefore be defined as follows: they are a set of methods and techniques designed to shorten the analyzed product life, accelerating the degradation of its performance while maintaining the fault modes unchanged. The purpose of these tests is to quickly obtain the data that, properly analyzed and modeled, produce the desired information on the useful life of the product in conditions of normal use. The direct advantage of the use of such tests is obviously the saving of time and costs [1].

Both the single components of the product and the complete mechanical component can be tested. The mechanical properties that can be tested during the accelerated life testing are fatigue and wear resistance, creep resistance or fracture toughness, corrosion resistance etc.

Reliability information are difficult to obtain due to experimental data processing. Moreover, it is necessary to obtain a mathematical model that can correlate the accelerated test results to the daily use in nominal conditions of operation of the product. It can be useful to use statistical models that allow the correlation between the few results obtained from the accelerated tests to the results expected during the use of the product at the nominal conditions.

Furthermore, unlike electronic components, just few studies have been carried out on the accelerated life testing of mechanical systems; this lack can be attributed to the high costs of the specimens compared to the electronic ones. Moreover, mechanical components are not characterized by a constant failure rate, unlike the electronic ones. In mechanical components there are generally different degradation mechanisms: fatigue, creep or wear, for example, each contributes in its own way to the total failure of the component. These factors lead to an intrinsic difficulty in the test modeling. In order to carry out accelerated life test, industries tend to invest a lot of money to implement a model for studying the reliability of their own components or products [3].

To better understand the useful life characteristics of the product until the failure in short time it is possible to perform two different accelerated test types [1]:

Qualitative accelerated tests;

Quantitative accelerated tests.

The accelerated qualitative tests allow to identify very quickly the cause or the main causes that lead to the product failure without focusing on the reliability of the same.

The accelerated quantitative tests instead are used to predict the useful life of the product under the nominal use conditions.

1.2 Qualitative accelerated tests

As briefly mentioned above, the purpose of these tests is to understand under what conditions the product fails; further purpose is to identify any design defects. These tests can be performed on the single component or on the full assembly.

It should be noted that qualitative accelerated tests do not work in the case of the main failure mechanism is wear, as the mechanism is compromised by the extreme conditions of the test [3].

Qualitative accelerated tests are also called Highly Accelerated Life Testing (HALT) because they are shorter than conventional accelerated life testing (ALT) [4].

The problem related with qualitative testing is that it is really difficult to carry out the test: it is essential to achieve the standard failure modes. Quality tests, if well executed, provide a general indication of how the sample can fail, is not an absolute result and must be validated at least through an accelerated quantitative test [4].

The most common highly accelerated test is generally called elephant test but, in the literature, it can be characterized by different names: killer tests, torture tests, shake and bake tests. This test, indeed, can be seen as an elephant walking on the product [1]: it is not known exactly at what stress levels the sample is subjected but you are sure to take it to extreme conditions of use, not associated with normal use of the product.

The elephant test procedure can be as follows [1]: it involves a single sample that will be subjected to extreme stress levels (e.g. extreme temperatures and tensions). This test will not certainly produce the failures that can occur during the normal use of the product but will tend to reveal the project flaws; in this regard, several elephant tests can be conducted to check different aspects of the product: what can happen if the product will be used at the South Pole at twice the recommended speed?

However, Nelson [1] points out that the elephant test is well performed when the same failures occur on the sample, in the same positions, which would be obtained under normal use. It is therefore particularly difficult to design this test as there is the risk of literally destroying the product without obtaining any information, especially in the case of a new product. It will then be necessary to gradually increase stress and understand how the product behaves before achieving the failure. This procedure is the most widely used to conduct the quantitative test type.

1.3 Quantitative accelerated tests

The aim of quantitative Accelerated Life Testing (ALT) is to obtain concrete information about the reliability of the product in a short period. These tests are also important to find, depending on the normal use of the product, the main failure mode and its location.

To carry out an ALT it is important to know several parameters: test duration, number of specimens, test goal, desired confidence interval, desired accuracy, costs, acceleration factor, test environment (temperature, pressure, humidity stress level (tension, frequency, amplitude...) and test conditions (material, surface treatment, heat treatment...) [4]

The key factor is the so-called acceleration factor [4], which allows the test to be carried out at a higher speed than the standard one. It is possible to define it because it is assumed

that there is a relationship between the stress level and the life of the product [5]. The acceleration factor (Equation 1.1) is a dimensionless number defined as the ratio between the life of the product assessed under nominal conditions and the life under accelerated conditions (overstress):

$$A_f = \frac{L_u}{L_a} \tag{1.1}$$

Where A_f is the acceleration factor, L_u is the life of the product at the nominal stress level and L_a is the product life under accelerated conditions. Experimental tests are required to know the acceleration factor.

Nelson and Silverman cited some experimental models to determine the acceleration factor (e.g. Arrhenius, Coffin-Manson, and Norris-Lanzberg models). The use of one of these models to determine the acceleration factor, is fast but not very accurate.

The most important condition to determine stress levels during the ALT is that the specimen should be subjected to the same failure for each level and that the failure is exactly the same that occurs during normal use.

If this cannot be achieved, it is necessary to simply speed up the work cycle: for example, increasing the test frequency.

Basically, two accelerated quantitative reliability test methodologies can be identified [1]: usage rate acceleration and overstress acceleration.

1.4 Usage rate acceleration

This methodology is implemented when the product is normally not used continuously (an elevator for example). In this case it is possible to test the product continuously, without the natural breaks, so the failure appears earlier. The limitation of this method is in products that by their nature, work practically continuously, (e.g. a computer). In such situations, the acceleration of the frequency of use is not effective in stimulating a failure mechanism, in this regard it is necessary to overstress the product, therefore accelerated overload is introduced.

1.5 Overstress acceleration

This methodology is to be implemented when the product works in continuous or with a very high rate of use (such as a bearing of a hydraulic turbine). In this case, higher loads will be applied; the overload can be achieved by increasing loads or temperature, speed or vibrational frequency etc. It is also possible to combine different stresses on the product. Like the previous test class, failure is achieved in a short time, and time-to-failure information (in overload conditions) is critical to obtaining failure data under normal usage conditions.

1.6 Stress and overload levels

The load applied during the test must be appropriately chosen before running the test [1]: it is necessary to apply high stresses in order to speed up the test, but not too high as they may induce different failure modes with respect to those occurring under nominal conditions. The stress levels should exceed the specifications, but cannot exceed the design limits: therefore, with regard to Figure 1, the design limits should not be overcome in both directions. If the different thresholds are not known, it is necessary to implement a qualitative test.

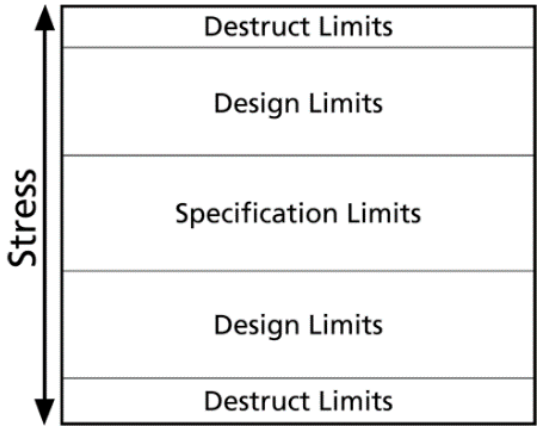

Figure 1: Product stress limits [1]

The type of stress applied may vary depending on the test one wants to perform. Constant, cyclical, step stress test, progressive or random stress [1] can be applied.
Constant stress is the most common load type for accelerated tests and each specimen is generally tested at the same stress level (Figure 2). There are some advantages in

implementing this model. First of all, many products are subject to constant load and tests could be very similar to reality; Moreover, it is relatively easy to implement a test that is characterized by constant stress.

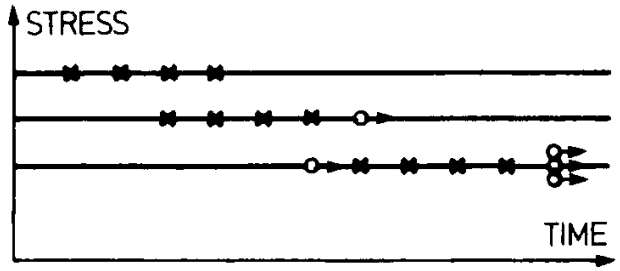

Figure 2: Constant stress test. (x) failure, (o) runout [1]

As explained by Nelson in [1], in step-stress loading, a specimen is subjected to successively higher stress levels. A specimen is first subjected to a specified constant stress for a specified length of time. If it does not fail, it is subjected to a higher stress level for a specified time. The stress on a specimen is thus increased step by step until it fails. Usually all specimens go through the same specified pattern of stress levels and test times. Sometimes different patterns are applied to different specimens. Figure 3 depicts two such patterns. Such data may be censored. Pattern 1 has six failures and three runouts.

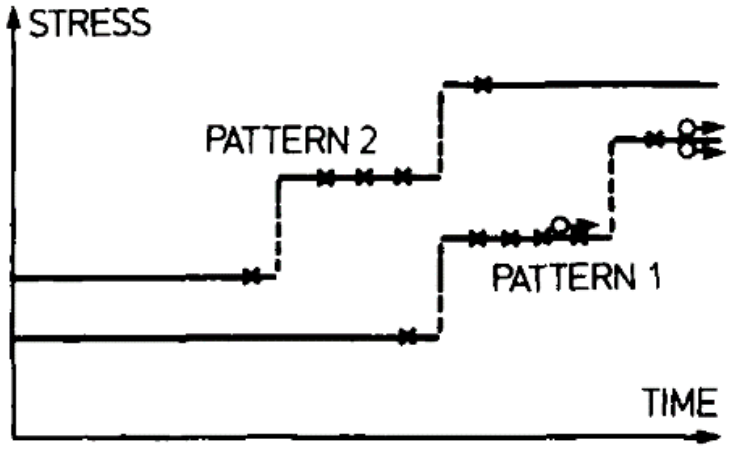

Figure 3: Step stress tests [1]

Implementing step stress allows to achieve product failure more quickly with respect to the constant stress method but there is also a disadvantage. Most products run at constant

stress - not step stress. Thus, the model must properly consider the cumulative effect of exposure at successive stress levels.

There are different laws to be applied during the step stress test. Nelson in [6] describes a step-stress model and data analysis. Schatzoff and Lane [7] use this model to optimize planning of a step stress test with read-out data. Goba [8] references such work on temperature accelerated testing of electrical insulation.

In progressive stress loading (Figure 4) the specimen is subjected to progressive increased load according to an appropriate law (generally linear). As it can be noticed, the specimens tested at low rate of stress tend to survive longer than in case of high rate stress.

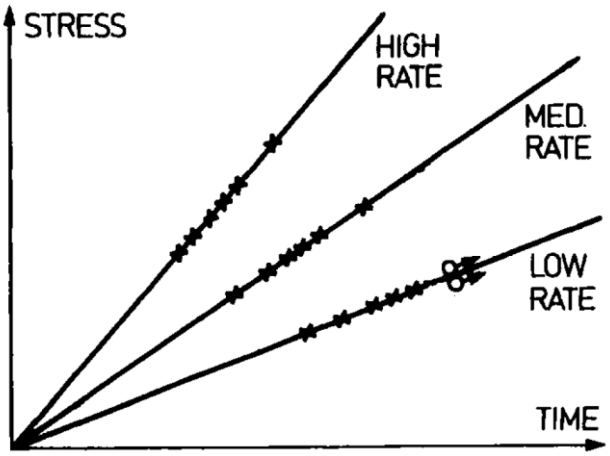

Figure 4: Progressive failure test [1]

It is also possible to carry out accelerated tests with cyclical stress (Figure 5), where the sample is subjected to the same constant cycle until the failure. This stress load is generally used to evaluate the fatigue behavior of the materials.

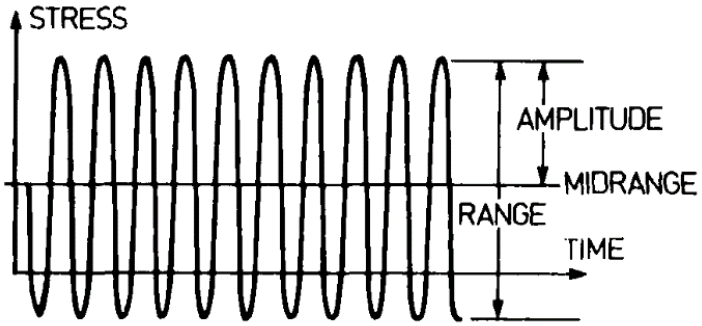

Figure 5: Cyclic stress loading [1]

Some products undergo randomly changing levels of stress during their use, as depicted in Figure 6. For example, bridge members and airplane structural components undergo wind buffeting.

Figure 6: Random stress loading [1]

Then an accelerated test typically employs random stresses with the same distribution as actual random stresses but at higher levels. Like cyclic stress tests, random stress models employ some characteristics of the stress distribution as stress variables (say, the mean, standard deviation, correlation function, and power spectral density). Then such a test is regarded as a constant stress test; this, of course, is simplistic but useful. The test can then be depicted as in Figure 2 where the horizontal line shows the mean stress. Moreover, specimen life is modeled with a constant stress model, and the data are analyzed accordingly [1].

2. ACCELERATED LIFE TESTING APPLIED TO A MECHANICAL DEVICE: A GENERALIZED METHODOLOGY APPLIED TO A CASE OF STUDY

2.1 Standard test and accelerated test

Many authors studied the statistical methods to be applied to accelerated life testing [1,3,4,6,9–12]. Almost all the studies dealing with accelerated life testing, that are present in the literature, are related to electronic component, due to their constant failure rate and therefore a greater simplicity of the study [1,4,6,10]. Few authors focused on accelerated life testing of mechanical components, but they mostly deal with very simple parts (ex. bearings). Issue of novelty of the present work is to develop an accelerated life testing procedure that can be applied to almost all the mechanical components, regardless their complexity grade. In complex mechanical components, indeed, the failure could be related to many different mechanisms. Moreover, the progressive degradation of a part of the assembly can affect the stresses on the other parts. In these cases, the evaluation of the actual service life of the components is not so trivial.

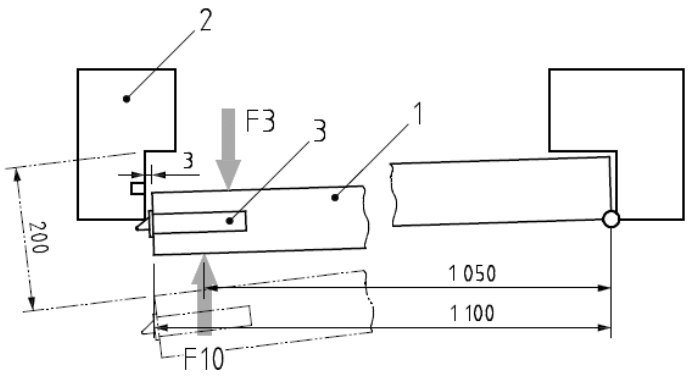

Figure 7: Durability test of the latch operating under a transverse force applied as recommended in EN 12209 [13]; (1) door fixture, (2) forend fixture, (3) lock component to be test

Through in this dissertation, focus is placed on products belonging to the lock-industry. Indeed, in these kinds of components, the standard durability test could be very expensive in terms of time and costs. For example the durability test of a door latch, when performed according to the EN 12209 [13] Standard, consist of different points. In the following, the

test methodology proposed by the Standard is briefly commented in order to highlight all the steps it requires, so as the reader can understand the fallout of such requirements in terms of cost. It is paramount to underline that similar requirements are set by many Standards dealing with product validation, not limited to the lock-industry. In order to develop the test, a force F3=120 N should be applied on the door (Figure 7). Then the door is opened to a distance of 200 mm from the frame and finally the door can be closed, and the cycle can restart. The minimum test duration is $2 \cdot 10^5$ cycles with a maximum frequency of 10 cycles/min. The test succeeds if all the components of the latch are still working at the end of the test. Due to the limited frequency set out by the standard, the whole test lasts approximately fourteen days. Besides increasing the test frequency, the test duration may be cut down by overstressing the components of the latch.In order to do so, it is mandatory to know the stress field along with the stress-life curves of the materials, as well as the possible sources of non-linearity.

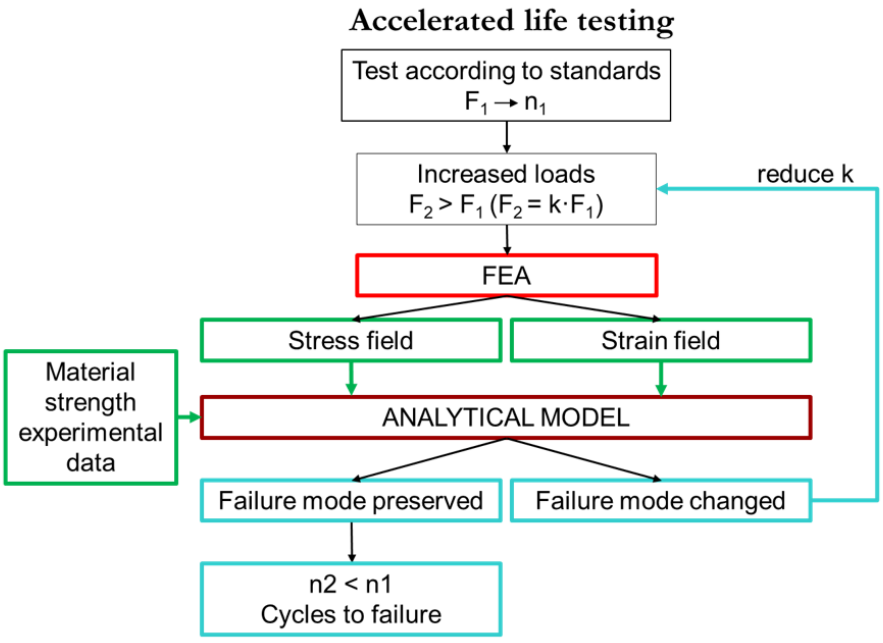

Figure 8: Accelerated life testing flowchart

In Figure 8 a flowchart suggests some basic steps that should be followed when designing accelerated life tests of complex mechanical products. The method herein proposed aims at determining whether the chosen increased loads F_2 suit the needs of product validation or not. In other words, prior to start testing with an increased load, it must be assessed if the stress and strain field which stem from such a magnification of the set of loads allows

preserving the failure modes normally displayed by the product (i.e. under nominal operating conditions) or if, on the flip side, it leads to an unacceptable change in the mode of failure. Such an assessment can obviously be made by trial and error but implementing a mixed numerical-analytical tool leads to considerable savings.

The first (implicit) step consists of assuming that testing under the actual load condition (F_1) is too expensive: thus, the product has to be tested under increased loads ($F_2=k\cdot F_1>F_1$).

Leveraging FEA, it is possible to evaluate the stress-strain field of all the components of the assembly involved in the test. At the same time, dedicated tests performed on the base materials (e.g. fatigue, wear, corrosion tests) or a thorough literature data scanning may provide useful thresholds of the base materials (e.g. fatigue limit). The FEA results, combined with the aforementioned experimental data could be input (in green) in the analytical model, which allows predicting the reduced service life of the components and to correlate it to the effective life during the standard use. This model is also conceived in such a way that it can detect if the failure mode changes due to the applied overload. In this case, the procedure reverts to the definition of the amplification factor k: e.g. k is reduced, and the cycle repeated until preservation of the standard failure mode is achieved. In the flowchart the outputs are represented in light blue.

2.2 Case study

As stated above, the developed methodology will be illustrated by making reference to a product belonging to the lock-industry (door latch): such a product will be referred to as “demonstrator” in the following. The object of investigation is shown in Figure 9. The operating principle of the mechanism will be briefly described in the following. The latch lever (Id. 5 in red) is initially engaged in the strike plate (Id. 7). To open the door, it is necessary to withdraw the latch. This operation can be done by applying a torque on the follower (Id. 4 in yellow), which in turn sets the latch lever (Id. 1 in green) into rotation. Such component is engaged onto the rightmost end of the latch rod (Id. 3 in blue) and permits to retract the latch itself.

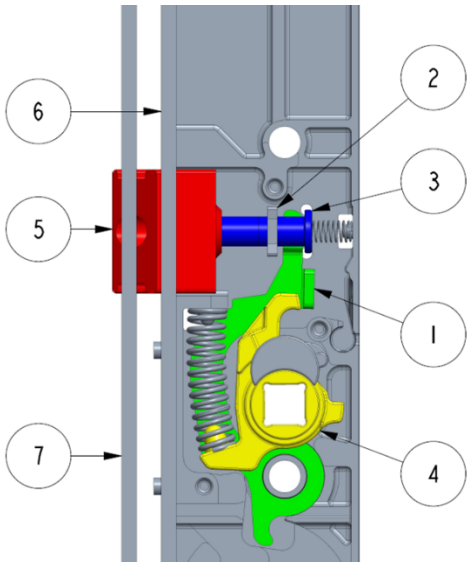

Id.	Name
1	LATCH_LEVER
2	BRACKET
3	LATCH_ROD
4	FOLLOWER
5	LATCH
6	FOREND
7	STRIKE_PLATE

Figure 9: Locking device object of the analysis

During testing, the latch repeatedly slides on the strike plate and on the forend (Id. 6 in grey). The relative motion between these parts, which takes place under non-negligible pressures, ultimately produces severe wearing of the latch. This component is usually made of materials like ZP5 zinc alloy [14], a material whose favorable cost makes it the preferred choice for mass-production applications like the one described here. These devices must sometimes work in a corrosive environment. In order to improve its corrosion resistance, the latch is coated by an electrodeposited nickel coating [15]. The friction coefficient between nickel and steel proved to be lower than the zinc alloy on steel one (see 4.2). Due to the wear of the latch, and therefore a mutation of the friction coefficient between the latch and the forend as well as between the latch and the strike plate, the components behind the opening chain are undergo a change in the stresses they are subjected to. The durability tests on this component shown that the main failure mechanism of the latch lever (made of S420MC [16]) and the latch rod (made of 11 SMnPb 30 [17]) is fatigue. The bracket is a component (made of DX51D alloy) that allows to guide the latch rod during the opening phase.

For the aforementioned reasons, it is particularly important to characterize the wear behavior of the latch (electrodeposited nickel coating over ZP5 zinc alloy base material) and the fatigue behavior of the S420MC steel and 11 SMnPb 30 free-cutting steel.

3. FINITE ELEMENT ANALYSES

In order to evaluate the stress field in terms of bending stresses and contact pressures of the components involved during the accelerated life testing, several finite element analyses were carried out by means of the ANSYS Workbench 17.1 software. As explained in the next chapter, the wear behavior of the latch introduces a transition of the friction coefficient during the test. So, different FEA were carried out using different friction coefficients in the relevant contactareas. Moreover, three different levels for the applied load were considered. The combination of the friction coefficient and the applied load brings to a total of nine FEanalyses. For the sake of synthesis, not all the FEA results will be shown in the following figures. In the last section of this chapter all the results will be summarized.

3.1 Materials behavior

In this section, the mechanical properties used during the FEA will be presented. The latch is made of ZP5 zinc alloy. The latch rod is machined from a bar of free cutting steel 11 SMnPb 30. The latch lever instead, is made of S420MC steel. Finally, the forend and the strike plate are made of AISI 304 whereas the bracket is made of DX51D alloy. The mechanical characteristics of these materials are reported in Table 1.

Table 1: Mechanical characteristic of the materials involved in the FEA

ZP5 EN 12844 [14]			
$Rp_{0,2}$	Yield strength	250	MPa
Rm	Ultimate tensile stress	330	MPa
A%	Elongation %	5	-
E	Elastic modulus	85,000	MPa
ν	Poisson's ratio	0.29	-
11 SMnPb 30 [17]			
$Rp_{0,2}$	Yield strength	480	MPa
Rm	Ultimate tensile stress	700	MPa
A%	Elongation %	14	-
E	Elastic modulus	210,000	MPa

ν	Poisson's ratio	0,3	-
AISI 304 [18]			
$Rp_{0,2}$	Yield strength	210	MPa
Rm	Ultimate tensile stress	520	MPa
A%	Elongation %	45	-
E	Elastic modulus	193,000	MPa
ν	Poisson's ratio	0,29	-
DX51D+AZ [19]			
$Rp_{0,2}$	Yield strength	140	MPa
Rm	Ultimate tensile stress	270	MPa
A%	Elongation %	22	-
E	Elastic modulus	210,000	MPa
ν	Poisson's ratio	0,29	-
S420MC [20]			
$Rp_{0,2}$	Yield strength	420	MPa
Rm	Ultimate tensile stress	480	MPa
A%	Elongation %	16	-
E	Elastic modulus	210,000	MPa
ν	Poisson's ratio	0,3	-

3.2 Latch action with a force applied FE model

In order to simulate the mechanism action that takes place during the tests, a numerical FE model conceived as follows has been developed. In particular the behavior of the components during the door opening was analyzed. In Figure 10 the static scheme of the mechanism is reported with an indication of the forces applied to the components during the tests.

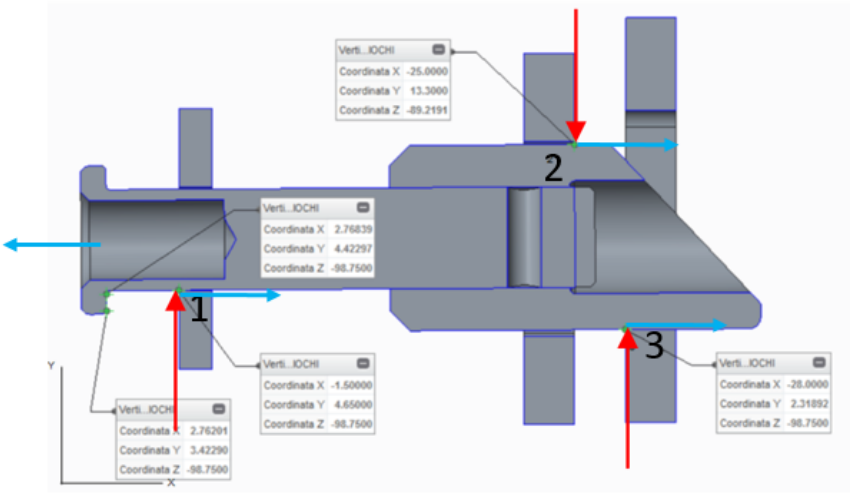

Figure 10: Static scheme of the mechanism

The problem is three-dimensional in nature, due to the geometry of components. Accounting for the symmetry, a half mechanism could be analyzed in order to reduce the computational cost. A symmetry region was therefore applied in the x-y plane (Figure 11). A fixed support was applied on the forend and to the bracket (A). The testing force F3/2 (B), equal to half the actual force applied during testing (owing to symmetry) was applied directly on the strike plate, which was in turn constrained to translate along the y direction (C). In order to simulate the door opening, a displacement (D) along the x direction was applied to the latch rod plate. A series of multistep analyses were carried out without considering (in this phase) the materials nonlinearities. At the first step the load F3 was applied on the strike plate. In the following steps the latch was retracted by the aforementioned displacement.

In Figure 12 the contacts used in the finite element model are shown. The contacts between the latch and the forend (A) and between the latch and the strike plate (B) were set as frictional and the friction coefficients were parameterized in order to test different friction coefficients. Indeed, as briefly noticed in the previous chapter, due to wear affecting the latch, a transition in terms of friction coefficients is likely to take place during the test. Consequently, three different friction coefficients were considered: 0.3, 0.7 and 0.9. These coefficients were selected, based on the outcomes of the experimental campaign involving wear tests that is going to be described in the next chapter. In the figures in this chapter the friction coefficient is always equal to 0.3. The contact between the latch rod and the bracket, instead, was also set as frictional with a constant friction coefficient of 0.15 (steel-steel contact), which is assumed not to change during the test (it

was validated by experimental tests). Finally, since simulating the actual stress distribution inside the bolted joint between the latch and the latch lever is outside the scope of this analysis, a bonded contact was applied there.

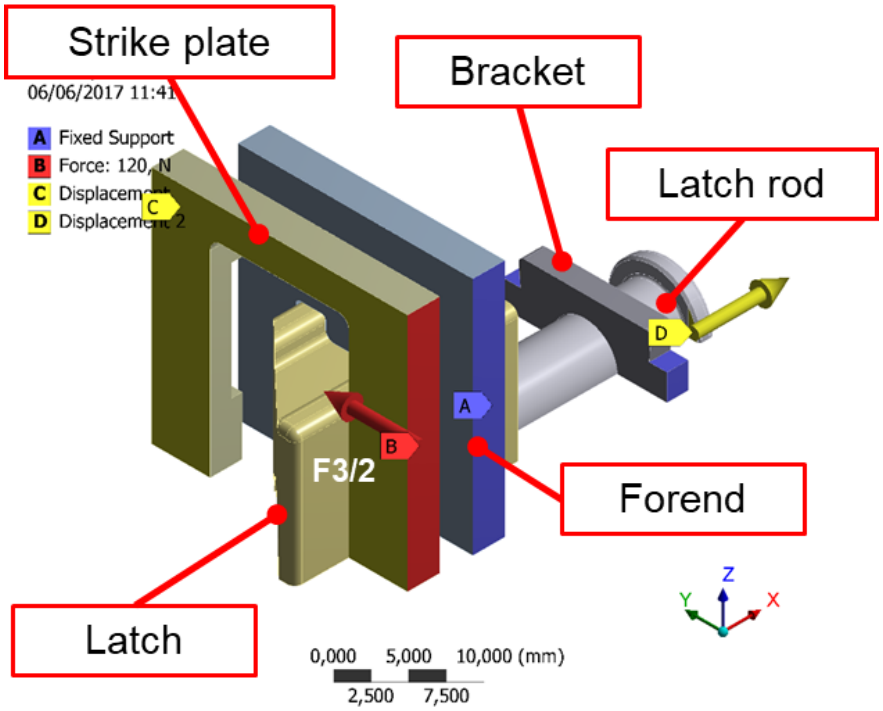

Figure 11: FEA of the latch action with a force applied (geometry and setup)

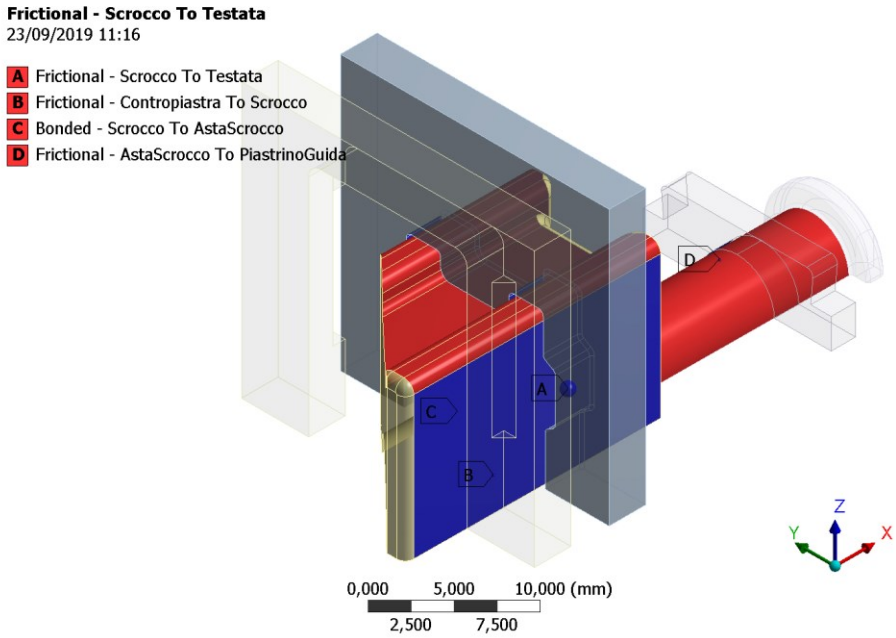

Figure 12: FEA of the latch action with a force applied (contact definition)

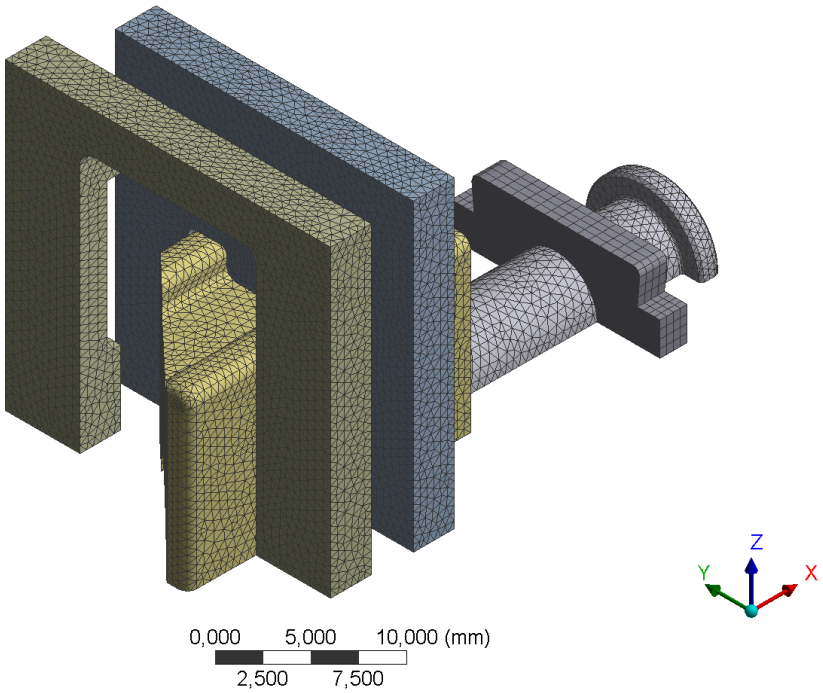

Figure 13: FEA of the latch action with a force applied (mesh)

In Figure 13, the mesh used during for the analyses is shown. A free meshing algorithm was used. The mean element dimension was set to 0.5 mm resulting into a total of 567,284 elements SOLID186 and SOLID187 and 801,576 nodes.

The results, in terms of von Mises stresses, during the opening phase are shown in Figure 14.

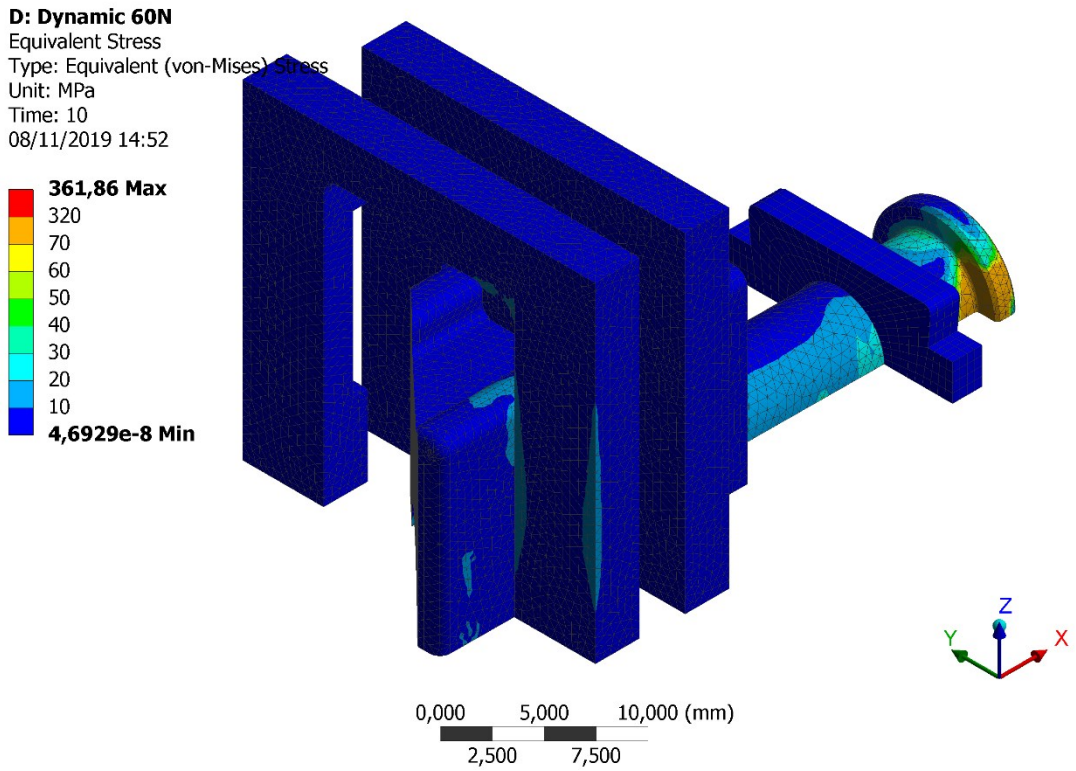

Figure 14: FEA of the latch action with a force applied (von Mises stress results)

It was assessed that the maximum stress occurs always on the latch rod during the opening phase. In order to evaluate the fatigue resistance of this component, the results in terms of bending stresses (normal x stress) were analyzed. In Figure 15 the normal x stress results are shown.

Finally, the contact pressure, between the latch and the strike plate and the latch and the latch rod plate, was analyzed: this result is useful for performing the following wear analysis, i.e. in order to evaluate the wear rate of the latch during the test. The contact pressure results are shown in Figure 16.

At last, the latch withdrawal force was analyzed, using the probe command in the simulation software, in order to carry out the further analyses presented in the next sections.

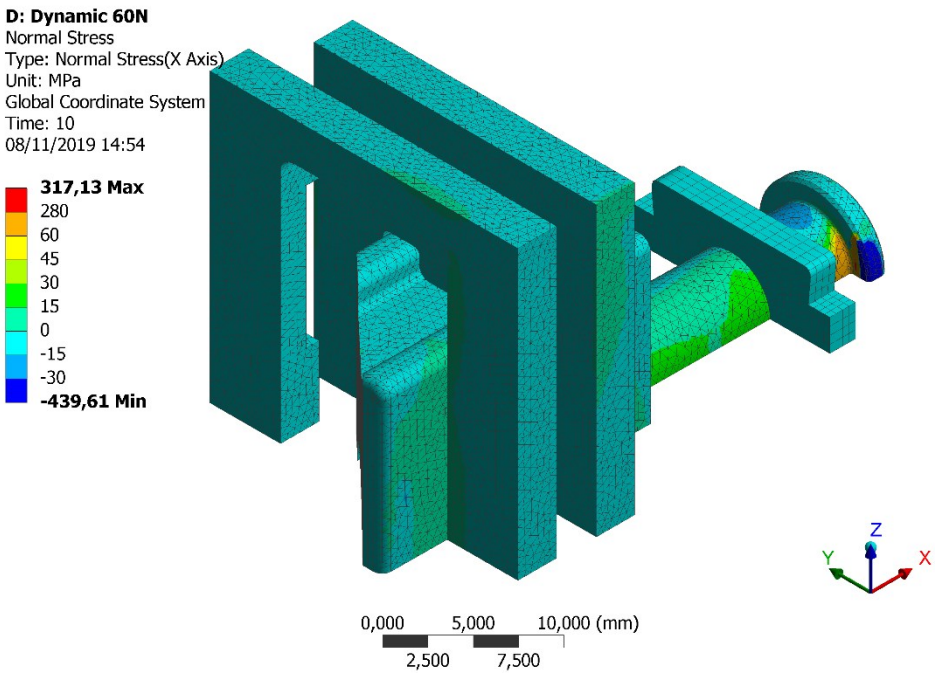

Figure 15: FEA of the latch action with a force applied (normal x stress results)

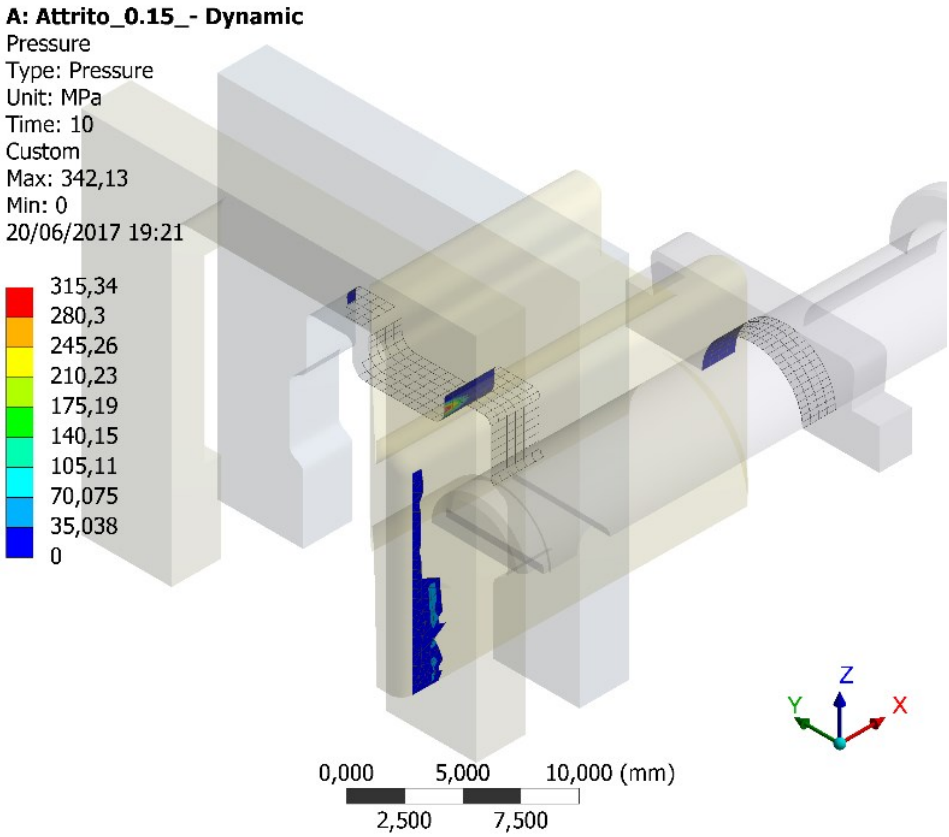

Figure 16: FEA of the latch action with a force applied (contact pressure results)

In order to evaluate the maximum load to be applied during the accelerated life testing, a series of FEA were carried out introducing the nonlinear material behavior. This check is important in order to understand if the overstress applied to the model is such that the intended failure mechanism can be maintained. In particular, a bilinear isotropic hardening material behavior was chosen. It was assessed that, following load increase during the accelerated test, the device could undergo a change in its failure mode. However, as pointed out in the first chapter, in order to properly run an accelerated life test, the failure mode of the standard test load must be kept unchanged. This means that, if additional plastic deformations are introduced during the test, the original failure is indeed improperly altered. As shown in Figure 17, as soon as the transverse force attains F3 = 260 N, the forend begins showing non-negligible plastic strains. For this reason, all the following analyses were limited to forces F3 $\leq$ 240 N, which means two-times the nominal value of force F3.

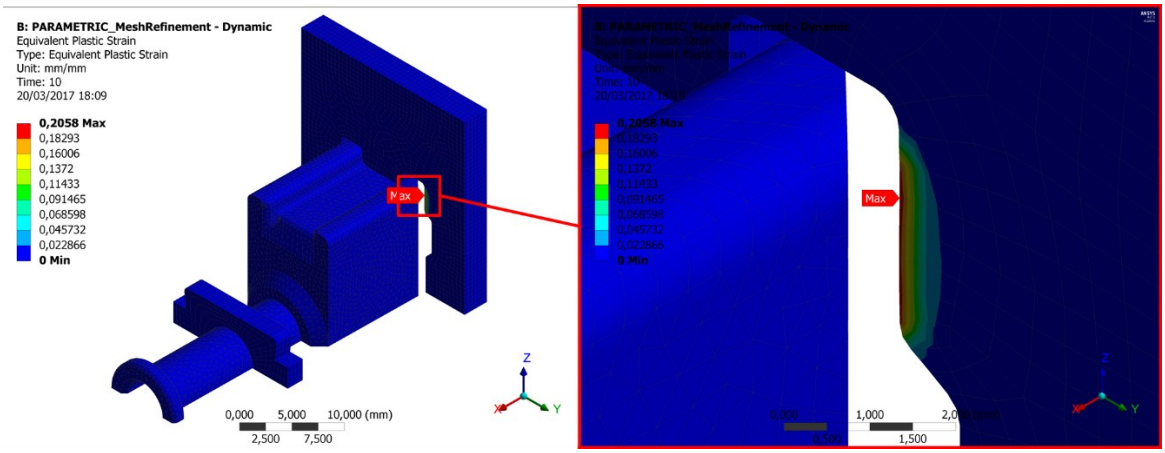

Figure 17: Equivalent plastic strain F3 = 260 N

3.3 Bending stress evaluation on the latch rod

In order to evaluate the actual bending stress on the latch rod plate, some simplified analyses were carried out. In particular, as shown in Figure 18, the latch rod was sliced and just the last part of it was analyzed (rightmost end in Figure 9). The latch withdrawal force, formerly evaluated by means of the probe tool in, was applied directly to the latch rod plate. A symmetry region was applied on the x-y plane whereas a fixed support was applied on the latch rod sliced surface. In this case also, the material nonlinearities were not considered.

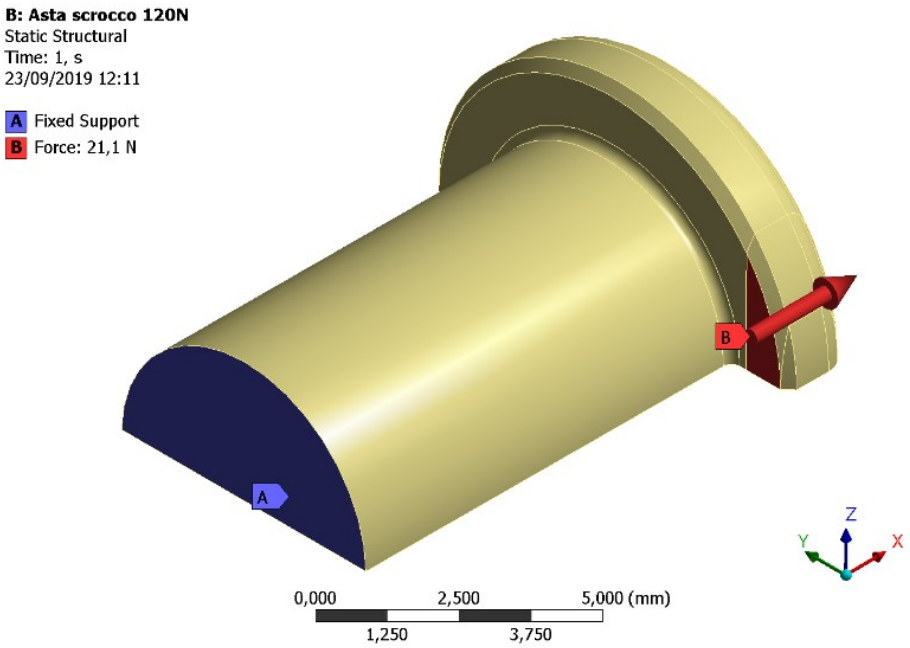

Figure 18: FEA bending stress on the latch rod plate (geometry and setup)

In order to evaluate the convergence of the solution a mesh refinement was applied on the rounded zone of the latch rod plate using a sphere of influence with a radius of 1 mm as shown in Figure 19. The mesh dimension in this zone was parameterized in order to carry out the convergence test. In this case also, the bending stress was extracted as the normal x stress.

Figure 20 shows the outcome of the convergence test. In order to achieve convergence of the solution, a mesh refinement with a mean element size, inside the sphere volume, as small as 0.02 mm was necessary.

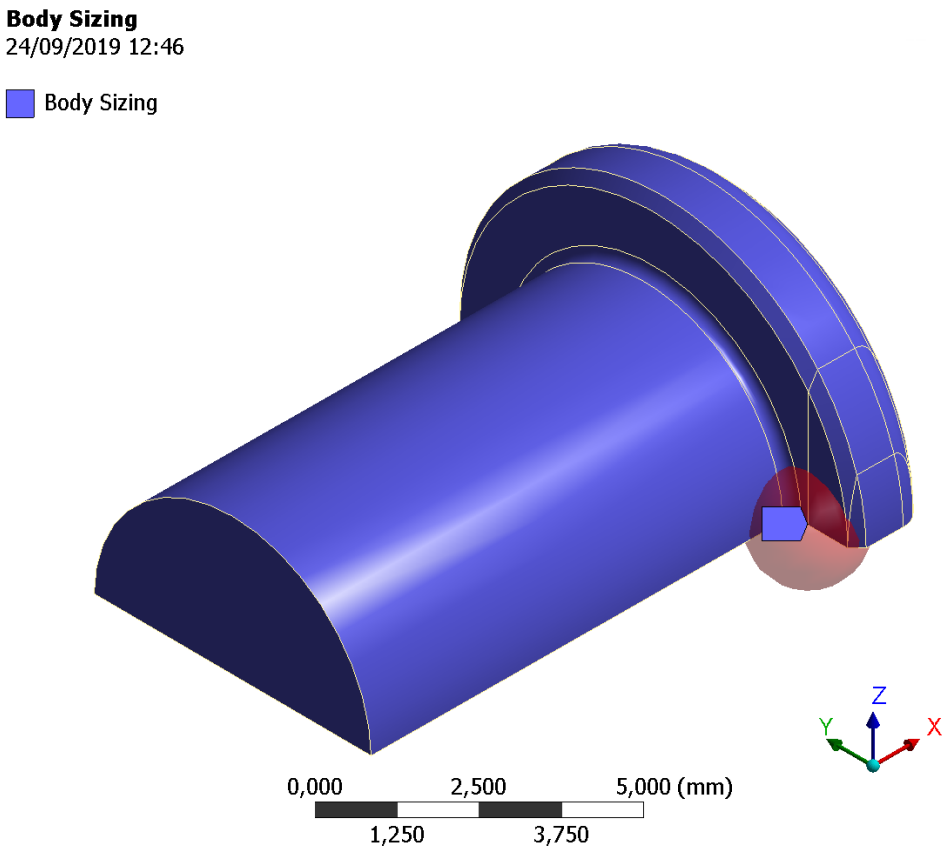

Figure 19: FEA bending stress on the latch rod plate (mesh refinement)

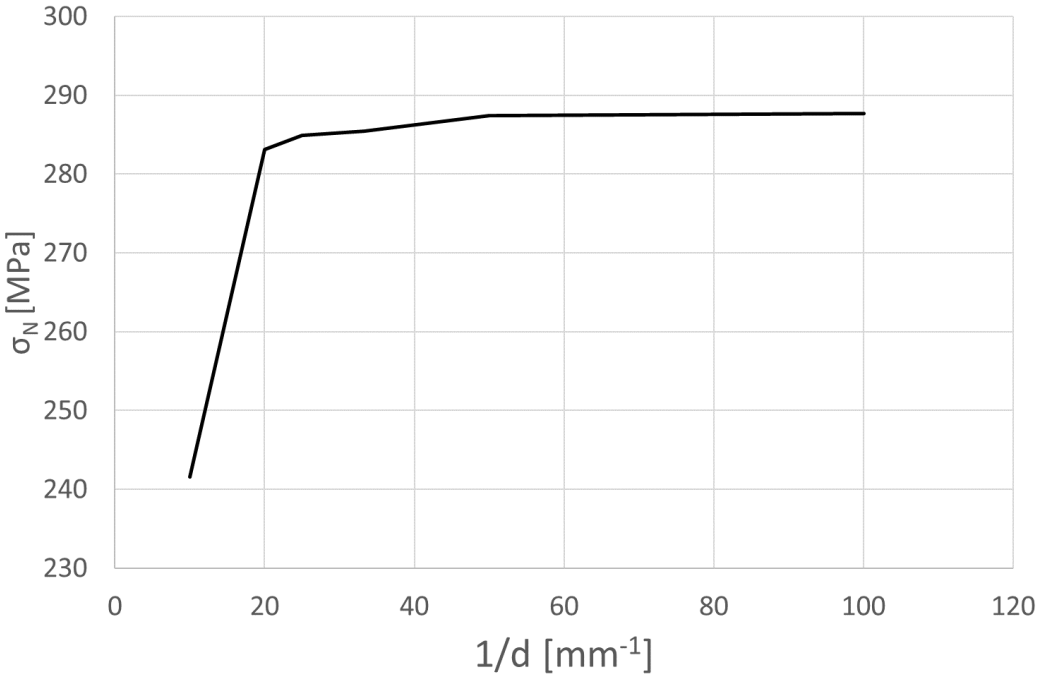

Figure 20: Convergence test

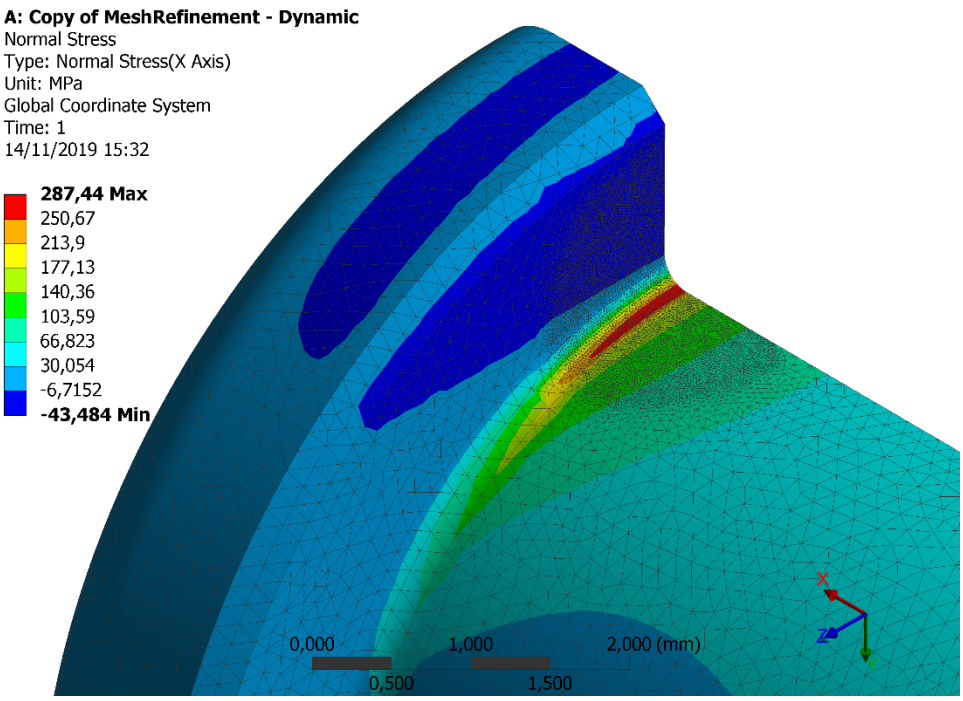

Figure 21: Bending stress on the latch rod plate; mesh refinement

The nominal stress at this point, calculated according to the beam theory, is 121 MPa and, comparing this one with the numerical one (287 MPa), it can be assessed that the stress concentration factor in this zone is equal to 2.37.

3.4 Latch lever stress analysis

In order to evaluate the stress field in the latch lever, some further analyses were carried out. As stated above, the latch withdrawal force was sampled by means of a probe tool in previous analyses. Due to symmetry, the aforementioned reading is a half of the actual force T (Figure 22), which must be borne by the latch lever.

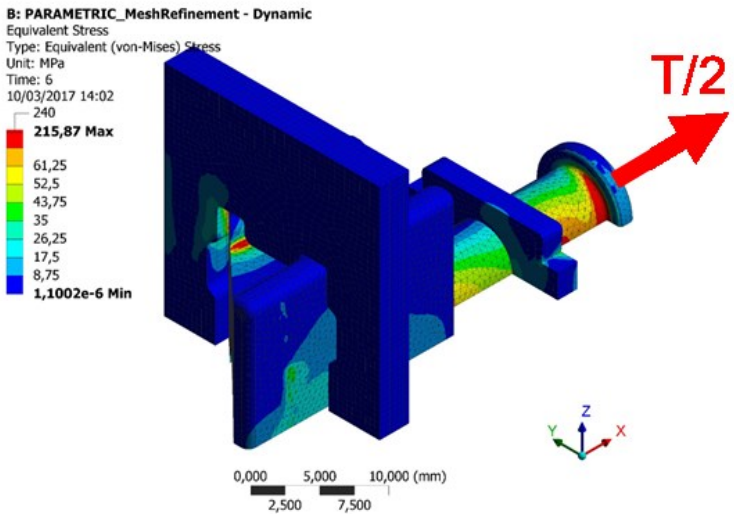

Figure 22: Latch withdrawal force evaluation

Force T was therefore applied to the latch lever (A), as shown in Figure 23. This component was constrained to rotate around y axis (D), by means of a cylindrical support placed at the hole center, which restrained translation along y- axis (C). Finally, in order to avoid any rigid rotations, a null x displacement was applied in (B). This last restraint aims at simulating the contact between the latch lever and the latch rod plate.

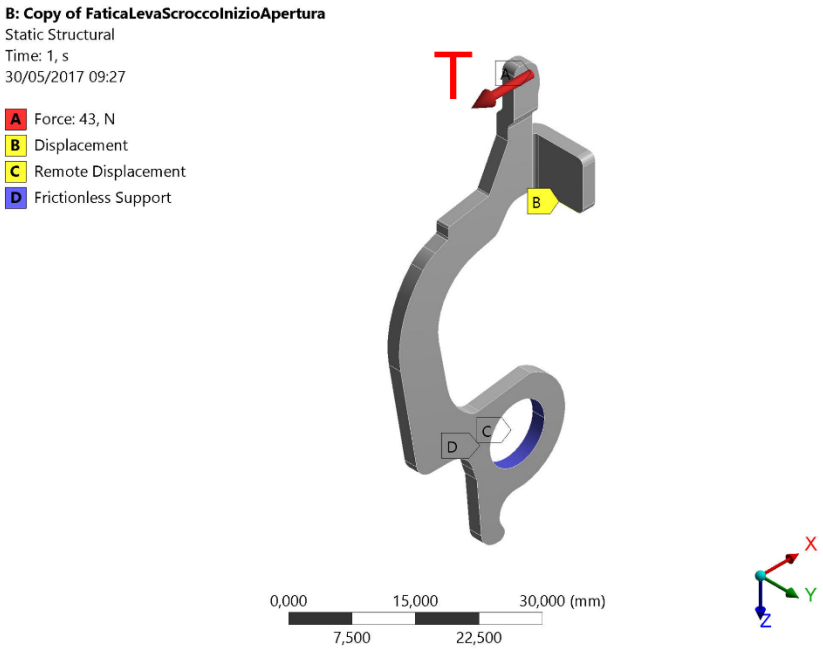

Figure 23: latch lever FEA setup and geometry

A Hex Dominant method mesh was used, with a body sizing of 0.5 mm resulting into 13,313 SOLID186 and 1,066 SOLID187 elements and a total of 60896 nodes as shown in Figure 24. The analyses were carried out using a linear material behavior. In Figure 25, the results, in terms of von Mises stresses are reported for the case of F3=120 N (baseline).

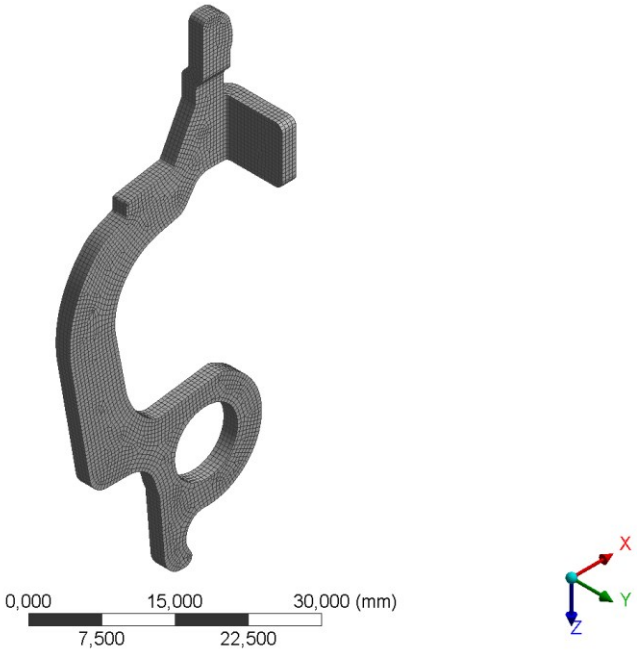

Figure 24: Latch lever mesh

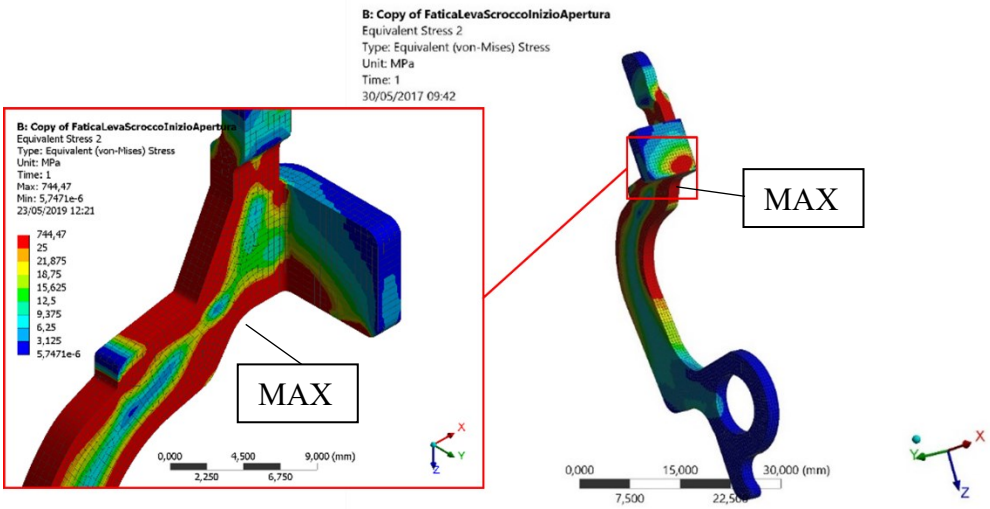

Figure 25: Latch lever FEA results (von Mises stresses)

As it can be noticed, the maximum stress on the latch lever shows up in the vicinity of the cross-section restriction, close to the upper constraint. Since the failure mode of this component is deemed to be fatigue, the maximum bending stress in this zone was thoroughly evaluated. In order to do so, a local coordinate system needed to be defined, in accordance with the picture of Figure 26. The origin was placed in the centroid of the maximum bending area surface whereas the z axis was directed in the maximum stress direction. The maximum bending stress was therefore evaluated for the all load conditions.

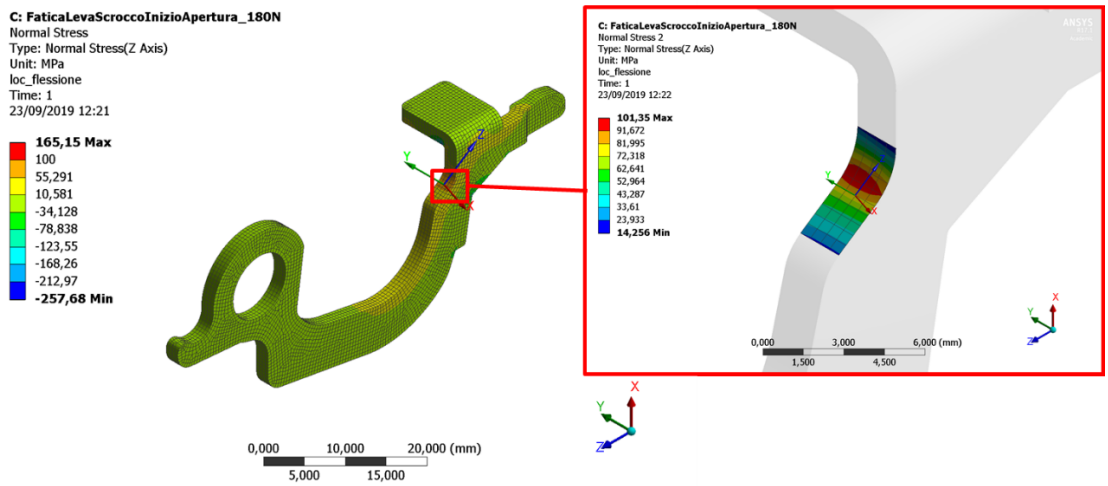

Figure 26: Latch lever maximum bending stress

3.5 Experimental validation

In order to validate the FE analysis, a series of experimental tests was carried out. A strain gauge (HBM 1-LY11-0.6/120) was applied to the latch lever as shown in Figure 27. This position was selected, based on the constant stress trend in this component, according to the FEA reported in Figure 30. A quarter bridge configuration plus dummy gauge for ΔT compensation was used. The latch lever was then mounted into the device, which was in turn constrained by means of suitable screws to a wooden plate (Figure 28). On the fixture, two sleds were provided, in order to constrain the strike plate to move only along the vertical direction. A downwards directed vertical force was then applied, by means of a mass of 12.2 kg (120 N) directly hanging on the strike plate. During the test, the voltage signal read by the strain gauge was processed through a NI9237 strain module, plugged

into a NI9184 carrier. Data sampling was made by means of a self-developed program written in LabView. A typical strain output behavior obtained during the tests is shown in Figure 29. The tests were carried out both in the lubricated and in the unlubricated conditions. Ten replications for the unlubricated condition and twelve replications for the lubricated one were totally carried out. The experimental results as a strain mean during the opening phase are reported in Table 2. As it can be noticed, the results for dry and lubricated surfaces are very close each other. This outcome can be related to the presence of lubrication applied upon the industrial assembly phase. Comparing the general mean of the two test conditions it is possible to assess that the strain is not affected by the lubrication of the latch. Considering then a Young's modulus of 210,000 MPa (Table 1) it is possible to evaluate the stress at the gage application area using the Hooke's law.

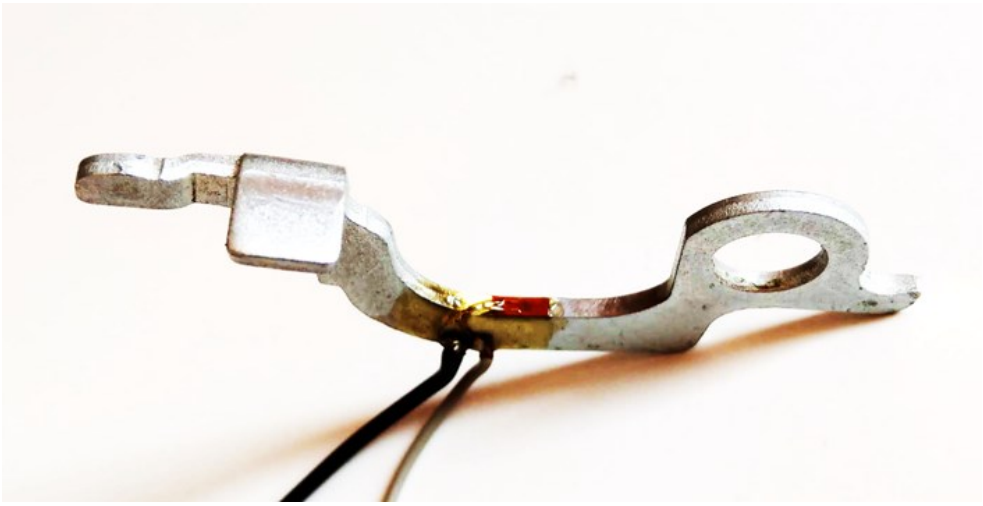

Figure 27: Strain gauge on the latch lever

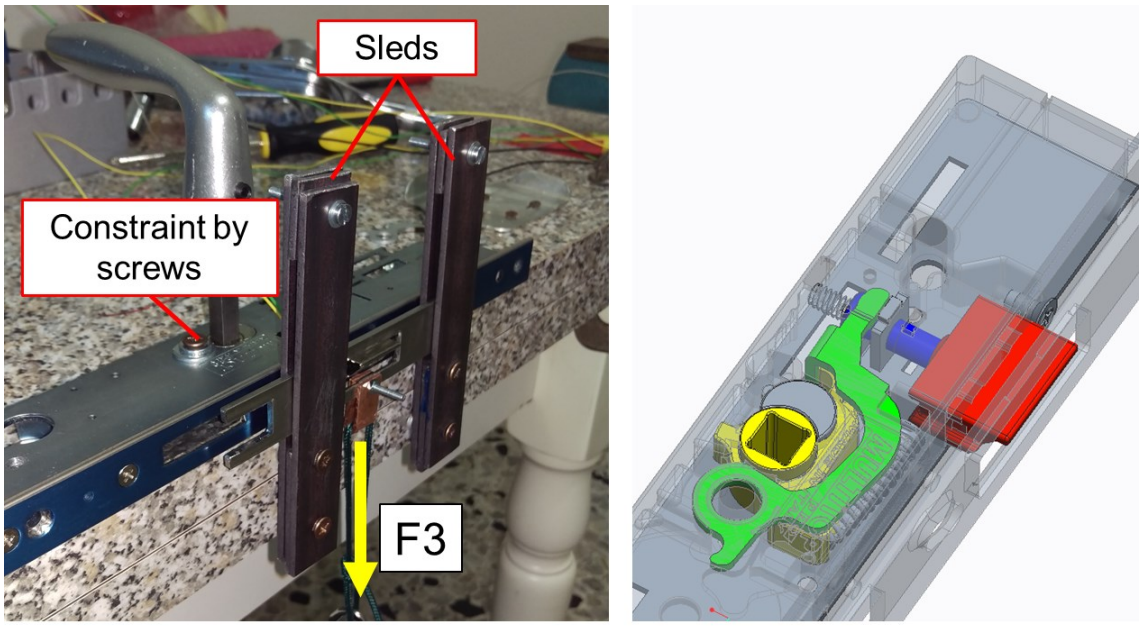

Figure 28: Experimental validation tests

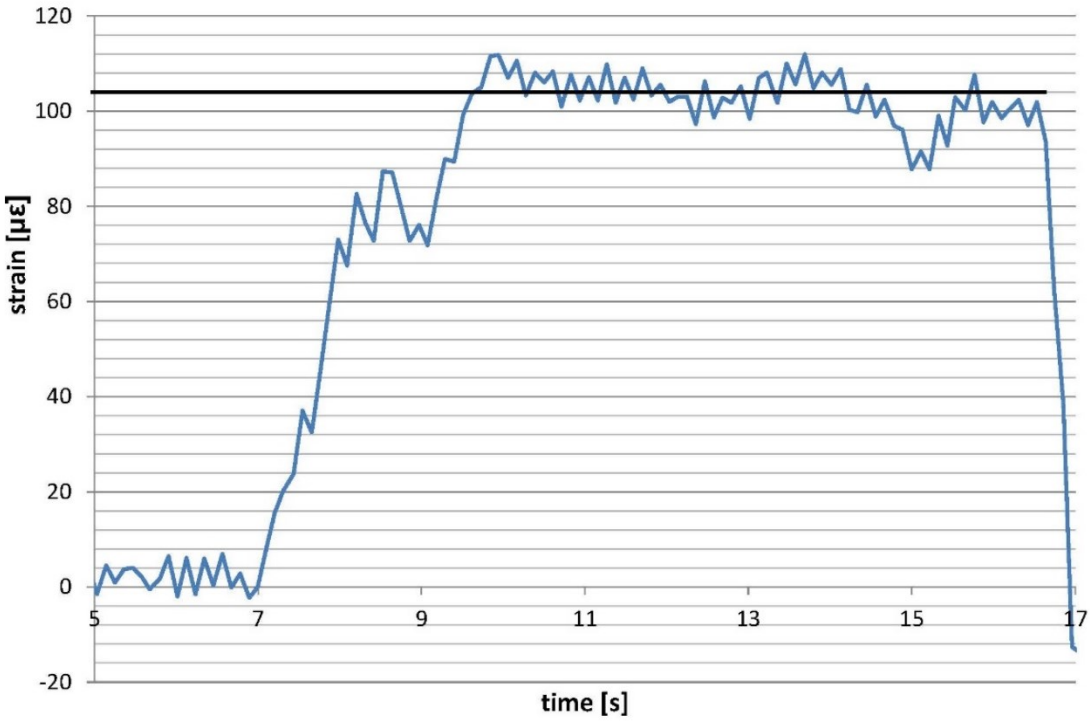

Figure 29: Strain gauge output during the tests

Table 2: Experimental results as a mean of the output strain

	Dry	Lubricated
Test N.	με	με
1	93	101
2	88	104
3	93	112
4	87	107
5	120	93
6	107	87
7	104	96
8	101	91
9	111	87
10	107	88
11		91
12		93
Mean	101	96
St. Dev.	11	8
Stress	21.2 MPa	20.1 MPa

The strain general mean ε_x = 98.5 με (for all the experimental tests) allows to assess that, at the gage application area, the normal stress is equal to σ_{exp} = 20.6 MPa (Figure 30). From the numerical FE models, it was assessed that, for the same load conditions, the stress is equal to σ_{num} = 21 MPa. It can be assessed that the model is therefore validated with an error of 2%.

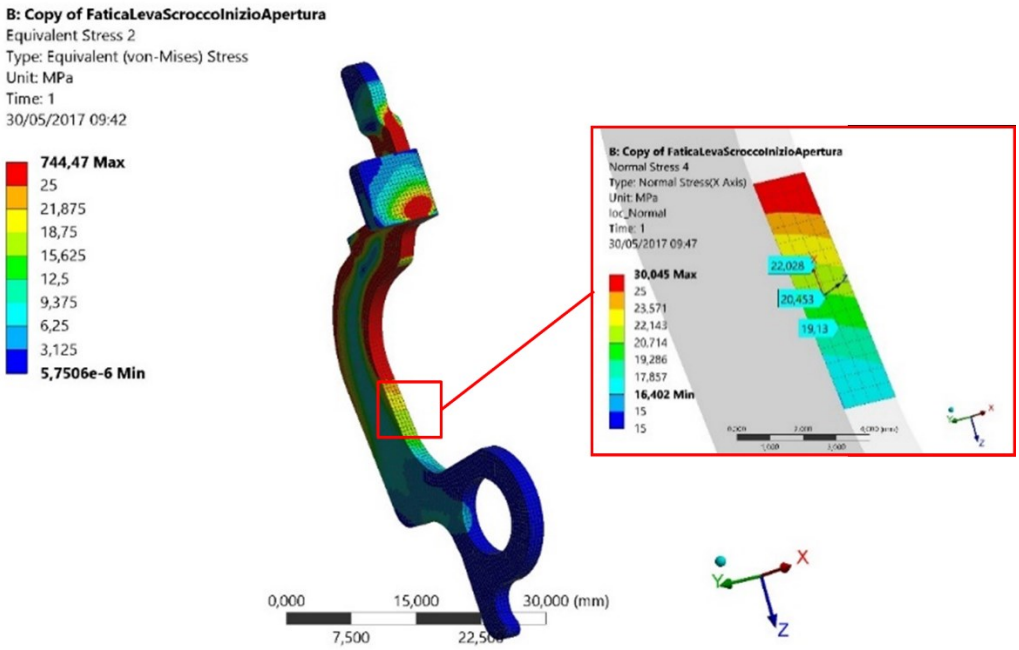

Figure 30: Latch lever results (bending stress evaluation)

3.6 Results summary

The aforementioned analyses were carried out considering different testing forces and different friction coefficients. For the sake of synthesis, not all the results have been presented in the previous section. In this section, a summary of the principal FEA results used in the analytical model presented in chapter 5 are reported. In Table 3, the maximum bending stress on the latch rod plate evaluated as explained in section 3.3 are reported. Moreover, in Table 4 the FEA results in terms of maximum contact pressure on the latch, evaluated according to section 3.2 are presented. Finally, in Table 5 the numerical results relevant to the maximum bending stress on the latch lever, evaluated as explained in section 3.4, are summarized.

Table 3: FEA results maximum bending stress on the latch rod plate [MPa] (normal x axis stress Figure 21)

	F3 = 120 N	F3 = 180 N	F3 = 240 N
μ = 0.3	250	290	328
μ = 0.7	280	324	367
μ = 0.9	300	346	394

Table 4: FEA results maximum contact pressure on the latch [MPa] (Figure 16)

	F3 = 120 N	F3 = 180 N	F3 = 240 N
μ = 0.3	115	180	266
μ = 0.7	130	220	280
μ = 0.9	140	230	290

Table 5: FEA results maximum bending stress on the latch lever [MPa] (Figure 26)

	F3 = 120 N	F3 = 180 N	F3 = 240 N
μ = 0.3	193	289	385
μ = 0.7	204	302	401
μ = 0.9	210	312	415

4. EXPERIMENTAL TESTS

In this chapter the experimental tests, needed to evaluate the mechanical behavior of the materials involved in the accelerated testing, will be presented. In particular the fatigue behavior of the free cutting steel 11 SMnPb 30 was experimentally determined (see 4.1). Concerning the fatigue behavior of S420MC steel, the data presented by Klemenc in [21,22], were used to develop the analytical model. Finally, the wear behavior of the electrodeposited nickel coating on the zinc alloy ZP5 was experimentally determined using slider on cylinder wear test (see 4.2).

4.1 Coating effect on the fatigue behavior of a free cutting steel [23]

Free cutting steels, which are commonly used in many mass production fields, such as the automotive industry and household appliances, contain sulfur lead and some other elements, which enhance machinability. For this reason, this class of materials is widely used in the lock-industry, which is characterized by very large production batches, in order to cut production costs. It must be observed that, in some cases, free cutting steel components must withstand remarkably high fatigue loads, even in harsh environment. For example, as indicated by Standard [13], the lock shall be mounted in a fixture being similar to a door application. Afterwards, it is sprayed by neutral salt for a defined duration: in this particular condition, it is required to comply with some standard requirements and to pass specific tests, to ensure its ability to operate after environmental exposure. To achieve acceptable material properties, thus improving wear resistance, even in harsh environments, considering cost issues as well, the widespread procedure in the lock industries is to use electrodeposited coatings over free cutting steel materials. This is a very serious issue, as the failure of the locking devices may arise both from too high wear, which is no longer compliant with the standard requirement, and from fatigue damage. In particular, some authors indicate that coatings may have a detrimental effect on the fatigue strength of the materials [24–28]. Therefore, it is important to clarify this point, depending on the involved materials and coatings, and, in case, to search a compromise. For these reasons, some free cutting steels have been investigated in the last years [29–35]. However, a literature survey still indicates a lack of knowledge in this field, in particular regarding the interaction between the material properties and the

coating alloy components and the related combined effect on the mechanical response with particular reference to fatigue.

Metal coatings may also be suitably applied to improve the mechanical response of leaf springs. Indeed, as indicated in [36] coatings yield the advantages of preventing fretting fatigue damage as well as significantly incrementing the wear resistance as an effect of friction reduction. However, the aforementioned reference, also confirms that coatings may have the serious drawback of reducing the fatigue strength of the treated components under cyclic loads. This outcome is often due to the weakening of the surface at the interface between the part and the coating. The described issue can be overcome by an additional surface treatment, for instance, a shot peening treatment with properly optimized parameters, to be performed before coating to strengthen the surface. However, such a treatment is not always affordable, due to its costs or the actual geometry of the parts to be processed. This point confirms and stresses the need for results concerning the fatigue response of coated parts, considering that the application of shot-peening or other surface treatments, to counterbalance the possible detrimental effect of coating, could not be available for many reasons.

11 SMnPb 30 is one of the most frequently used free cutting steels. In order to prevent corrosion, electrodeposited nickel and zinc coatings are commonly applied on these materials. The literature indicates that these coatings have some issues arising from thickness control difficulties during the electrodeposition process. For this reason, they are currently used mainly for decorative purposes, whereas, very few studies deal with their industrial applications [37,38]. In the literature there are no data regarding the effect of the coatings on the fatigue behavior of the free cutting steel 11 SMnPb 30. Moreover, in this study, an ANOVA-based statistical method was used, making possible to assess the significance or not significance of the aforementioned effects.

4.1.1 Materials and methods

The testing campaign involved 11 SMnPb 30 EN 10087 [17] (also referenced with the number 1.0718), whose chemical composition is reported in Table 6. The fatigue testing procedure was based on ISO 1143 Standard for rotating bending fatigue testing [39]. The Standard defines the testing procedure, the load scheme and the specimen geometry. The samples were manufactured with 6 mm diameter at gage and 10 mm diameter at the heads as a good compromise to reduce production costs, while ensuring agreement with the

Standard. A sample drawing including its dimensions, as well as dimensional and geometrical tolerances, is shown in Figure 31.

Table 6: Chemical composition of free cutting steel 11 SMnPb 30 [16]

C	Si max	Mn	P max	S	Pb
≤0.14	0.05	0.90 to 1.30	0.11	0.27 to 0.33	0.20 to 0.35

Three different sets of specimens were involved in the experimental campaign: one sample for each set is shown in Figure 32. The first set, referenced as 1, involved samples that were fabricated without coating (in the "as received" conditions). Set 2 consisted of samples that were treated by an electrodeposited zinc coating, referenced as Fe/Zn5/a, according to ISO 2081 [40]. This process provides a 5-µm minimum zinc thickness and a finishing by a clear chromate conversion process. Finally, Set 3 involved specimens treated by an electrodeposited nickel coating Fe/Cu1/Zn5s in the framework of ISO 1458 [41]. This process provides a coating consisting of 1 µm (minimum) ductile, levelling copper, plus 5 µm (minimum) sulfur-free nickel.

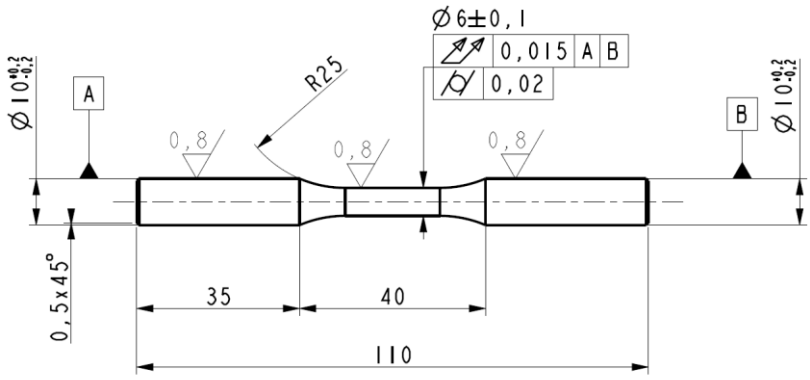

Figure 31: Smooth sample for fatigue tests under rotating bending according to [17]

The experimentation was preceded by dimensional checks and roughness measurements that involved every sample. The measurements were made, using a micrometer screw gage and a portable surface roughness tester as indicated in [42]. Measurements were carried out with 4 replications at each head and with 6 replications at gage. Surface roughness on both the heads and on the gage were measured over 8 replications. In particular, roughness was averaged over 4 mm runs along the longitudinal axis, considering 90° angled spots with two repetitions for each. Measurement at the gage was

performed only on the samples that got broken during fatigue testing, due to the impossibility to correctly align the roughness tester in the unbroken ones. The retrieved measurements were anyway sufficient to get evidence of the roughness mean value at gage and to ensure the fulfilment of drawing specifications in the case of Set 1. Average values of the diameter and surface roughness measurements are provided in Table 7 with reference to the three sample Sets.

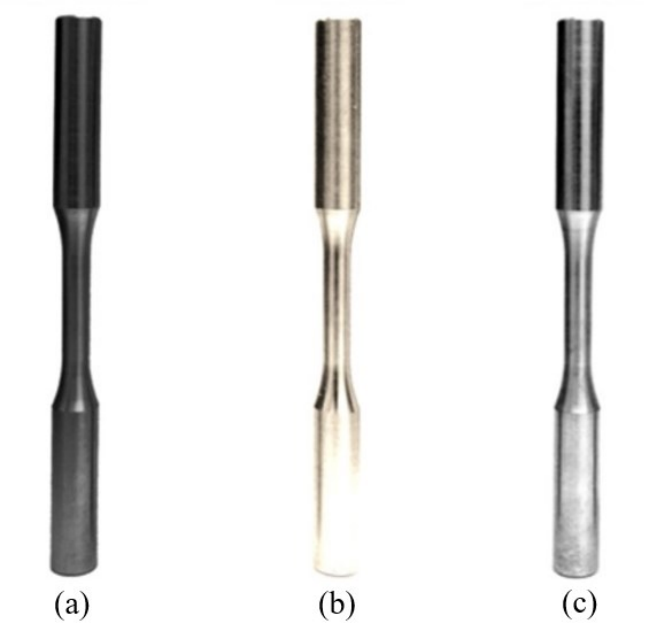

Figure 32: Specimens sets (a) Set 1: as received, (b) Set 2: zinc coated Fe/Zn5/a, (c) Set 3: nickel coated Fe/Cu1/Ni5s

The specimens were tested under rotating bending fatigue loads, at the Alma Mater Labs, using a four-point rotating bending machine configuration, where the sample is loaded under constant maximum nominal bending moment [42–46]. The fatigue testing was aimed at the determination of the S-N curves and the endurance limits. A staircase method was applied, to determine the endurance limit, according to Standard ISO 12107 [47]. A life duration of $5 \cdot 10^6$ cycles was set as run-out threshold. A confidence analysis (90% confidence level) was also performed based on the standard deviation of the endurance limit (scattering of the experimental results) and on the size of the sequence that led to its computation. The data in the finite life domain were processed according to the Standard: both the linear and the quadratic model were worked out and the general linear test was then applied, to assess the significance of the improvements arising from the latter. Lower

and upper bounds to be wrapped around the curves were determined, considering failure probabilities of 10% and 90% and with a 90% confidence level.

Table 7: Dimensional and roughness (Ra) measurements

Specimen ID	Gage diameter		Roughness Ra [µm]	Specimen ID	Gage diameter		Roughness Ra [µm]	Specimen ID	Gage diameter		Roughness Ra [µm]
	Mean[mm]	St. dev. [mm]			Mean[mm]	St. dev. [mm]			Mean[mm]	St. dev. [mm]	
1.1	5.989	0.012	2.105	2.1	6.007	0.011	1.515	3.1	6.069	0.008	1.748
1.2	5.999	0.007	0.897	2.2	6.009	0.011	1.590	3.2	6.060	0.017	1.715
1.3	5.995	0.005	0.825	2.3	6.015	0.007	-	3.3	6.063	0.005	1.815
1.4	5.996	0.012	-	2.4	6.010	0.005	0.757	3.4	6.060	0.009	1.767
1.5	5.987	0.005	1.067	2.5	6.025	0.004	1.153	3.5	6.059	0.011	1.705
1.6	5.992	0.007	0.780	2.6	6.012	0.005	-	3.6	6.058	0.009	-
1.7	6.007	0.007	1.842	2.7	6.039	0.009	0.527	3.7	6.055	0.009	2.198
1.8	5.989	0.015	1.165	2.8	6.009	0.009	1.427	3.8	6.048	0.007	2.357
1.9	5.988	0.005	1.010	2.9	6.014	0.005	0.653	3.9	6.058	0.008	1.002
1.10	5.997	0.006	0.825	2.1	6.012	0.004	0.650	3.10	6.058	0.013	1.882
1.11	6.001	0.010	1.620	2.11	6.014	0.006	0.680	3.11	6.041	0.014	-
1.12	5.996	0.007	1.235	2.12	6.018	0.004	0.660	3.12	6.059	0.008	1.353
1.13	5.989	0.005	1.098	2.13	6.015	0.004	0.645	3.13	6.050	0.010	2.472
1.14	6.010	0.007	1.505	2.14	6.015	0.008	-	3.14	6.052	0.011	-
1.15	5.992	0.012	0.827	2.15	6.020	0.006	0.810	3.15	6.068	0.010	1.373
1.16	5.994	0.009	-	2.16	6.013	0.006	-	3.16	6.052	0.013	-
1.17	6.002	0.011	-	2.17	6.009	0.009	1.645	3.17	6.056	0.010	-
1.18	5.994	0.007	0.770	2.18	6.008	0.004	-	3.18	6.044	0.009	2.133
1.19	5.995	0.006	-	2.19	6.012	0.006	0.790	3.19	6.054	0.012	3.072
1.20	5.997	0.009	-	2.20	6.017	0.008	-	3.20	6.051	0.011	-
1.21	5.995	0.009	0.767	2.21	6.011	0.004	0.875	3.21	6.062	0.010	-
1.22	5.997	0.004	1.185	2.22	6.015	0.004	0.745	3.22	6.047	0.015	2.355
1.23	6.004	0.010	0.987	2.23	6.007	0.007	-	3.23	6.062	0.010	1.532
1.24	6.004	0.009	-	2.24	6.016	0.003	0.952	3.24	6.061	0.016	-
1.25	5.998	0.008	-	2.25	6.038	0.015	-	3.25	6.056	0.011	1.437

At the end of the fatigue testing, crack surfaces were carefully analyzed for the individuation of the crack nucleation point and of possible internal defects. For this purpose, a Stemi 305 stereo microscope (by ZEISS, Oberkochen, Germany) was used.
Finally, further specimens coming from the same sets were used to experimentally characterize the ultimate tensile strength (UTS) and the yield point ($Rp_{0.2}$) of the material with and without coatings. For this purpose, tensile tests were carried out.

4.1.2 Results

The experimental fatigue results are reported in Table 8 to Table 10. The tables provide the sample identifier, as well as the maximum nominal bending stress (corresponding to the stress amplitude) at the gage and the number of cycles to failure. Furthermore, in the fourth column, an indication of the trial outcome ("Run out" or failure) is reported. In particular, "Run out" indicates that the specimen survived testing after 5·106 cycles whereas, "Yes" indicates failed specimens. It is necessary to point out that the failures always occurred at the gage, far from the fillet. Finally, in the fifth column the samples involved in the staircase are highlighted along with the indication of the related ordinal number in the Failure/Run out sequence.

Table 8: Results of the fatigue tests on the samples of Set 1

SET1				
Sample ID	Stress Amplitude [MPa]	Life cycles (N) to failure	Failure	Stair-case sequence
1.1	311	5,006,836	Run out	6
1.2	358	490,983	Yes	-
1.3	406	153,978	Yes	-
1.4	333	5,008,744	Run out	2
1.5	382	309,689	Yes	-
1.6	431	74,745	Yes	-
1.7	346	365,613	Yes	1
1.8	431	24,028	Yes	-
1.9	406	61,905	Yes	-
1.10	382	113,586	Yes	-
1.11	358	334,720	Yes	-
1.12	346	353,105	Yes	3
1.13	333	422,380	Yes	4
1.14	322	3,298,272	Yes	5
1.15	322	3,580,666	Yes	7
1.16	311	5,012,908	Run out	8
1.17	322	15,476,393	Run out	9
1.18	333	2,514,009	Yes	10
1.19	322	5,000,243	Run out	11
1.20	333	5,110,789	Run out	12
1.21	346	954,747	Yes	13
1.22	333	1,902,361	Yes	14
1.23	322	3,200,363	Yes	15

Table 9: Results of the fatigue tests on the samples of Set 2

SET 2				
Sample ID	Stress Amplitude [MPa]	Life cycles (N) to failure	Failure	Stair-case sequence
2.1	431	118,543	Yes	-
2.2	406	192,357	Yes	-
2.4	382	500,898	Yes	-
2.5	358	1,580,338	Yes	-
2.6	333	5,124,090	Run out	2
2.7	431	139,889	Yes	-
2.8	406	142,735	Yes	-
2.9	382	439,301	Yes	-
2.10	358	1,509,506	Yes	-
2.11	346	2,297,939	Yes	1
2.12	346	2,975,560	Yes	3
2.13	333	2,491,952	Yes	4
2.14	322	5,083,675	Run out	5
2.15	333	2,550,607	Yes	6
2.16	322	5,096,147	Run out	7
2.17	333	4,813,658	Yes	8
2.18	322	5,002,900	Run out	9
2.19	333	2,460,925	Yes	10
2.20	322	5,000,046	Run out	11
2.21	333	3,702,551	Yes	12
2.22	322	3,794,098	Yes	13
2.23	310	5,000,032	Run out	14
2.24	322	1,342,276	Yes	-
2.25	322	5,021,102	Run out	15

Table 10: Results of the fatigue tests on the samples of Set 3

SET 3				
Sample ID	Stress Amplitude [MPa]	Life cycles (N) to failure	Failure	Stair-case sequence
3.1	431	65,084	Yes	-
3.2	406	318,587	Yes	-
3.3	382	644,277	Yes	-
3.4	333	2,264,165	Yes	3
3.5	358	1,783,627	Yes	-
3.6	311	5,342,366	Run out	-
3.7	431	122,675	Yes	-
3.8	406	230,720	Yes	-
3.9	382	708,774	Yes	-
3.10	358	929,903	Yes	-
3.11	333	5,256,344	Run out	1
3.12	346	1,664,834	Yes	2
3.13	322	1,101,409	Yes	-
3.14	322	5,057,756	Run out	4
3.15	333	2,859,260	Yes	5
3.16	322	5,714,704	Run out	6
3.17	333	5,015,858	Run out	7
3.18	346	2,135,676	Yes	8
3.19	333	4,663,273	Yes	9
3.20	322	5,066,694	Run out	10
3.21	333	5,004,859	Run out	11
3.22	346	2,825,175	Yes	12
3.23	333	1,966,023	Yes	13
3.24	322	5,069,751	Run out	14
3.25	333	2,667,202	Yes	15

The results were then processed, in order to retrive the S-N curves in the finite life domain and the endurance limits at Run out for the three specimen sets. S-N curves, together with their upper (90% failure probability) and lower (10% failure probability) bounds at the 90% confidence level are respectively shown in Figure 33 to Figure 35 for the Sets 1, 2 and 3. These curves, plotted using a double logarithmic scale, were obtained by linear regression, as the linear model always proved to be the most suitable, according to the general linear test [47]. In the same figures, some specifications, with regard to the specimen set and its feature, the load ratio and the testing frequency, are reported. Arrows indicate the run outs.

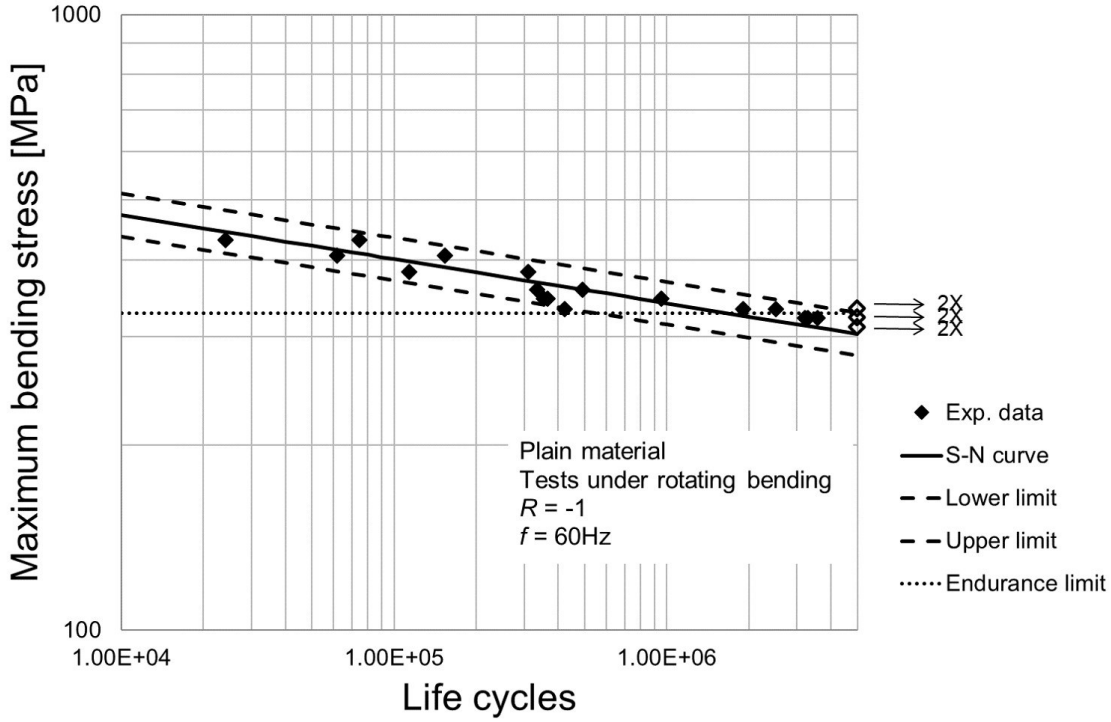

Figure 33: S-N Curve along with his confidence bands and the endurance limit at 5 million cycles for Set 1

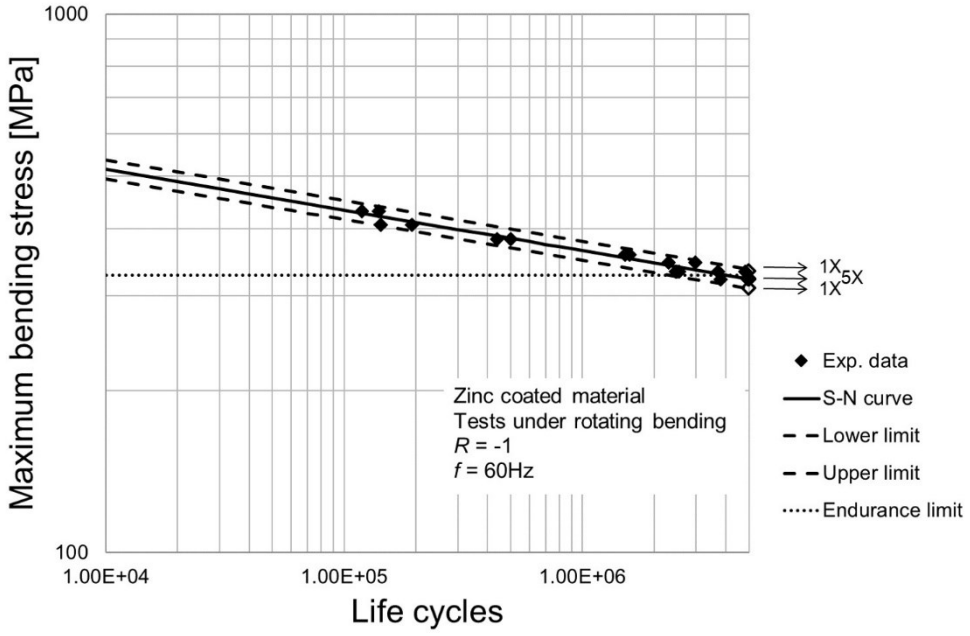

Figure 34: S-N Curve along with his confidence bands and the endurance limit at 5 million cycles for Set 2

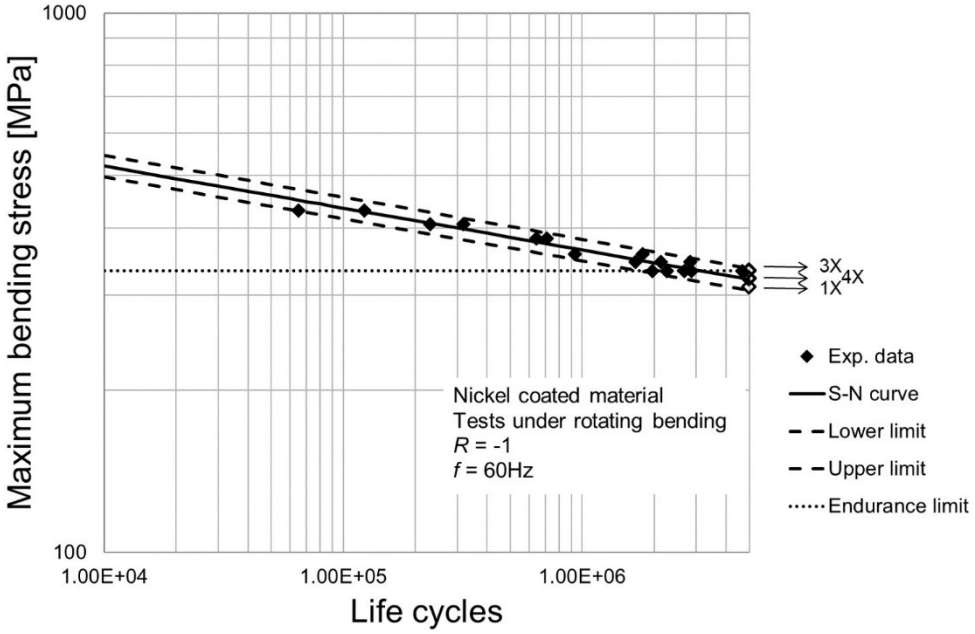

Figure 35: S-N Curve along with his confidence bands and the endurance limit at 5 million cycles for Set 3

The relevant equations are provided in Table 11, in the terms of the coefficients of the formulas in Equations 4.1 and 4.2, which refer to the (i-th) Set.

$$Log(N) = b_0 + b_1 \cdot Log(\sigma_i) = b_0 + b_1 \cdot S_i \tag{4.1}$$

$$\sigma_i = 10^{-b_0/b_1} \cdot N^{1/b_1} \quad (4.2)$$

Table 11: Coefficients of the determined S-N curves, according to the linear model of [23] with reference to Equations (4.1-4.2)

Set ID	b_0	b_1	$10^{-\frac{b_0}{b_1}}$	$\frac{1}{b_1}$
1	41.30	-13.94	915	-0.072
2	39.95	-13.26	1031	-0.075
3	38.91	-12.85	1066	-0.078

The results of the tensile tests are reported in Table 12 to Table 14..

Table 12: Tensile test results for Set 1

Specimen ID	E [GPa]	$Rp_{0.2}$ [MPa]	UTS [MPa]
1.24	183	570	614
1.25	187	600	634
1.26	190	580	614
1.27	209	570	614
1.28	208	580	614
1.29	196	570	614
Mean	195	578	617
St Dev.	11.1	11.7	8.3

Table 13: Tensile tests results for Set 2

Specimen ID	E [GPa]	$Rp_{0.2}$ [MPa]	UTS [MPa]
2.3	191	570	617
2.26	195	570	617
2.27	197	610	640
2.28	198	590	638
2.29	174	580	617
2.30	196	570	610
Mean	192	582	623
St Dev.	9.1	16.0	12.5

Table 14: Tensile tests results for Set 3

Specimen ID	E [GPa]	$Rp_{0.2}$ [MPa]	UTS [MPa]
3.26	203	600	631
3.27	204	580	628
3.28	202	590	632
3.29	203	600	632
3.30	200	590	631
Mean	203	592	631
St Dev.	1.3	8.4	1.5

Experimental stress-strain curves with regard to specimens of the three sets are depicted in Figure 36, where the graphical constructions for the estimation of the yield points is also shown.

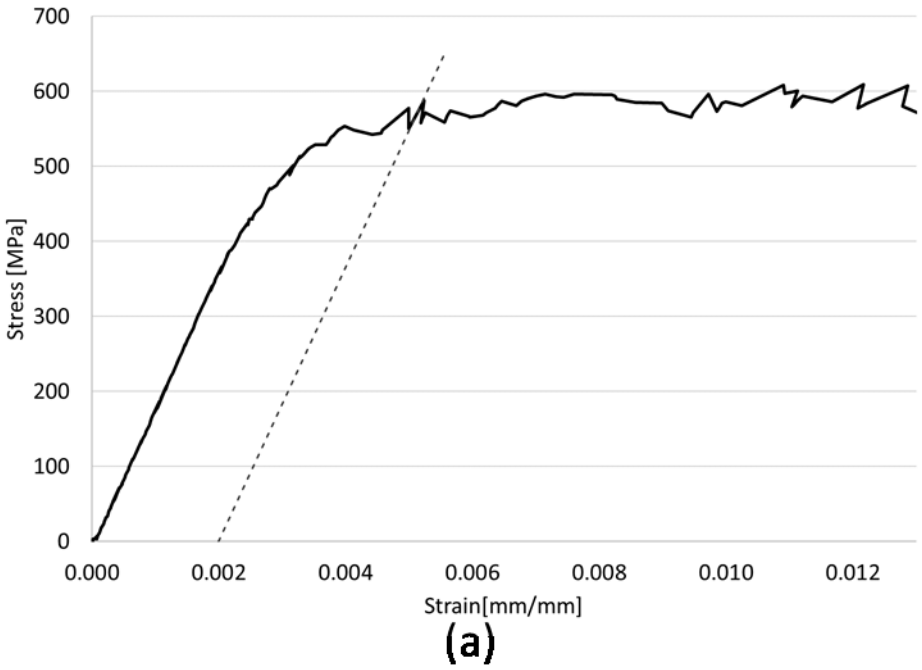

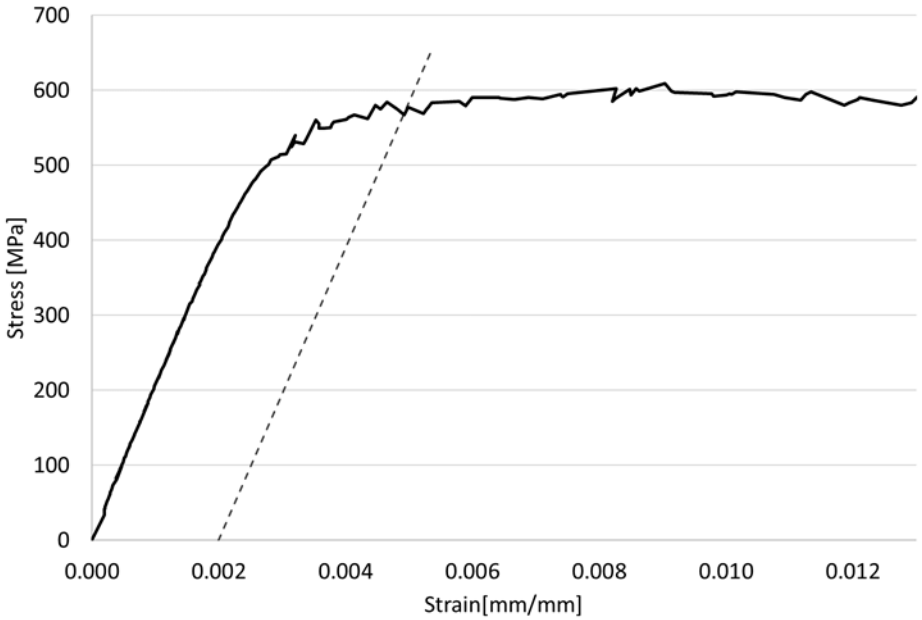

(b)

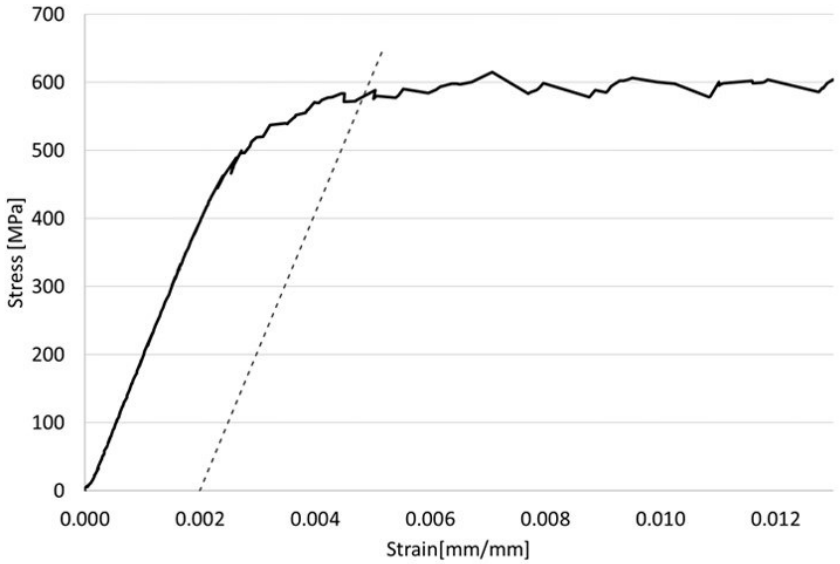

(c)

Figure 36: Stress-strain curves: (a) specimen 1.24, (b) specimen 2.26 and (c) specimen 3.27

4.1.3 Discussion

The results were processed by the statistical tools of Design of Experiment: in particular, the innovative analysis of variance (ANOVA)-based methodology introduced in [48] and successfully applied in [42,49] was used to compare the fatigue curves over the investigated life span. The Fisher test (F-test) was subsequently applied [50,51], to assess

if the coatings had a significant effect (5% significance level) on the fatigue strength of the material. The S-N curves related to the Sets 1, 2 and 3 are plotted together with the related experimental data in Figure 37.

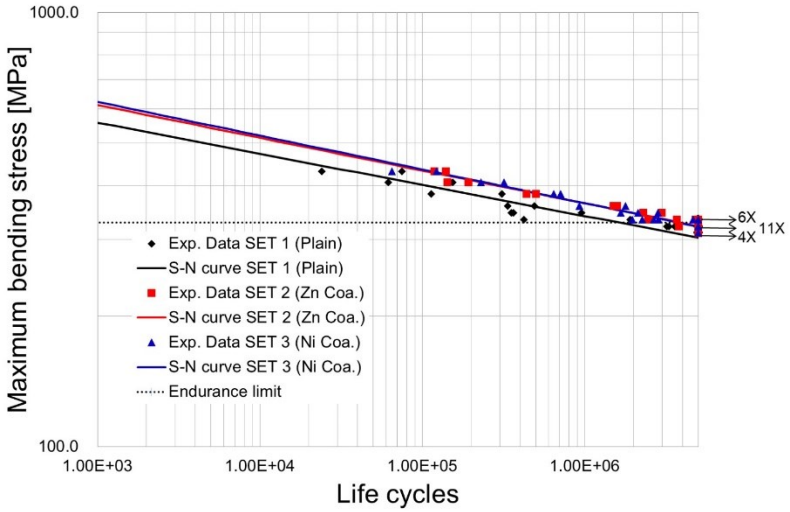

Figure 37: S-N Curves for Sets 1 to 3 plotted together with all the experimental data and the average endurance limit at 5 million cycles

One-way ANOVA, as specifically described in [42,48,49], was applied to compare the three curves (black, red and blue) corresponding to the Sets (1, 2 and 3). In particular, the different strengths in the considered lifespan, i.e. the differences among the S-N curves, were compared with respect to the experimental uncertainty. This was estimated as the sum of the squares of the residuals, corresponding to the deviations between the experimental and the predicted strengths, based on the S-N curves. The performed statistical test indicates that the differences among the three curves are not significant. In other words, it can be finally assessed that the three curves are statistically the same, as the differences are confounded by the data scattering. The further step consisted in the computation and subsequent comparison of the endurance limits at 5 million cycles, following the determination of their confidence bands. The outcome of this processing is depicted in the bar graph in Figure 38. The results are all very close with overlapped bands, which suggests the endurance limits are not significantly affected by the presence of coatings. As it can be noticed, for all sets, at an average, these limits turn out to be 53% of the general UTS. This ratio is also in agreement with the commonly accepted ratios for metallic materials.

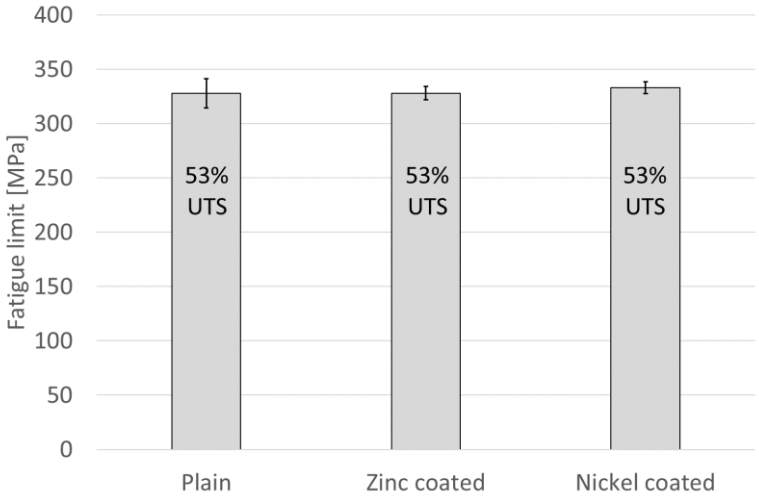

Figure 38: Endurance limits at 5 million cycles with regard to the three Sets

Moreover, the tensile test results were also statistically processed by the same tool of One-Way ANOVA. The outcome indicates that all the main features related to the static response, i.e.: the Young's modulus, the yield and the ultimate strengths are not significantly affected by coatings, consistently with the previous outcomes concerned with fatigue.

Finally, the facture surface was analyzed by the aid of a stereoscopic microscope and an optical microscope, in order to detect the fatigue crack initiation point. Some examples of fractures initiating from the surface are depicted in Figure 39 and Figure 40 with examples for each of the three Sets involved in the experimental campaign. It was found that the crack always starts from the surface for all the Set types. It can be remarked that, considering the coated specimens, i.e. Sets 2 and 3, the presence of the coating did not have a relevant role at triggering the nucleation. Indeed, the conducted surface analyses indicate that the flaws started just beneath the external coated layer, from the external surface of the steel part. This occurrence, highlighted in the detail of Figure 41, which refers to the same sample of Set 2 in Figure 39, indicates a well comparable failure mechanism with respect to that of the uncoated samples (Set 1).

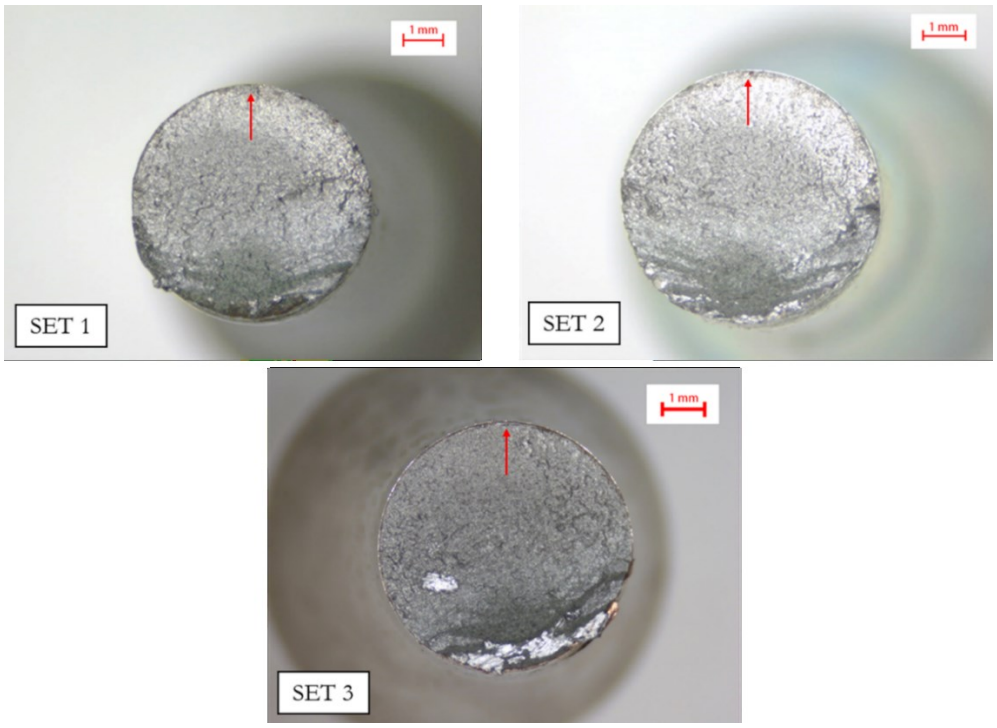

Figure 39: Fracture surfaces observed by stereoscopic microscope for the three Sets. (Set 1): specimen 1.18, 333 MPa, 2,514,009 cycles; (Set 2): specimen 2.13, 333 MPa, 2,491,952 cycles; (Set 3): specimen 3.13, 322 MPa, 1,101,409 cycles

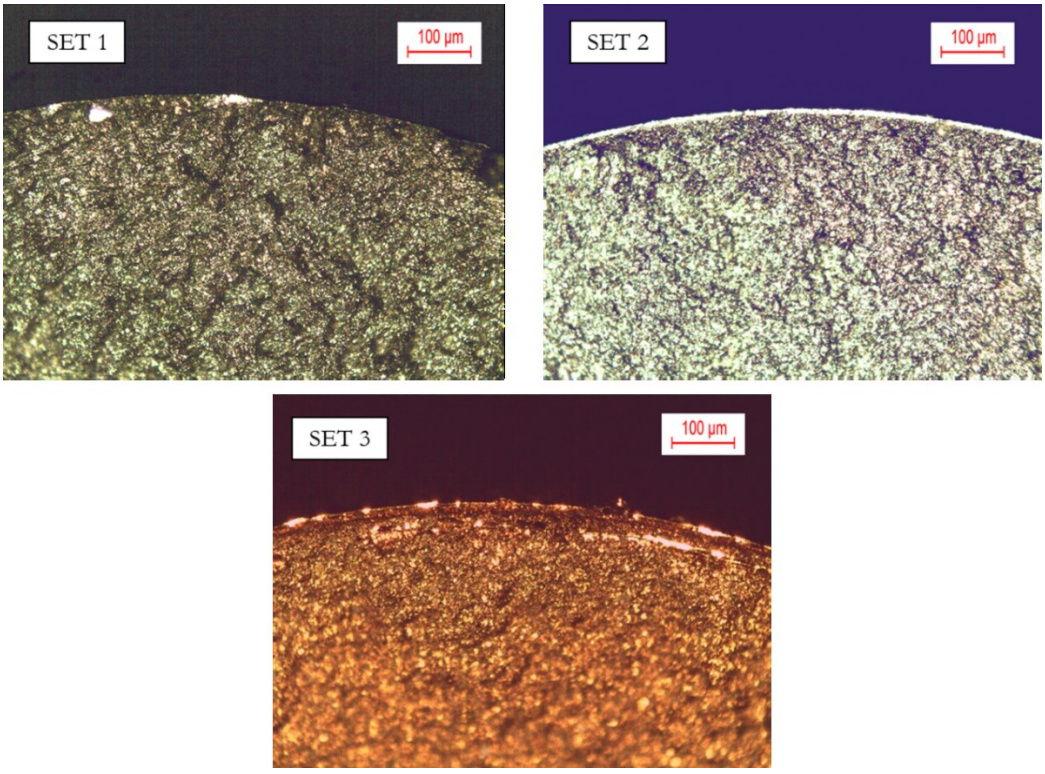

Figure 40: Fracture surfaces observed by optical microscope for the three Sets. (Set 1): specimen 1.7, 346 MPa, 365,613 cycles; (Set 2): specimen 2.8, 406 MPa, 142,735 cycles; (Set 3): specimen 3.13, 322 MPa, 1,101,409 cycles

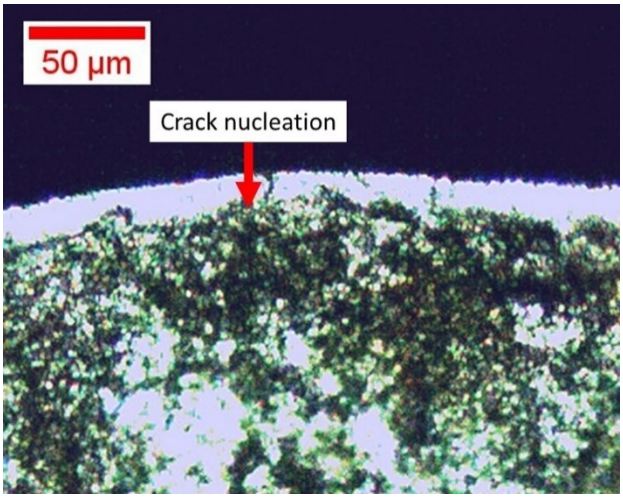

Figure 41: Fracture surface of the specimen 2.13 observed by optical microscope

4.1.4 Summary of the fatigue tests

This section dealt with the effect of coating on the fatigue strength of a free cutting steel. Three specimen sets were considered. One Set was tested in the "as received" conditions, without coatings, a second one underwent a treatment of zinc coating and a third one was nickel coated. All the experimental results were processed for the determination of the S-N curves in the finite life domain and of the endurance limits at 5 million cycles. Some specimens were utilized for tensile static tests, in order to estimate the Young's modulus, the yield strength and the ultimate tensile stress of the material. The results, statistically processed, have indicated that the differences among the three sets, in terms of fatigue strength, endurance limit and static mechanical properties, are not significant. The average endurance limit, accounting for the three specimen Sets is 53% of the corresponding ultimate tensile stress, consistently with the common accepted ratios for metallic materials. The fracture surface analyses indicate that the fatigue cracks always initiated from the specimen surfaces and that the presence of the external coating did not trigger of facilitate flaw nucleation.

As remarked in the section 4.1, the scientific literature in the field of coatings for the studied class of materials indicates these are mainly used to improve wear resistance or to protect from corrosive environment. However, there is concern they may have a detrimental effect on the fatigue response. The most interesting and original outcome of this work is that the here studied electrodeposited Zinc and Nickel coatings do not

negatively affect the fatigue response and lead conversely to well comparable results to those of the plain material. This consistency reflects also to the static properties of the material.

Therefore, these results are likely to have a great relevance, considering the possible application of coatings in the field of leaf springs, where they are mainly used to avoid fretting wear occurrence. This study ensures the fatigue response under cyclic loads is not compromised by the presence of external coatings, which makes it possible to avoid additional expensive surface treatments, such as shot-peening, to strengthen the surface. Moreover, these outcomes are expected to have a beneficial impact on the lock industry, where coatings are widely utilized to improve the tribological behavior, even in harsh environments.

Finally, considering the reported promising results for free-cutting steels: a follow-up of this research will investigate in further details the improvement from the tribological point of view the here involved coatings are able to provide.

4.2 Wear behavior of electrodeposited nickel coating on ZP5 zinc alloy [52]

Die-casting components, made of low strength materials, such as zinc alloys, are often used in the industry due to their favorable manufacturing-related features and low cost. These components must sometimes withstand cyclic loading in a corrosive environment. As explained in the European Standard 12209 [13], which deals with the standard test procedure for new lock components, these parts and devices should be tested in different conditions. In particular, this Standard defines different product grades and the related testing conditions. Each product, to be conforming to this Standard, must therefore pass different tests (e.g. durability test of the latch action with a force applied, corrosion resistance, …), aimed at assessing different features or capabilities. As explained in the previous chapters, during the durability test of the latch action, the lock must be mounted to a fixture, which is similar to a door. Afterwards, the door is opened by a force that is cyclically applied for several cycles. During this process, the components may experience a severe wear, due to the sliding between the components.

Due to process cost, the most widespread procedure adopted to improve the wear resistance is to use electrodeposited nickel coatings on zinc alloys EN 12844 [14]. Indeed, the combination of cheap materials as well of nickel coatings leads to cheaper products.

The testing procedure according to the current standard is very expensive in terms of time and costs. In order to respond to this issue, Accelerated Life Tests can be a very promising alternative to more economically assess the reliability of the product. Available methodologies and applications have been proposed by several authors [53–59].
Many studies on the wear behavior of metal coatings were run [60–62], however, few of them concern electroless nickel coatings [63–72], and, to the best of the authors' knowledge, none of them is focused on the wear behavior of electrodeposited nickel coating [15]. Therefore, the aim of this work is to determine the wear behavior of electrodeposited nickel coating on ZP5 zinc alloy, assessing the influence of coating thickness and applied load.

4.2.1 Materials and Methods

In the lock component under investigation, the latch is initially engaged in the strike plate. Rotating the latch lever, it is possible to retract the latch rod. This component, bonded on the latch, makes it possible to disengage the latch from the strike plate. The analyzed test is focused on the latch durability under an applied load. As explained in the second chapter, according to Standard [13], the testing procedure consists of different stages (Figure 7): i- applying a force F3 equal to 120 N on the door; ii- opening the door by the force F10; iii- closing the door. The minimum test duration is $2 \cdot 10^5$ cycles at a maximum frequency of 10 cycles per minute. Since the wear mechanism occurs in the contact and repeated sliding between the latch (made in ZP5 EN 12844 [14] Zn/Cu1Ni5s ISO 1458 [15]) and the forend (made in AISI 304 [18]), the wear behavior in an interaction between these materials has been analyzed.
Laboratory tests were carried out by a slider-on-cylinder tribometer [73] (block-on-ring contact geometry, according to ASTM G77 Standard [74]), in the unlubricated condition and at ambient conditions (room temperature and humidity). The test scheme, according to the aforementioned standard is shown in Figure 42. The test parameters were chosen in order to simulate the actual test condition.

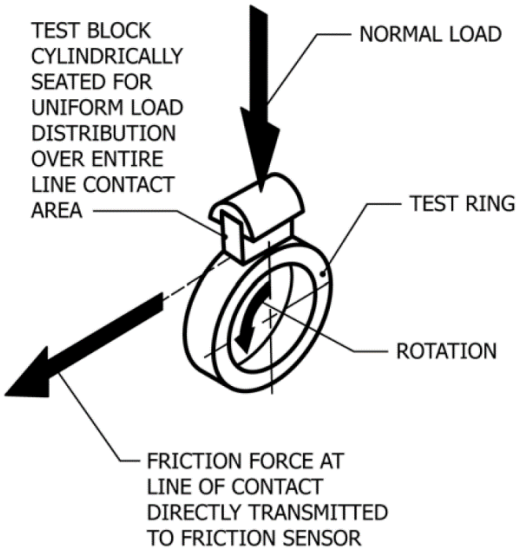

Figure 42: Block on ring wear tests [74]

In the slider on cylinder wear test (Figure 43), the slider represents the static element, while the cylinder is the rotating one. Sliders were obtained directly from the actual components (as shown in Figure 44): using a micro cutting machine, some 5x5x21 mm^3 specimens were extracted from each latch. This component is made of ZP5 die-casting alloy and treated by the electrodeposited nickel coating Zn/Cu1Ni5s ISO 1458 [15]. This process provides a first layer of pure copper with a minimum thickness of 1 μm and a subsequent layer of pure nickel coating with a minimum thickness of 5 μm. In order to perform the test, the 5x5x21 mm^3 specimens were fixed in a sample holder. As counter material, a rotating AISI 304 cylinder with 40 mm diameter was used.

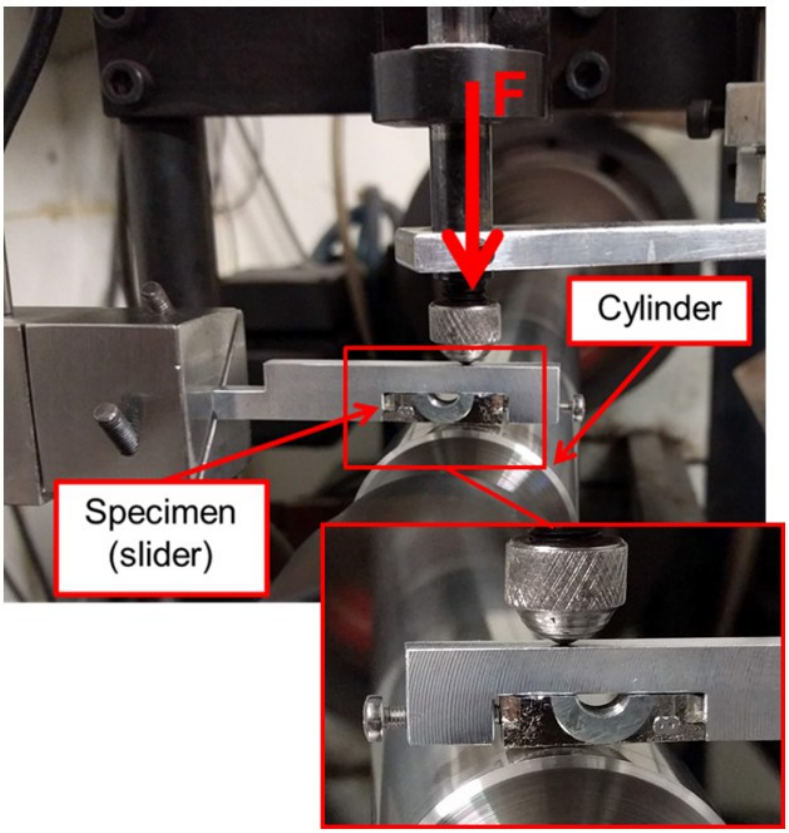

Figure 43: Slider on cylinder wear test

The hardness of the coating, experimentally evaluated by a micro-indentation test, was 430 HV 0.01. The hardness of the cylinder was evaluated by a Rockwell indentation test and was estimated as 29 HRC. Moreover, the cylinder roughness (Ra) was equal to 0.2 µm whereas the slider roughness (Ra) was equal to 0.7 µm. The electrodeposition process is known to provide a variable coating thickness on the components [75], as it is hard to accurately control its actual extent during the manufacturing process. Indeed, as indicated in the Standard [15] just the minimum coating thickness should be prescribed. The actual coating thickness was measured (for each specimen) on a metallographic section using an optical microscope (as shown in Figure 45). Five measurements per specimen were done, thus determining the average values. The specimens were split into 3 groups, depending on the total coating thickness (LOW coating thickness: 5-10 µm; MEDIUM coating thickness: 10-15 µm; HIGH coating thickness: 15-20 µm; Table 15).

Table 15: Measured coating thickness.

Group	Specimen ID	Cu thickness	Ni thickness	Total coating thickness
Low	2	4.4	5.0	9.4
	6	3.8	6.1	9.9
	7	4.1	5.7	9.8
Medium	9	3.7	7.4	11.1
	5	4.2	10.5	14.7
	3	4.5	7.9	12.4
High	1	7.8	8.9	16.7
	4	5.5	13.3	18.8
	8	7.1	10.2	17.3

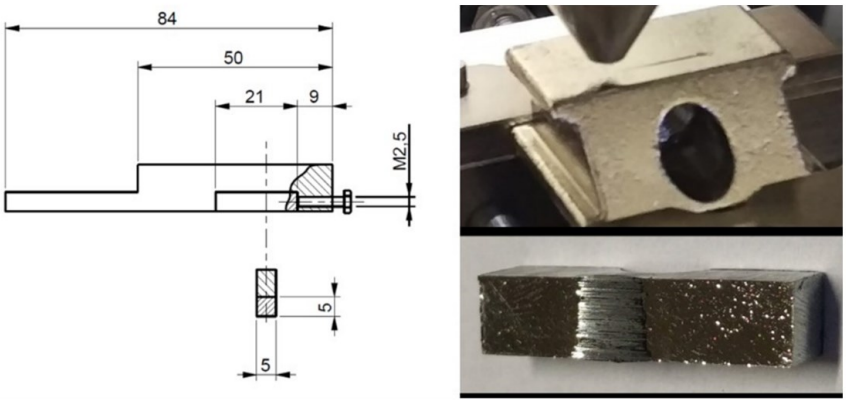

Figure 44: Static specimen (slider)

The sliding tests were carried out by applying a vertical force on the slider. Tre different levels of force (5 N, 10 N and 15 N) were used during the test, in order to investigate the effect of contact pressure on the wear resistance of the coating. In particular, specimens 1, 2, and 3 were tested using 5 N of applied force, specimens 4, 5 and 6 were tested at 10 N whereas specimens 7, 8 and 9 were tested at 15 N. Moreover, in order to determine how the wear resistance is affected by the aforementioned factors, with a sufficient statistical evidence, the tests were replicated. In total, three replications per combination of coating thickness and applied load (contact pressure) were performed. On a single

specimen three tests were made considering three different locations. A total of twenty-seven wear test were made on nine specimens as indicated in Table 16.

The sliding velocity was set at 0.3 m/s (143,3 rpm) and the total distance was set at 500 m for each test. This distance was selected, in order to replicate the total actual sliding distance of the durability test of the latch action with a force applied for the maximum grade (Grade X: 200,000 cycles). The Standard, indeed, provide different product grades and for which one provide a different test duration. During the test normal load, friction force and vertical displacement were constantly monitored by bending load cells and a linear variable displacement transducer (LVDT) respectively. The LVDT provides an output signal being related to a combination of the wear of both the slider and the cylinder. With the aim to determinate the contribution of the slider alone, profilometric measurements of wear tracks were carried out at the end of each test by stylus profilometry (tip with a 5 μm curvature radius): for each track, three measurements were made. Finally, wear tracks on the sliders were observed by means of a 3D digital microscope.

Table 16: Design of the experiment

		COATING THICKNESS [μm]		
		5-10	10-15	15-20
APPLIED FORCE [N]	5	Specimen 2	Specimen 3	Specimen 1
	10	Specimen 6	Specimen 5	Specimen 4
	15	Specimen 7	Specimen 9	Specimen 8

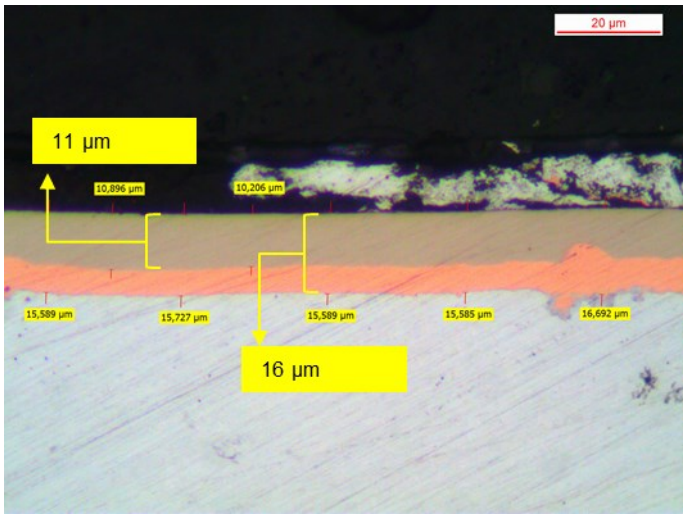

Figure 45: Metallographic section: coating thickness analysis (fresh specimen)

According to [74] the wear volume loss was evaluated by Equation 4.3:

$$Sr = \frac{4 \cdot r^2 \cdot t}{8} \cdot \left[2\sin^{-1}\frac{b}{2r} - \sin\left(2\sin^{-1}\frac{b}{2r} \right) \right] \tag{4.3}$$

where r represents the cylinder radius, t is the specimen width, and b is the track width as indicated in Figure 46.

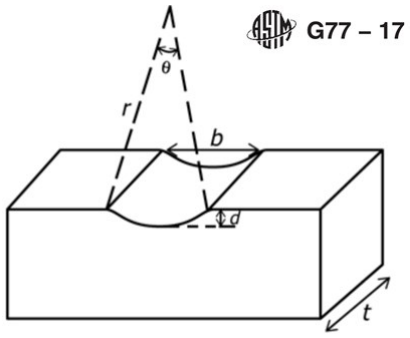

Figure 46: Evaluation of the scar volume according to ASTM G77-17 [74]

4.2.2 Results

During the tests, the applied force, the tangential force and the LVDT output signal were sampled. Such procedure made it possible to investigate the evolution of the friction coefficient throughout a test. Typical trends of friction coefficient and of system wear

versus distance are shown in Figure 47. An abrupt transition, in terms of friction coefficient, was generally retrieved after 70-150 m. At the same distance, the system wear also significantly increases. There is a second phase where the fiction coefficient increase (after 300-350 m) while the system wear remains constant. This particular behavior could be related with the material transfer between the mating surfaces that does not allow to produce wear debris.

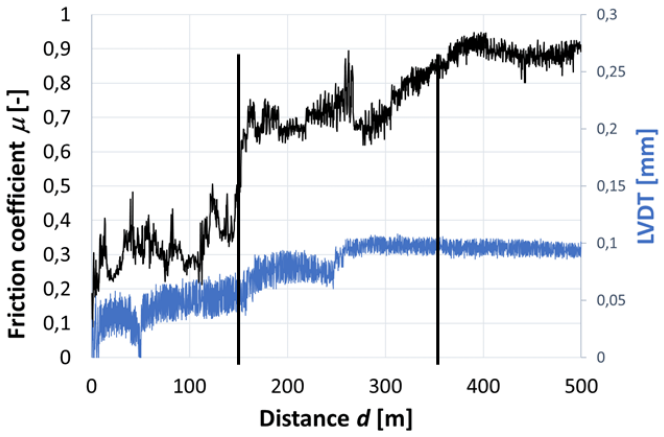

Figure 47: Friction coefficient and system wear trends during the slider on cylinder tests (specimen 7, test 1)

As for the wear tracks, the mean values of the three measurements of track widths are reported in Table 17.

Table 17: Wear track measurements

Load [N]	Specimen ID	Wear track	Width [mm]
5	1	1	2.499
		2	2.174
		3	2.175
	2	1	2.675
		2	1.748
		3	2.350
	3	1	2.878
		2	2.149
		3	2.025
10	4	1	2.938
		2	3.088
		3	3.208
	5	1	3.151
		2	2.670
		3	3.117
	6	1	3.519
		2	3.123
		3	3.262
15	7	1	4.143
		2	3.904
		3	3.537
	8	1	3.904
		2	3.928
		3	3.867
	9	1	3.965
		2	3.927
		3	4.239

In Figure 48 shows some representative 3D digital micrographs of wear tracks, taken on high coating thickness sliders: a severe wear regime may be recognized. It can be noticed that both the nickel coating and copper interlayer have been removed upon sliding, confirming the results of the profilometric investigations. Under both load levels, the substrate is clearly visible at the center of the wear tracks while, at the edges, a few debris of the copper interlayer can be detected.

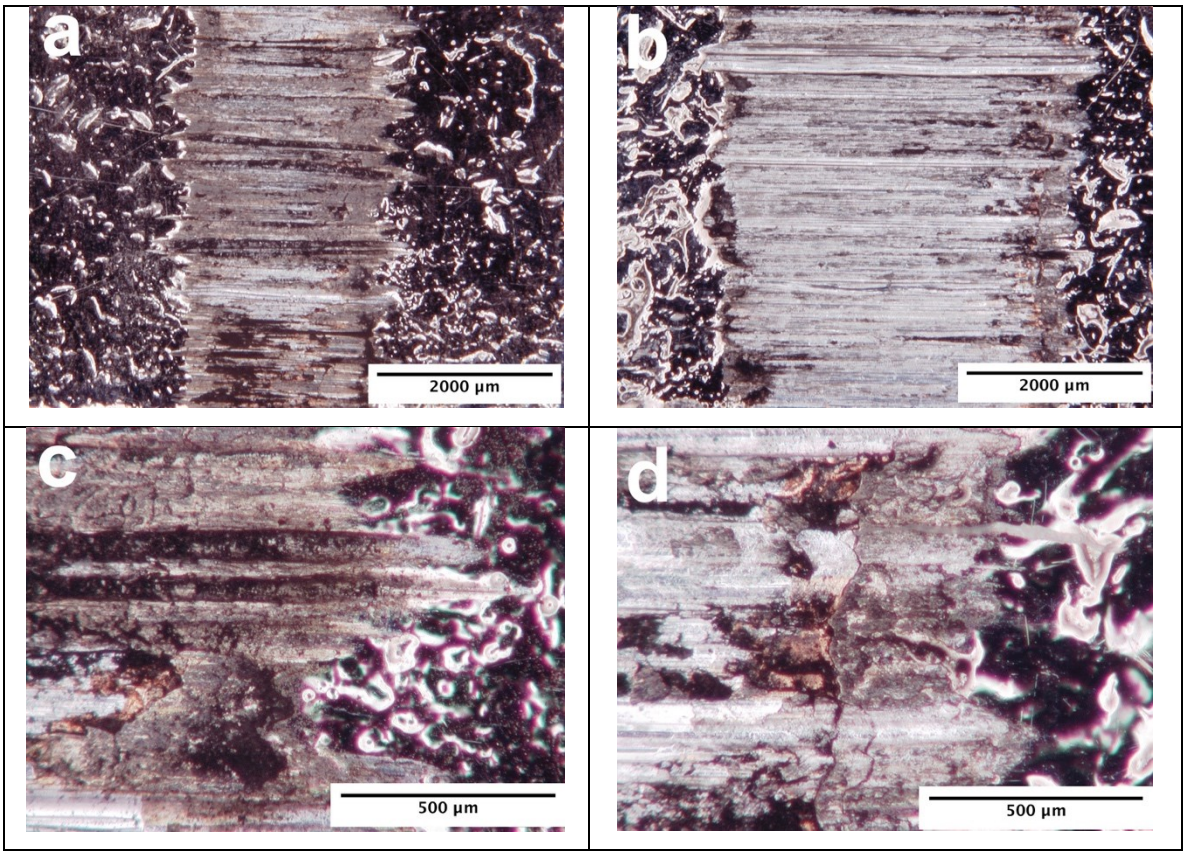

Figure 48: 3D digital micrographs of wear tracks on sliders: a) and b) low magnifications of tracks on specimen 1 and 8 respectively, c) and d) high magnifications of tracks edges on specimen 1 and 8 respectively

4.2.3 Discussion

Based on the test outputs it can be pointed out that there is a transition, in terms of friction coefficient, after 100-150 m of total travel. This outcome suggests that the entire coating thickness was worn out completely at this stage. Indeed, this transition can be due to the change of the tribological state of the contact. Initially, there is a contact between the AISI 304 bar and the nickel coating. After the aforementioned distance, , as an effect of wearing of the coating, the contact involves the base material (ZP5), thus producing the aforementioned abrupt variation of the friction coefficient. Moreover, focusing on the LVDT, it can be noticed that the transition of the friction coefficient can be related to a suddenly increase of the system wear.

After the tests, all the wear tracks were measured in order to calculate the volume loss. Using the results reported in Table 17 and Equation 4.3 it was possible to obtain the scar

volume reported in Table 18. The same results are compared in Figure 49 in the form of a bar graph with the indication of the scatter bands from maximum to minimum measured values.

In order to detect the impact of each factor on the wear volume loss, these results were treated by the statistical tools of two-way ANOVA and Fisher test. These tools make it possible to assess if the factors involved in the experimental tests have a significant effect on the wear volume loss.

The outcome of the performed analysis indicate that wear is strongly affected by the applied load (p-value=$2.4 \cdot 10^{-8}$). Furthermore, there is no significant effect of the coating thickness on the wear volume loss. This outcome, as mentioned before, suggests that the coating thickness is worn out completely during the first stages of the test. Finally, no significant interactions were found between applied load and coating thickness.

Table 18: Scar volume loss after 500 m evaluated with the Equation 4.3

Specimen ID	Wear track	*Sr* [mm^3]
1	1	0.3253
	2	0.2143
	3	0.2144
2	1	0.3991
	2	0.1113
	3	0.2705
3	1	0.4974
	2	0.2068
	3	0.1730
4	1	0.5292
	2	0.6156
	3	0.6898
5	1	0.6530
	2	0.5484
	3	0.6324
6	1	0.9100
	2	0.6354
	3	0.7242
7	1	1.4863
	2	1.2427
	3	0.9236
8	1	1.2427

	2	1.2663
	3	1.2076
	1	1.3020
9	2	1.2648
	3	1.5917

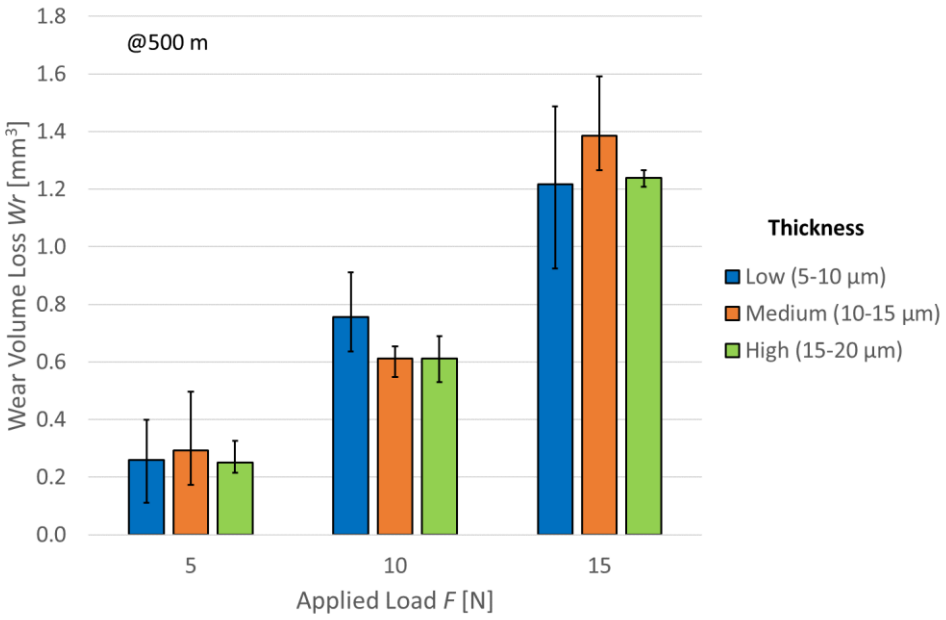

Figure 49: Wear volume loss after 500 m on the slider on cylinder test

4.2.4 Further experimental tests at reduced distance

In order to evaluate a possible effect of the coating thickness on the wear behavior of the nickel coating, further experimental tests were carried out. Focusing on the outcomes of the aforementioned experimental tests it was decided to repeat the slider on cylinder wear tests using a reduced sliding distance of 150 m corresponding to the sliding distance until the transition between the two friction coefficient levels. Also in this case, three different levels for the applied load (5 N, 10 N and 15 N) and three different levels for the coating thickness (LOW coating thickness: 5-10 µm; MEDIUM coating thickness: 10-15 µm; HIGH coating thickness: 15-20 µm) were analyzed. The coating thicknesses of the tested specimens are reported in Table 19. However, in this case, a total of six replicates for

each condition were made. The wear volume loss Sr (reported in Table 20) was still evaluated by the Equation 4.3.

Table 19: Measured coating thickness for specimens used in the "reduced-distance tests"

Group	Specimen ID	Cu thickness	Ni thickness	Total coating thickness
Low	16	4.3	5.5	9.8
	19	4.1	5.6	9.7
	17	3.8	6.1	9.9
Medium	14	4.1	9	13.1
	10	4.3	10.3	14.6
	26	3.9	10.1	14.0
High	20	6.5	12.9	19.4
	22	4.8	15.1	19.9
	15	6.2	12.7	18.9

Table 20: Wear track width and wear volume loss after 150 m evaluated with Equation 4.3

Specimen ID	Wear track	Width [mm]	*Sr* [mm^3]
10	1	2.219	0.2278
	2	2.381	0.2815
	3	2.555	0.3477
	4	2.543	0.3430
	5	2.307	0.2561
	6	2.827	0.4714
14	1	1.880	0.1384
	2	1.893	0.1413
	3	1.846	0.1310
	4	1.865	0.1351
	5	1.358	0.0521
	6	1.615	0.0877
15	1	2.747	0.4325
	2	2.564	0.3516
	3	2.604	0.3683
	4	2.732	0.4252
	5	2.242	0.2350
	6	2.606	0.3692

17	1	2.862	0.4889
	2	2.682	0.4025
	3	2.648	0.3873
	4	2.574	0.3555
	5	2.598	0.3658
	6	2.582	0.3589
19	1	2.541	0.3422
	2	2.574	0.3555
	3	2.698	0.4095
	4	2.391	0.2849
	5	2.244	0.2356
	6	2.364	0.2755
20	1	2.089	0.1899
	2	1.516	0.0725
	3	2.032	0.1749
	4	1.674	0.0977
	5	1.933	0.1506
	6	2.071	0.1851
22	1	2.419	0.2952
	2	2.326	0.2623
	3	2.831	0.4734
	4	2.255	0.2391
	5	2.345	0.2688
	6	2.467	0.3130
26	1	2.848	0.4820
	2	2.722	0.4208
	3	2.814	0.4647
	4	2.998	0.5620
	5	2.730	0.4242
	6	3.094	0.6182

The two-way ANOVA and F-Test were then used in order to determine the influence of each factor on the nickel coating wear behavior. Again, the contact pressure proved to be the only factor affecting the wear volume lost (p-value $3 \cdot 10^{-17}$). Moreover, it was assessed that there is a low interaction between the applied load and the coating thickness (p-value $2 \cdot 10^{-2}$). In Figure 50 the results obtained during the tests are reported in form of bar graph with the related error bands. Is simple to see that the wear volume is affected simply by the applied load.

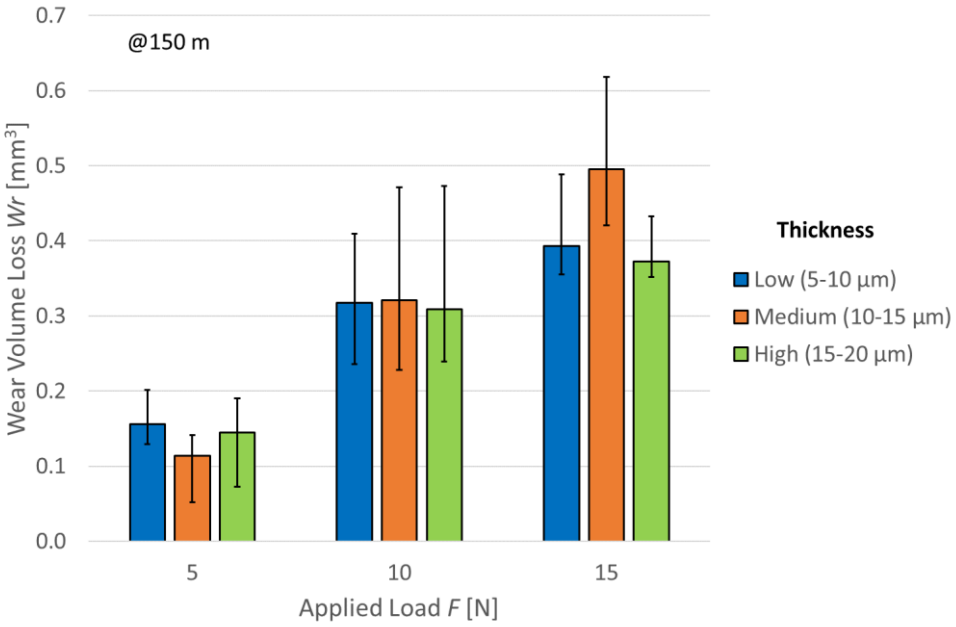

Figure 50: Wear volume loss after 150 m on the slider on cylinder test

4.2.5 Summary of the wear tests

The wear behavior of an electrodeposited nickel coating on a zinc alloy was analyzed. The specimens were obtained directly from the actual component used in a lock application. According to the ASTM G77-17 Standard [74], a 5x5x23 mm^3 bars were machined. Since in the actual application, wear occurs between the electrodeposited nickel coating and an AISI 304 steel component, slider on cylinder wear tests were run, using an AISI 304 cylindric geometry as the rotating element.

The specimens were prepared by the aid of a metallographic section, in order to determine the actually generated coating thickness of the single specimen. So, the specimens were split into three groups, depending of their uniform coating thickness. The wear tests were run, with three different load levels.

It was assessed that there is a transition in terms of friction coefficient during the first stage of test. This outcome indicates that the entire coating thickness was worn out at this stage. The total wear volume that was lost after 500 m was evaluated according to the American Standard [74]. In order to evaluate the significance of the effects of the applied

load and coating thickness on the wear of the tribological system, the wear volume results were treated by statistical tools, in particular two-way ANOVA and F-test.

It was assessed that the applied load has a strong influence on the wear behavior of the electrodeposited nickel coating. Conversely, the coating thickness does not significantly affect the wear. This outcome also suggests that the whole coating is completely worn out at the first stage of the test. Finally, it was assessed that the interaction between the applied load and the coating thickness is not significant, meaning that load keeps its significance regardless of coating thickness in the investigated range.

Focusing on the aforementioned wear tests results it was decided to carry out further analyses at a reduced sliding distance of 150 m.

It was assessed that, the total volume lost after the wear tests, is strongly affected by the applied load and there is a low interaction between the two factors. Finally, it was stated that there is no significant effect of the coating thickness on the wear rate.

5. ANALYTICAL MODEL

As explained in the second chapter, in order to set up an accelerated life testing (Figure 51, it is mandatory to know the stress-strain field of the components involved in the test as well as the stress-life curves of the materials. It is also necessary to evaluate every possible source of nonlinearities.

In chapter 3, the FEAs that have been developed in order to define the stress field, in terms of bending stresses (that brings until the fatigue failure of the components) and contact pressures (that influence the wear rate of the material), have been presented. Indeed, in order to accelerate the test, it is necessary to increase the load applied on the device. This means that the components are therefore subjected to stresses that are not necessarily linearly dependent on the applied load.

In chapter 4, the experimental tests were presented in order to define the fatigue behavior of the 11 SMnPb 30 free cutting steel and the wear behavior of the electrodeposited nickel coating on a zinc alloy. It was assessed that the fatigue behavior of the free cutting steel is not influenced by the coatings. Moreover, the wear behavior of the nickel coating was proven to be affected just by the applied load (see chapter 5).

In this chapter, the analytical model able to predict the actual service life of the lock components, written in the software Wolfram Mathematica, is eventually discussed.

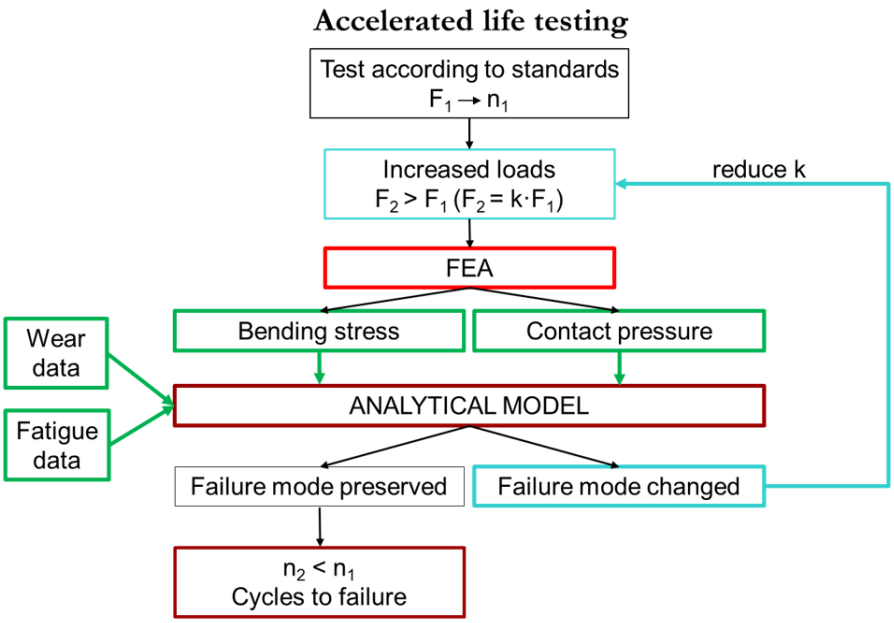

Figure 51: Accelerated life testing flowchart. A method applied to a case of study

5.1 Fatigue characterization

Since it is necessary to represent the fatigue behavior of the materials involved in the accelerated life testing, the data presented in section 4.1 were used to describe the fatigue curve of the free cutting steel 11 SMnPb 30. Moreover, the fatigue data reported in [22] were used to describe the fatigue curve of the S420MC. The stress-life curve of the materials, indeed, can be described by Equations 5.1 and 5.2 reported here below for the sake of clarity.

$$Log(N) = b_0 + b_1 \cdot Log(\sigma_i) = b_0 + b_1 \cdot S_i \tag{5.1}$$

$$\sigma_i = 10^{-b_0/b_1} \cdot N^{1/b_1} \tag{5.2}$$

Regarding the free cutting steel, the coefficients b_0=41.3 and b_1= -13.94 were chosen from Table 11 for the uncoated material type. This choice was made because the validation test (which will be used later to assess the accuracy of the analytical model) has been carried out using a latch rod without any coating. The fatigue curve of this material is shown in Figure 52 in double-logarithmic scale.

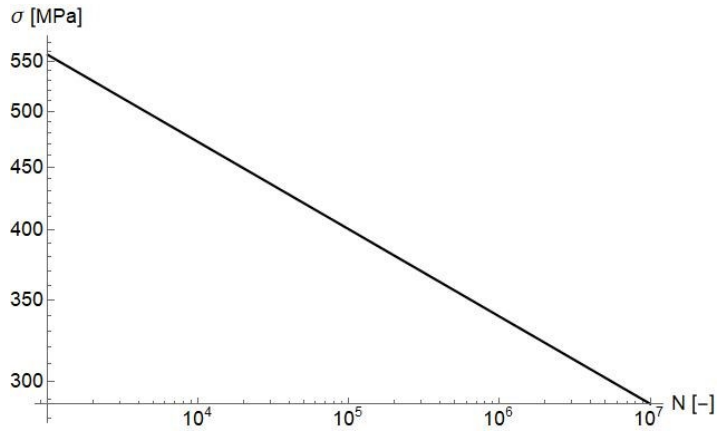

Figure 52: Free cutting steel 11 SMnPb 30 fatigue curve

Regarding the S420MC steel, the aforementioned analysis was carried out. In order to describe its fatigue curve, the coefficients b_0=25.15 and b_1= -8.16 were used [22] and the relative plot is reported in Figure 53 in double-logarithmic scale.

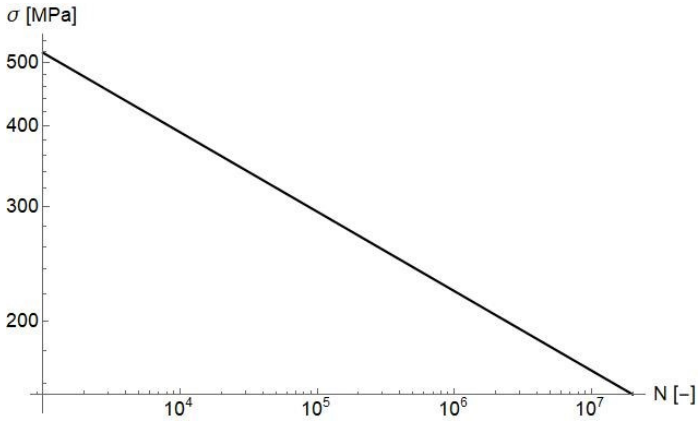

Figure 53: S420MC steel fatigue curve

5.2 Wear characterization

The wear behavior analytical analysis was carried out focusing on the results presented in the section 4.2. It was assessed that the applied load is the only factor affecting the wear rate, that was therefore modeled focusing just on this parameter. During the experimental tests, the applied load (F) produce a certain contact pressure $p_0(F)$, that can be evaluated, according to the Hertz's theory [76], by the Equations 5.3 and 5.4

$$a = \sqrt{\frac{4 \cdot F \cdot R}{\pi \cdot E^*}} \tag{5.3}$$

$$p_0(F) = \frac{2 \cdot F}{\pi \cdot a} = \sqrt{\frac{F \cdot E^*}{\pi \cdot R}} \tag{5.4}$$

where a represents the semi contact width, F the applied load R the radius of the cylinder bar. The equivalent elastic modulus E* can be expressed by equation 5.5 as follows:

$$E^* = \frac{1}{\frac{1-\nu_1^2}{E_1} + \frac{1-\nu_2^2}{E_2}} \tag{5.5}$$

where E represent the Young's modulus of the materials and ν the Poisson's ratio of the materials involved in the experimental tests. The Hertz's theory is not fully applicable in this case, but still keeps the best method, according to standard practice, to evaluate the actual contact pressure during the test. However, there is indeed an issue being related to

the accurate evaluation of the actual contact area during the test. The standard practice is to evaluate the contact pressure using the Hertz's theory. In particular, regarding the AISI 304 bar $E = 195GPa$ [77] and $\nu = 0.3$ were used whereas for the electrodeposited nickel coating $E = 205GPa$ [78] and $\nu = 0.31$.

After the slider on cylinder wear test, all the wear tracks were measured as explained in section 4.2. It was therefore possible to evaluate the wear volume loss using Equation 4.3. Since wear is affected just by the applied load, the wear volume loss was evaluated grouping the results based on the applied load. The experimental results are reported in Table 21.

Table 21: Experimental wear test results

Applied Load [N]	5	10	15
Contact pressure [MPa]	66.2	93.6	114.7
Wear volume lost after 500 m [mm^3]	0.268	0.660	1.281
Standard deviation (500 m) [mm^3]	0.121	0.112	0.186
Wear volume lost after 150 m [mm^3]	0.138	0.316	0.420
Standard deviation (150 m) [mm^3]	0.041	0.075	0.077

The wear rate was obtained by simply dividing the wear volume by the total sliding distance. The data were fitted using a 4th-order function as shown in Equation 5.6.

$$Wr(p_0) = 1.571 \cdot 10^{-5} \cdot p_0 - 3.513 \cdot 10^{-7} \cdot p_0^{\,2} + 3.56642 \cdot 10^{-9} \cdot p_0^{\,3} \qquad (5.6)$$

In Figure 54 the wear rate graph is reported as a function of the contact pressure.

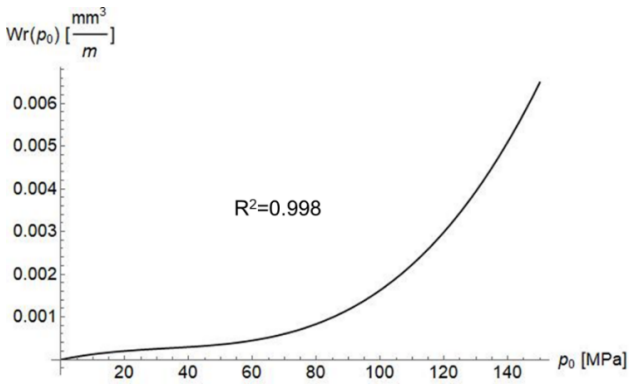

Figure 54: Wear rate as a function of the contact pressure

Focusing on the slider on cylinder outputs (Figure 47) it was assessed that there is a first transition in terms of friction coefficient after 150 m (from 0.3 to 0.7) and a second one after 350 m (from 0.7 to 0.9). It was therefore evaluated the critical volume that brings to these transitions. For the sake of synthesis all the measurements are not reported here. It was assessed that the critical volume at the first transition stage is equal to $W_{Cr\_1} = 0.47\ mm^3$ whereas the second critical volume (second transition) is equal to $W_{Cr\_2} = 1.11\ mm^3$.

It is therefore possible to describe the friction coefficient as a function of the wear volume loss as shown in Figure 55.

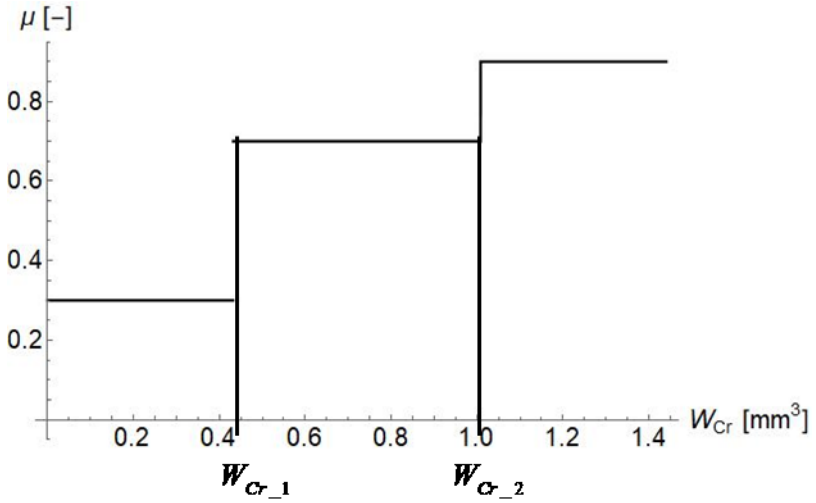

Figure 55: Friction coefficient as a function of the wear volume loss

Combining the wear rate results with the critical volume it is possible to evaluate how many cycles are necessary to have the first transition (or the second as well) of the friction coefficient on the latch.

5.3 Stress characterization

As explained in the third chapter too, the friction coefficient on the latch introduces a nonconstant maximum stress on the component involved in the opening chain. For this reason, several FEA were carried out in order to determine the stresses on the locking device parts. In particular, three different loads were considered for the durability test: 120 N (standard test), 180 N and 240 N and three different levels for the friction

coefficient, namely 0.3, 0.7, 0.9. The FEA outputs were used to obtain the bending stresses as a function of the applied load for the aforementioned friction coefficient. The fitting law was chosen linear and in Equation 5.7, the three formulas represent the curve of the maximum contact pressure at the latch ($p\_latch_{(F3)}$) as functions of the applied load F3

$$\begin{aligned} p\_latch(F3)_{\mu=0.3} &= -5.914 + 1.111 \cdot F3 \\ p\_latch(F3)_{\mu=0.7} &= -2.571 + 1.186 \cdot F3 \\ p\_latch(F3)_{\mu=0.9} &= -0.857 + 1.229 \cdot F3 \end{aligned} \tag{5.7}$$

In Equations 5.8 and 5.9, are reported the relative curves of the maximum bending stress on the latch rod and on the latch lever respectively, for the three different friction coefficients. In this case also, the contacts do not introduce any nonlinearities on the stresses, so a linear law was used.

$$\begin{aligned} \sigma\_latch\_rod(F3)_{\mu=0.3} &= 29.543 + 1.389 \cdot F3 \\ \sigma\_latch\_rod(F3)_{\mu=0.7} &= 33.114 + 1.553 \cdot F3 \\ \sigma\_latch\_rod(F3)_{\mu=0.9} &= 35.257 + 1.665 \cdot F3 \end{aligned} \tag{5.8}$$

$$\begin{aligned} \sigma\_latch\_lever(F3)_{\mu=0.3} &= 0.171 + 1.604 \cdot F3 \\ \sigma\_latch\_lever(F3)_{\mu=0.7} &= 1.171 + 1.671 \cdot F3 \\ \sigma\_latch\_lever(F3)_{\mu=0.9} &= 0.829 + 1.729 \cdot F3 \end{aligned} \tag{5.9}$$

In this case also, the contacts no introduce nonlinearities on the stresses, so a linear law was used.

The force versus pressure and stresses curves are reported in Figure 56

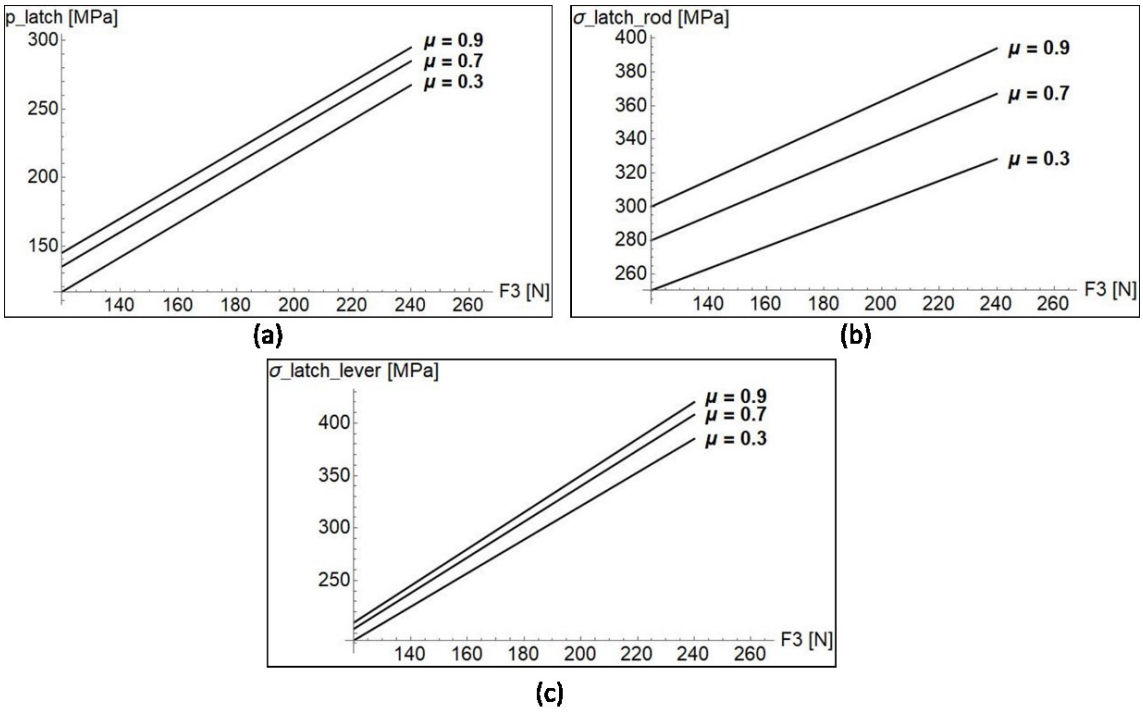

Figure 56: FEA results as a function of the friction coefficient and of the applied force: a) maximum contact pressure on the latch, b) maximum bending stress on the latch rod, c) maximum bending stress on the latch lever

5.4 Predictive analytical model

In order to evaluate the actual service life of the device, during the accelerated test, it is necessary to develop an analytical model taking as an input the experimental data and the FEA results, and capable of giving in output the number of cycles to failure of the components. As explained before, due to the contact pressure on the latch, wear introduces a source of nonlinearity. During the opening phase, indeed, there is a transition in terms of friction coefficient between the latch and the forend and the strike plate. This transition introduces a stress increment on the components that are downstream the opening mechanism.

It is important to point out that (almost always) the latch failure mechanism is wear, whereas the latch rod and the latch lever often fail because of fatigue.

The critical wear volumes, up to the transition of the friction coefficient, were analyzed and used to determine the actual number of cycles at each stress condition. Using a cumulative damage model (Miner's rule), it is then possible to predict the number of cycles up to fatigue failure of each component.

From Equation 5.6, it is possible to evaluate the wear rate as a function of the applied load and therefore of the contact pressure. The Equations 5.10 allow then to evaluate the actual number of cycles up to the transitions of the friction coefficient.

$$n_{Cr\_1}(p\_latch(F3)) = \frac{W_{Cr\_1}}{Wr(p\_latch(F3)) \cdot L_{track}}$$
$$n_{Cr\_2}(p\_latch(F3)) = \frac{W_{Cr\_2} - W_{Cr\_1}}{Wr(p\_latch(F3)) \cdot L_{track}} \quad (5.10)$$

Where $n_{Cr\_1}(p_0)$ represent the number of cycles to the first transition, $n_{Cr\_2}(p_0)$ the number of cycles to the second transition, and L_{track} represent the total sliding length on the latch during the accelerated test (equal to 3 mm in the case study). The number of cycles at each friction coefficient depends on the contact pressure that depends on the applied force. Therefore, the number of cycles $n_{Cr\_1}(p_0)$ and $n_{Cr\_2}(p_0)$ depend on the applied load.

Using the Miner's rule (reported in Equation 5.11), it is therefore possible to evaluate the actual number of cycles up to failure for each component involved in the accelerated test.

$$\sum_i \frac{n_i}{N_i} = 1 \quad (5.11)$$

Where *n* represents the actual number of cycles at a determined stress and *N* is the number of cycles up to fatigue failure at the same stress value.

In the case study, there are three stress levels corresponding to three friction coefficients. The Miner's rule can be written as follows (Equation 5.12) for the latch lever:

$$\frac{n_{Cr\_1}(p\_latch(F3))}{N(\sigma\_latch\_lever(F3)_{\mu=0.3})} + \frac{n_{Cr\_2}(p\_latch(F3))}{N(\sigma\_latch\_lever(F3)_{\mu=0.7})} + \\ + \frac{n_{latch\_lever}(p\_latch(F3))}{N(\sigma\_latch\_lever(F3)_{\mu=0.3})} = 1 \quad (5.12)$$

Solving the equation, it is therefore possible to obtain the number of cycles to failure of the latch lever that, for the sake of synthesis, will not be reported here. In Figure 57, the stress life curve obtained by solving Equation 5.8 in double logarithmic scale.

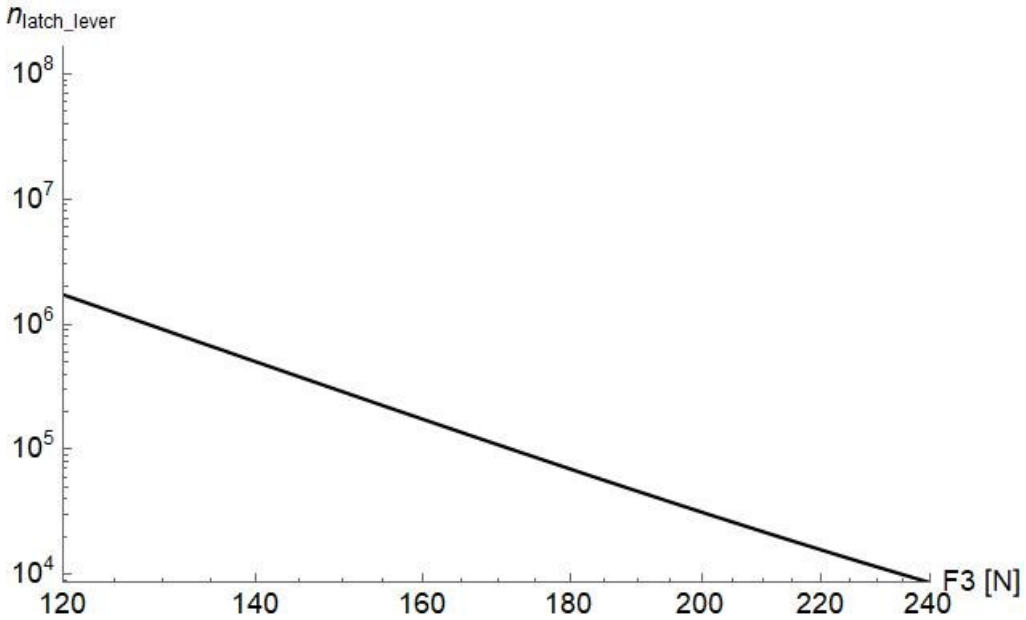

Figure 57: Number of cycles until latch lever failure as a function of the force applied F3 given by the equation 5.12

The same analysis made for the latch lever can be carried out for the latch rod. In Equation 5.13 the Miner's rule applied to the rod plate is reported, whereas in Figure 58 the relative stress strain curve is reported in double logarithmic scale.

$$\frac{n_{Cr\_1}(p\_latch(F3))}{N(\sigma\_latch\_rod(F3)_{\mu=0.3})}+\frac{n_{Cr\_2}(p\_latch(F3))}{N(\sigma\_latch\_rod(F3)_{\mu=0.7})}+ \\ +\frac{n_{latch\_lever}(p\_latch(F3))}{N(\sigma\_latch\_rod(F3)_{\mu=0.3})}=1 \tag{5.13}$$

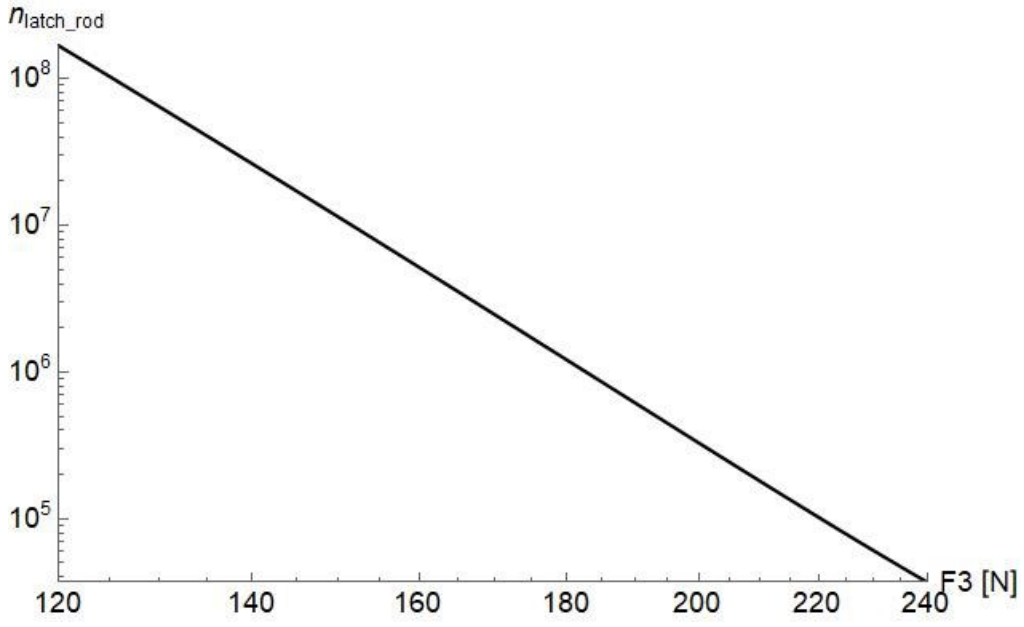

Figure 58: Number of cycles until latch rod prediction failure as a function of the force applied F3 given by the equation 5.13

As it can be noticed, increasing the force F3, it is possible to reduce the actual service life of the components involved in the accelerated life testing. A comparison between the two curves plotted in Figure 57 and Figure 58, suggests that failure should always occur on the latch lever.

5.5 Validation of the analytical model

In order to validate the analytical model, a series of experimental accelerated life tests were carried out on a dedicated testing machine. The force was applied directly to the door. Three load levels were considered: 120 N, 180 N and 240 N. A total of three replications were made. The run out was set at $2 \cdot 10^6$ cycles. In Table 22 are reported the results in terms of number of cycles up to the device failure. The failure always occurred on the latch lever.

Table 22: Experimental validation tests

Applied Load [N]	120	180	240
Test 1	200,000	68,341	7,124
Test 2	200,000	61,974	7,932
Test 3	200,000	62,757	6,798

Mean	200,000	64,357	7,285
St. Dev.	-	3472	584

The experimental results were used in order to validate the analytical model. In Table 23 the number of cycles up to failure given by the analytical model are reported.

Table 23: number of cycles up to failure given by the analytical model

Applied Load [N]	120	180	240
Number of cycles up to failure latch lever	1,725,310	69,682	8,608
Number of cycles up to failure latch rod	167,123,000	1,209,830	36,996

It can be stated that the device failure always occurs on the latch lever due to fatigue degradation of this component. The analytical model results were therefore compared with the experimental ones. In Table 24 the comparison is reported with the indication of the error committed using the analytical model. The first force level (120 N) was not taken into account because both the experimental and the analytical model shows that the device survive at 200,000 cycles.

Table 24: Comparison between the analytical model and the experimental test

Applied Load [N]	180	240
Experimental failure	64,357	7,285
Latch lever prediction failure	69,682	8,608
Error	5,325	1,323
Error %	8.3%	18.2%

As it can be noticed there is a good agreement between the analytical forecast and the experimental one. The same results are also collected in Figure 59, where the curve deals with failure prediction by the analytical model, whereas the red points indicate actual failures, which occurred during the experimental validation tests.

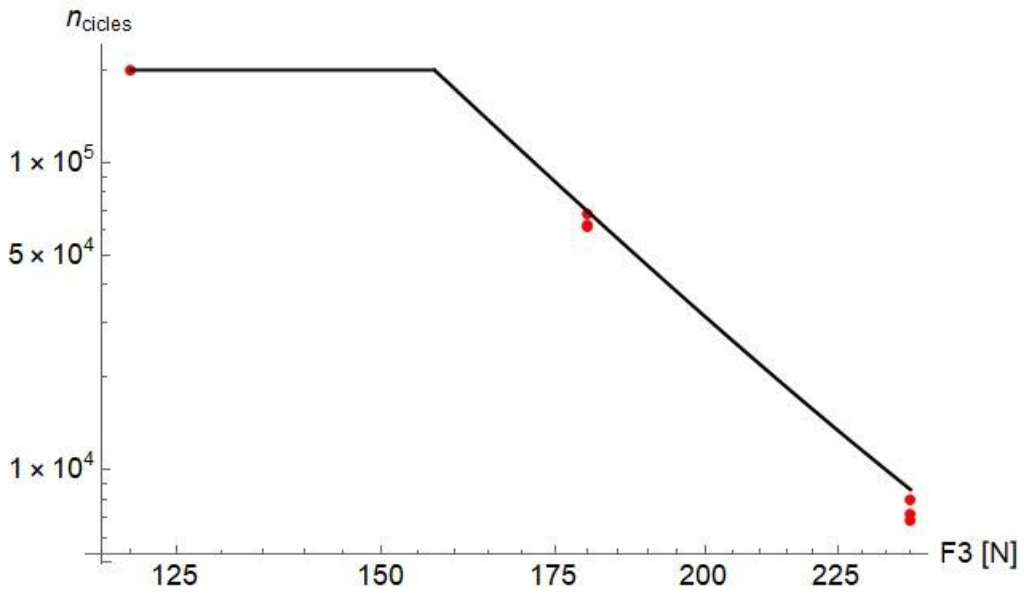

Figure 59: Comparison between the failure predicted by the analytical model and the experimental results

5.6 Generalization of the case of study

In order to develop this study a locking device was used as a demonstrator. In this section a generalization of the described method will be presented. For example, in the single-axis hinges, of lift-off or fixed pin type, for use on access windows and doors (Figure 60), the European Standard EN 1935 [79], many tests should be carried out. Hinges suitable for side-hanging use are usually strong enough for top-hanging applications with hinged elements of the same mass. However, the load bearing and wearing surfaces are totally different for the two types of application.

Figure 60: Hinge

The Standard [79] provide different tests on these kind of devices: static loads, shear strength and allowable wear during durability cycling. In this section, focus is placed on the durability test. In order to carry out the test, it is mandatory to mount the device on the testing machine shown in Figure 61 and it is necessary to load the hinged test element with a certain force. Then, in order to test the device, it necessary to operate the hinged element through the lesser of 92,5° ± 2,5° or the full angular movement permitted by the hinge for 200,000 cycles. After that, the horizontal and vertical gaps between the hinged element and the datum surfaces must measure ensuring that the fastenings used to fix the hinge to the test apparatus maintain the same torque as at the beginning of the test. The testing frequency is equal to 10 cycles/min that means that, in this case also, the whole test duration is approximately 14 days.

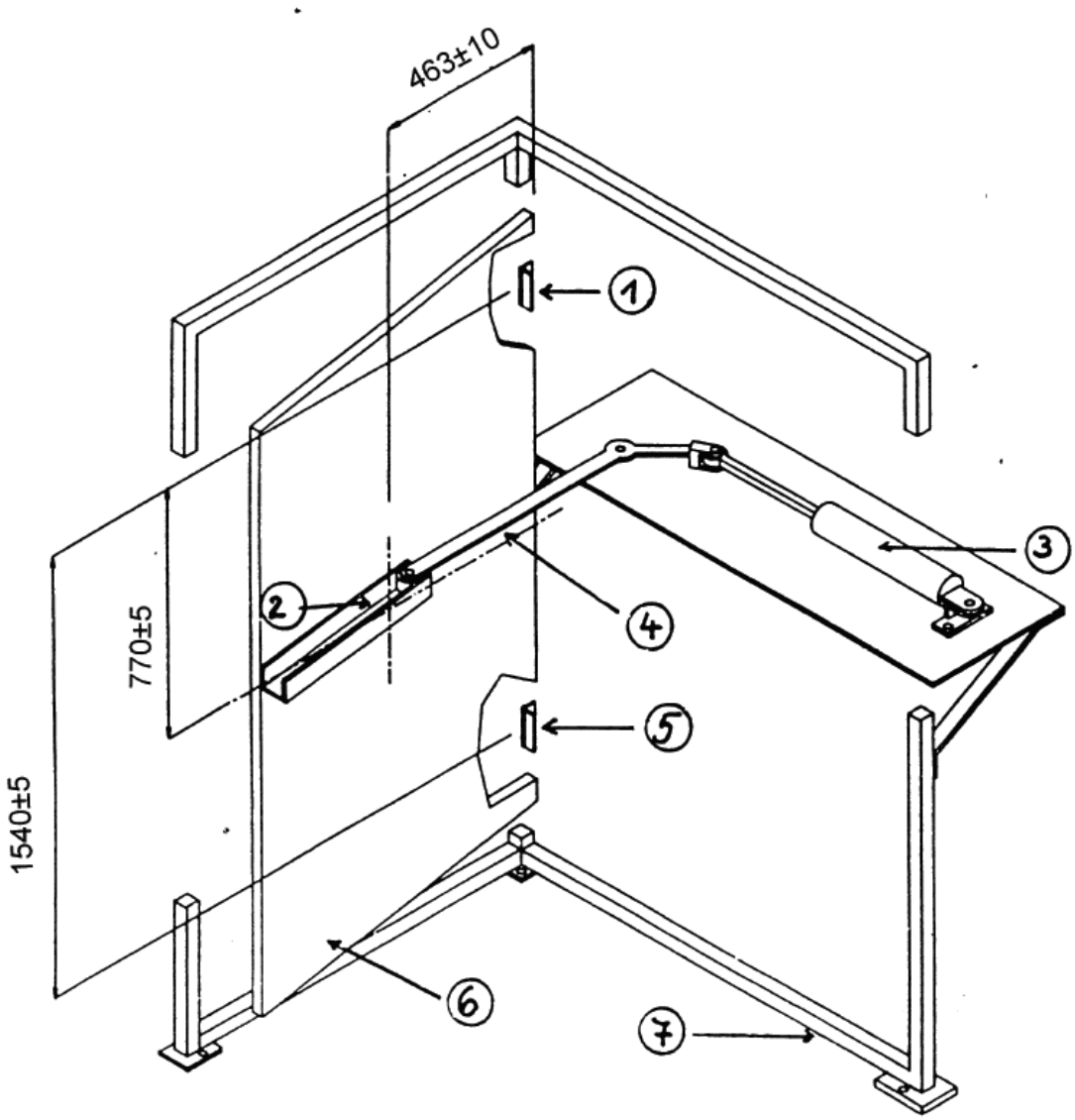

Figure 61: Test apparatus. (1) Hinge under test. (2) roller wheel in guide channel. (3) Pneumatic or hydraulic cylinder. (4) Typical mechanism for applying a force at 90º. (5) Lower hinge for support horizontal forces only. (6) Interchangeable door. (7) Rigidly secured main frame.

During this test it is possible that the wear introduces a variation of the forces to which the hinge is subjected and therefore the stresses in the device can increase. In order to accelerate this test, it is possible to increase the door mass, but this can lead to a severe wear and consequently a rapid degradation of the fatigue resistance of the hinge.

6. ACCELERATED LIFE TESTING MACHINE DESIGN

As explained in the first chapter, the test can be accelerated in two different ways. In the previous chapters, focus was placed on the accelerated life testing by an incremented load. Here, a new testing bench machine, which makes it possible to accelerate the test by increasing the testing speed, is going to be presented.
The Standard [13], indeed, provides the test door specifications to carry out the test as follows.
The test door leaf shall be 2,100 mm high and 1,100 mm wide. It shall have means of attaching weights to the door to enable the door mass to be in the center of the door. The test door and its frame shall have enough rigidity such that any distortion perpendicular to the plane of the test door, taking place during the test sequence shall be no more than 5 mm at any position. The door mass to carry out the test should be above 200 kg door mass as specified by the manufacturer. This means that, due to the inertial forces, the test speed cannot be more that 10 cycles/min.
In order to speed up the test, is therefore necessary to reduce the moving masses. In the next section a new test bench will be presented.

6.1 General design

The principle of the new design is to reduce the moving masses. So, it is necessary to remove the door. For this purpose, a pneumatic actuator can be utilized in order to apply the force on the latch. Moreover, since the device should be fixed in the testing machine that must be rigid enough, the idea is to move the strike plate. The conceptual design of such movement is shown in Figure 62. As it can be noticed, the pneumatic actuator is integrated with the strike plate that can consequently be rigid enough. In this way, it is possible to apply the load on the latch, simply introducing a pressure in the actuator chamber. In order to simulate the door opening, it is necessary to introduce a mechanical mechanism, such as a cam that, working on the lock device handle pin, makes it possible to simulate the actual door movement. This coupling can be regarded as an efficient system characterized by minimum wear over the elapsed testing time, so that almost no maintenance is required.
A magnification of the conceptual mechanism, sketched in a section view to show the lock device, is shown in Figure 63.

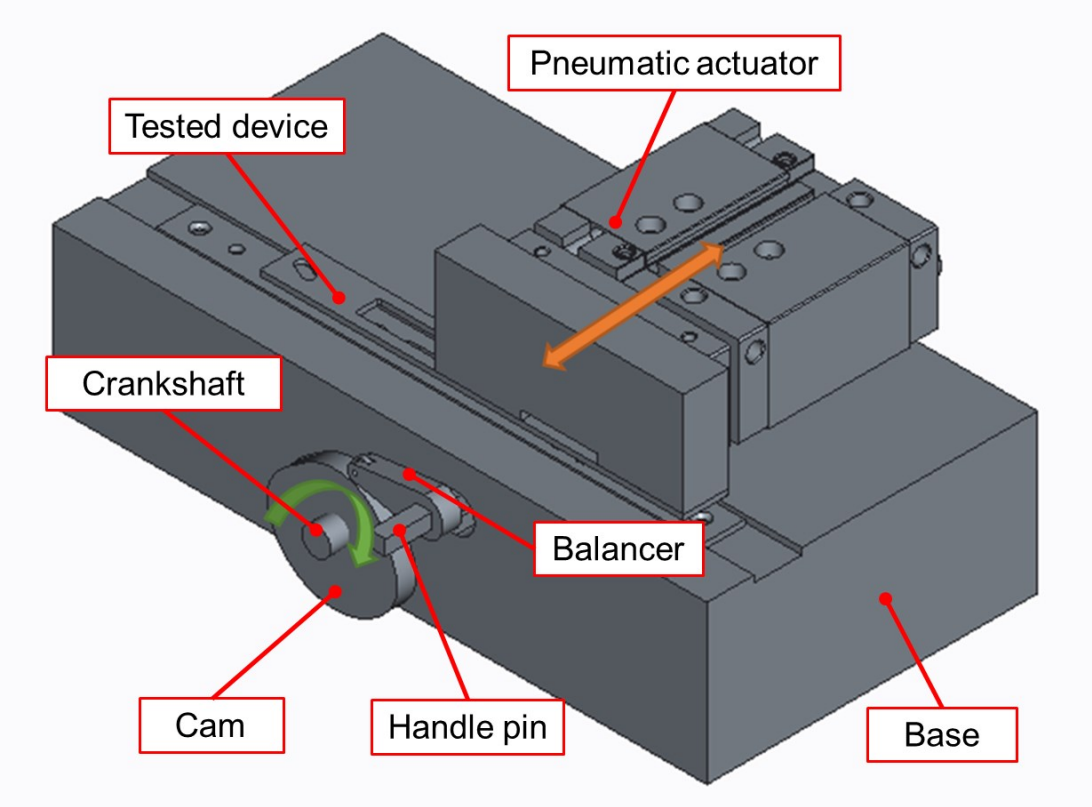

Figure 62: Test bench conceptual design

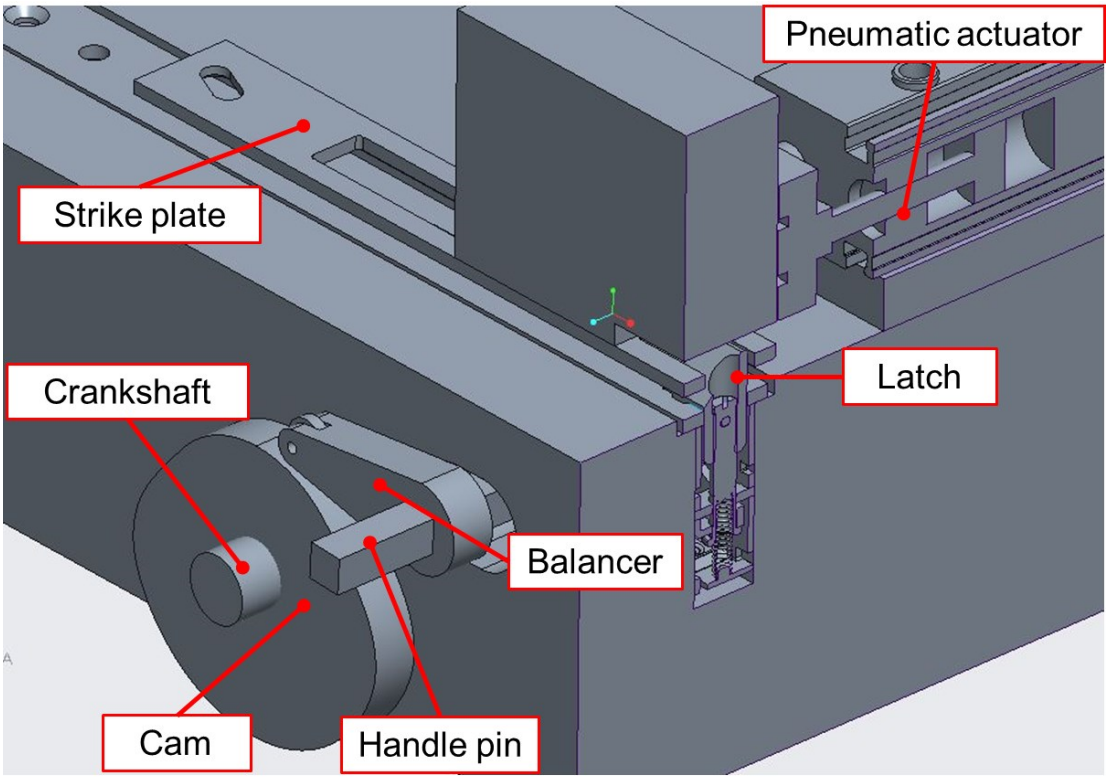

Figure 63: Test bench conceptual design magnification

6.2 Cam design

The cam is the organ that makes it possible to transform the rotary motion of the crankshaft into the alternating motion of the handle pin. The transformation takes place through the coupling, on the surface of the cam, of a wheel keyed on the rocker, which is, in turn, connected to the square pin.

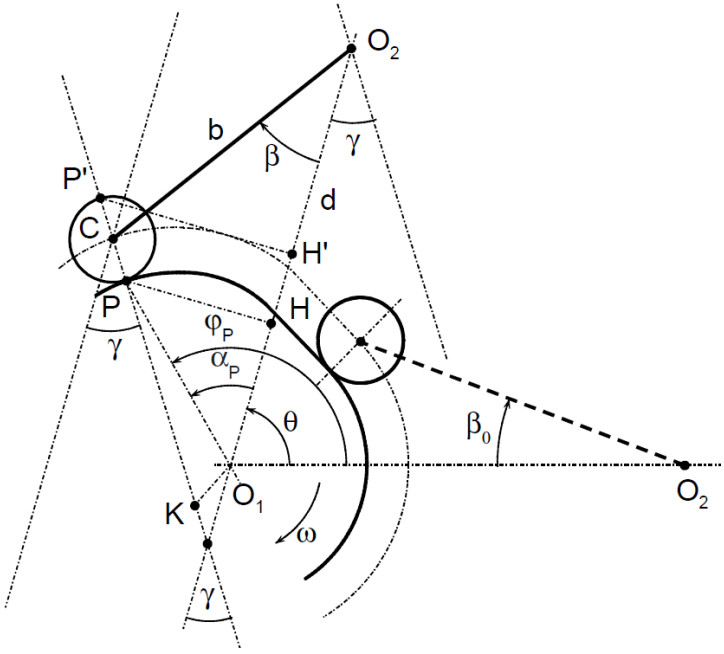

Figure 64: Cam profile design

Referring to Figure 64, in order to correctly size the riser, it is necessary to work out the angle β as a function of the rotation of the cam (or of the time). To derive the β function, a fifth degree interpolating polynomial fitting was used (Equation 6.1).

$$y(t) = a_0 + a_1 \cdot (t - t_i) + a_2 \cdot (t - t_i)^2 + a_3 \cdot (t - t_i)^3 + a_4 \cdot (t - t_i)^4 + a_5 \cdot (t - t_i)^5 \qquad (6.1)$$

Where the constant a_0, a_1, a_2, a_3, a_4 and a_5 can be write as follow (Equation 6.2).

$$
\begin{aligned}
a_0 &= y_i \\
a_1 &= v_i \\
a_2 &= \frac{1}{2} \cdot a_i \\
a_3 &= \frac{20 \cdot (y_f - y_i) - (8 \cdot v_f + 12 \cdot v_i)T - (3 \cdot a_f - a_i)T^2}{2T^3} \\
a_4 &= \frac{30 \cdot (y_f - y_i) + (14 \cdot v_f + 16 \cdot v_i)T + (3 \cdot a_f - 2 \cdot a_i)T^2}{2T^4} \\
a_5 &= \frac{12 \cdot (y_f - y_i) - 6 \cdot (v_f + v_i)T - (a_f - a_i)T^2}{2T^5}
\end{aligned}
\tag{6.2}
$$

Where y(t) is the angular position of β, v is its speed, a is the acceleration, t is the time. The subscript i represents the initial state, whereas the subscript f indicates the final one. The rotational speed of the crankshaft was imposed at n=60 rpm. The others boundary condition of the case of study and the definition of the period T is defined as in the next formulae (Equation 6.3).

$$
\begin{aligned}
&y_i = 0\ ^\circ\text{; initial position} \\
&y_f = 13\ ^\circ\text{; final position} \\
&v_i = 0\ ^\circ/\text{s; initial speed} \\
&v_f = 0\ ^\circ/\text{s; final speed} \\
&a_i = 0\ ^\circ/\text{s}^2\text{; initial acceleration} \\
&a_f = 0\ ^\circ/\text{s}^2\text{; final acceleration} \\
&t_i = 0.05\text{s; initial time corresponding to the start of the lift} \\
&t_f = 0.43\text{s; final time corresponding at the maximum angle } \beta \\
&T = t_f - t_i
\end{aligned}
\tag{6.3}
$$

The resulting law is reported in Equation 6.4.

$$
y(t) = 41.4 \cdot (-0.05 + t)^3 - 163.2 \cdot (-0.05 + t)^4 + 171.8 \cdot (-0.05 + t)^5 \tag{6.5}
$$

Introducing the relation between the time and the angle (Equation 6.6)

$$
t = \frac{\theta}{n} = \frac{\theta}{2 \cdot \pi} \tag{6.6}
$$

The movement of the handle pin can be plotted as a function of the crankshaft rotation angle (Figure 65).

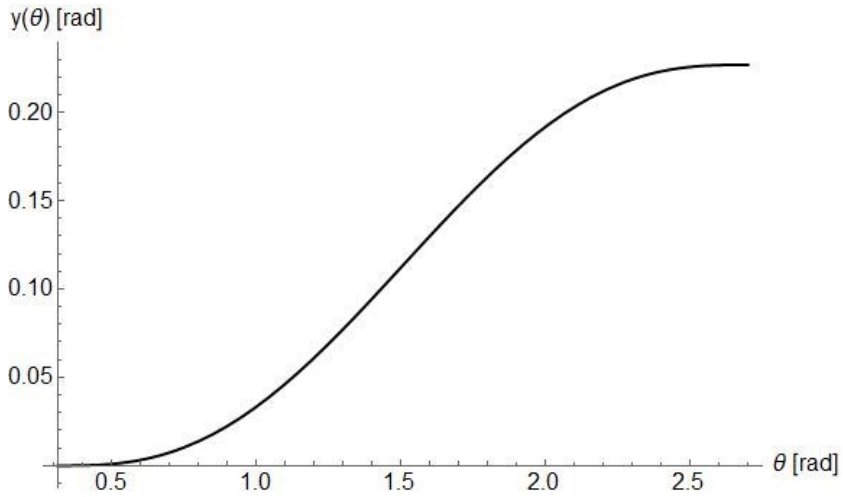

Figure 65: Handle pin movement as a function of the crankshaft rotation angle (outward phase)

Using the same criteria, it is therefore possible to evaluate the movement in the return phase, considering the related boundary conditions in Equation 6.7.

$y_i = 13$ °; initial position
$y_f = 0$ °; final position
$v_i = 0$ °/s; initial speed
$v_f = 0$ °/s; final speed
$a_i = 0$ °/s^2; initial acceleration (6.7)
$a_f = 0$ °/s^2; final acceleration
$t_i = 0.48$ s; initial time corresponding to the start of the lift
$t_f = 0.73$ s; final time corresponding at the maximum angle β
$T = t_f - t_i$

For the sake of synthesis only the law (Equation 6.8) and the movement graph (Figure 66) are reported here.

$$y(t) = 13 - 145.2 \cdot \left(-0.5 + \frac{\theta}{2\pi}\right)^3 + 871.3 \cdot \left(-0.5 + \frac{\theta}{2\pi}\right)^4 - 1394.1 \cdot \left(-0.5 + \frac{\theta}{2\pi}\right)^5 \quad (6.8)$$

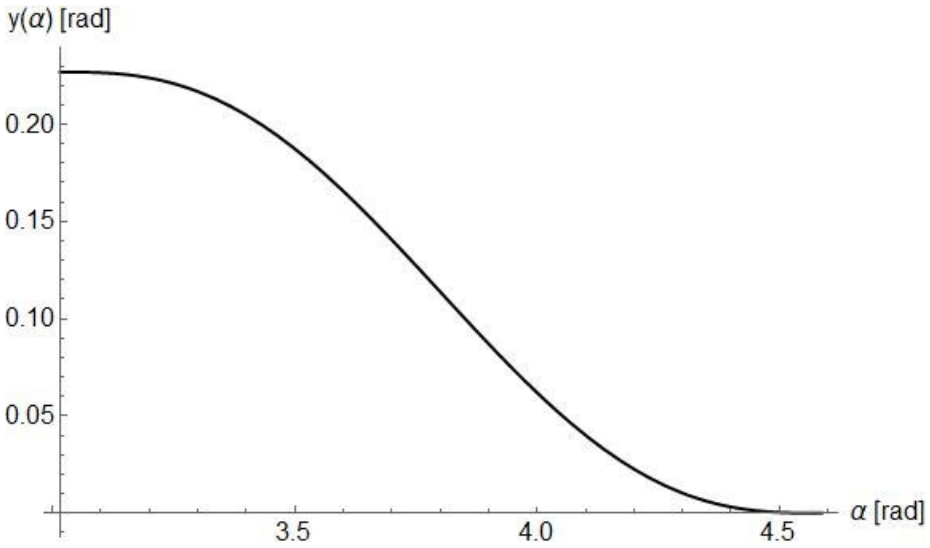

Figure 66: Handle pin movement as a function of the crankshaft rotation angle (return phase)

Based on the desired geometrical position of the handle pin, it is finally possible to work out the primitive profile of the cam, coming then to its final drawing.

$\beta_0 = 30$ °; initial angle of the barbell
b = 36.74 mm; length of the barbell, measured center-center
d = 55.75 mm; distance between the rotation axes of the cam and the rocker

Referring to Figure 64, it is possible to describe the pitch curve in polar coordinates as follows (Equation 6.9).

$$O_1C = \sqrt{(b \cdot \sin\beta_a)^2 + (d - b \cdot \cos\beta_a)^2} \tag{6.9}$$

And the final cam profile as in Equation 6.10.

$$O_1P(\theta) = \sqrt{\left[b\ Sin(\beta_a) - R_r\ Sin(\gamma)\right]^2 + \left[d - b\ Cos(\beta_a) - R_r\ Cos(\gamma)\right]^2} \tag{6.10}$$

The pitch curve and the cam profile yielded by the previous analyses are depicted in Figure 67 the pitch curve and the cam profile obtained from the previous analyses. For

the sake of completeness in Figure 68, the balance movement during an entire cycle is shown.

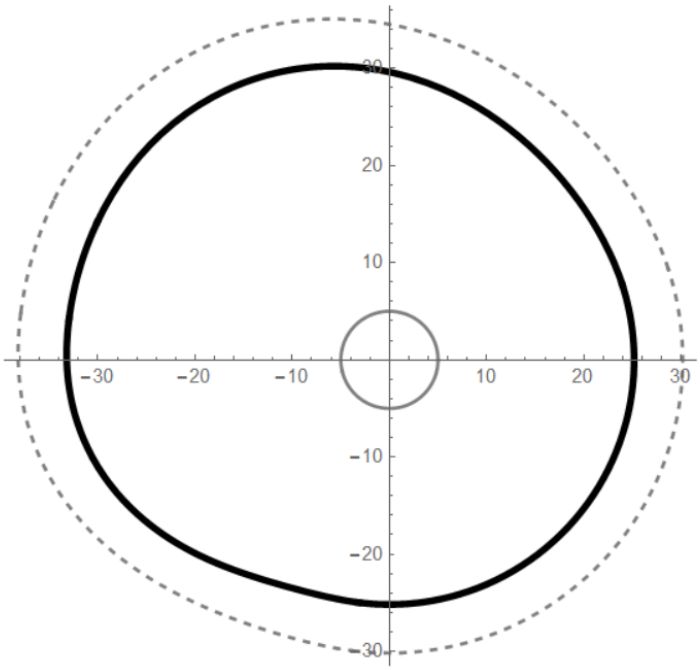

Figure 67: Cam design. Profile curve (dashed line) and cam profile (continuous line)

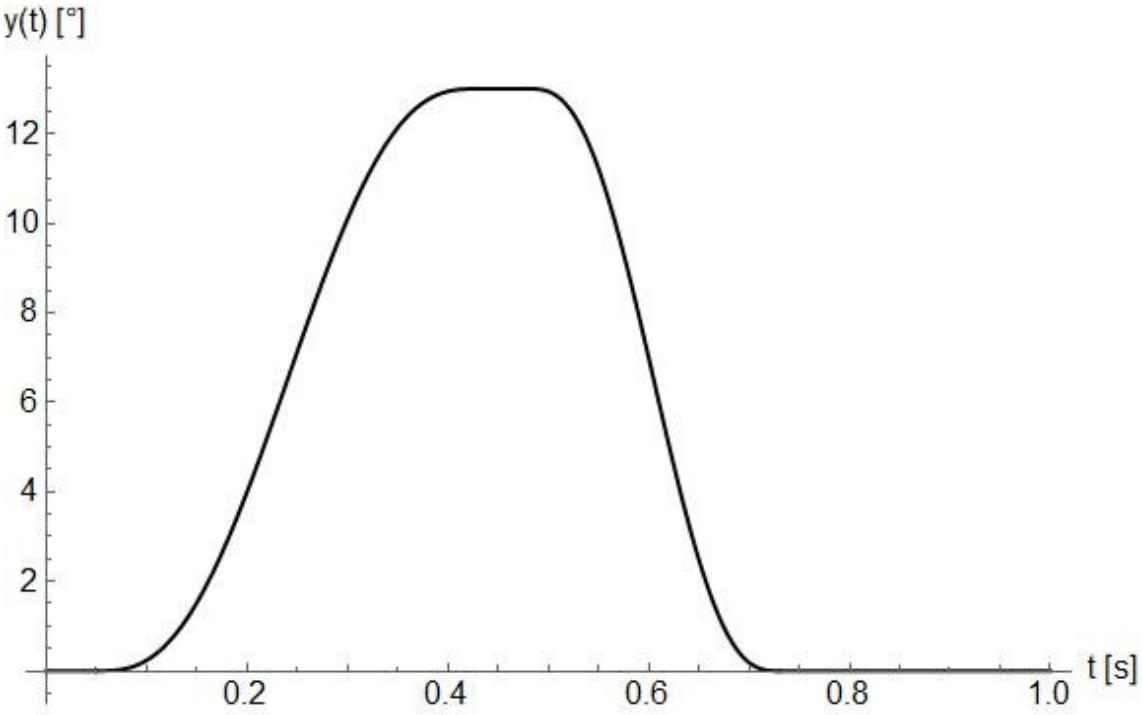

Figure 68: Balance movement as a function of the time (one cycle)

6.3 Actuator movement

In order to carry out the test, the pneumatic actuator should apply the force at the correct time. Thus, the movement of the actuator was studied, so that it was synchronized with that of the crankshaft. The different phases are reported in Figure 69. The displacement law must be consistent with the motion of the latch defined by the cam: first, the actuator must put the strike plate and the latch in contact together (phase 1). Subsequently, when, through the cam, the handle pin is lifted, and therefore the latch is retracted, the actuator must bring the strike plate to a position, so that the lock disengaged (phase 2 and 3); then, the actuator stops briefly to allow for the latch to return to its initial position (phase 4). Finally, the actuator returns to its initial position, thus simulating the door closing (phase 5 and 6).

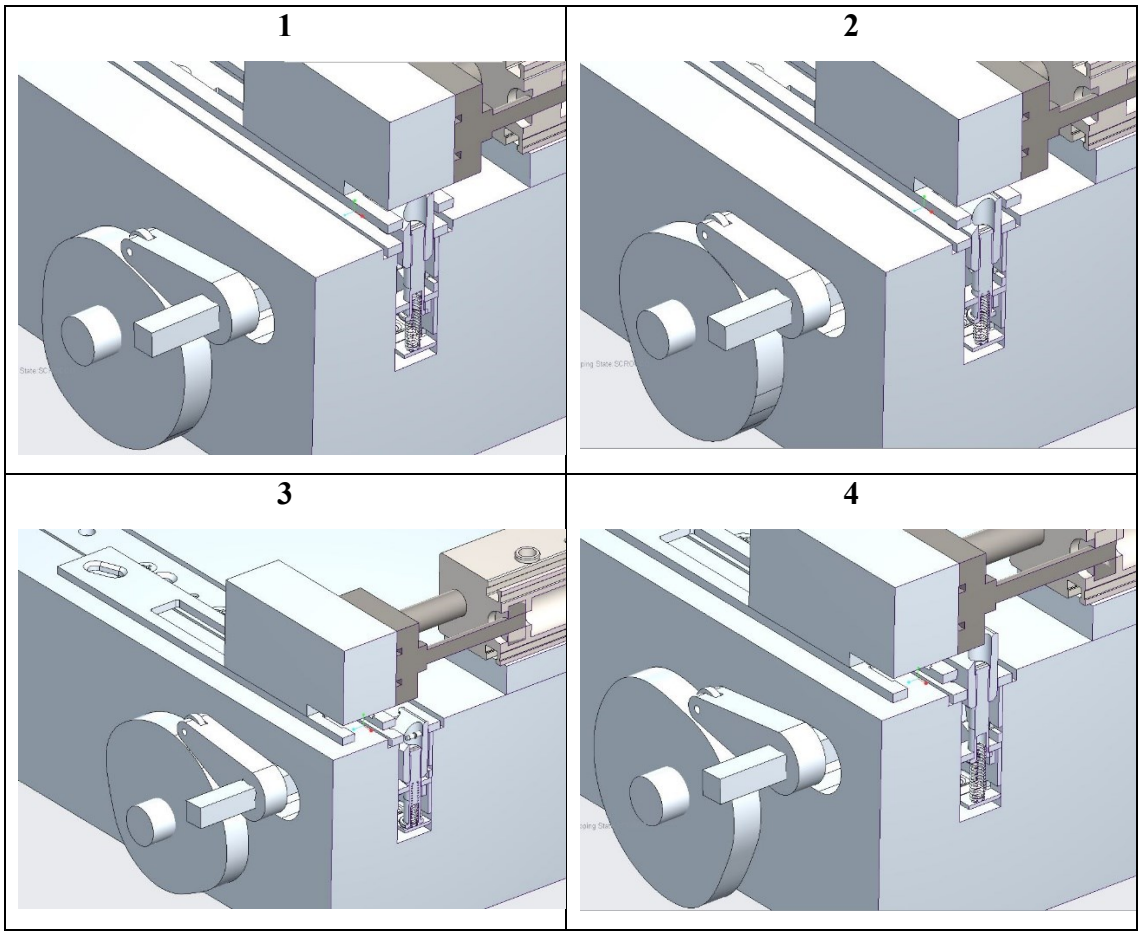

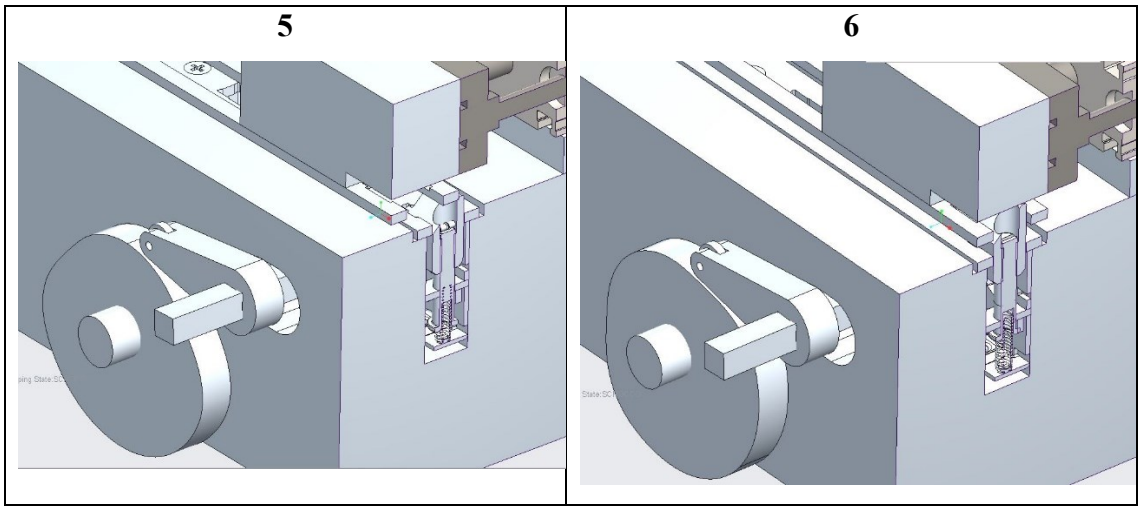

Figure 69: Testing phases

The reciprocal motion was studied by PTC Creo Parametric 5.0 as reported in Figure 70. The strike plate in the initial phase, undergo in contact with the latch. This position persist until the latch is retracted and the actuator is free to reach its final position; finally, it can come back to the start position.

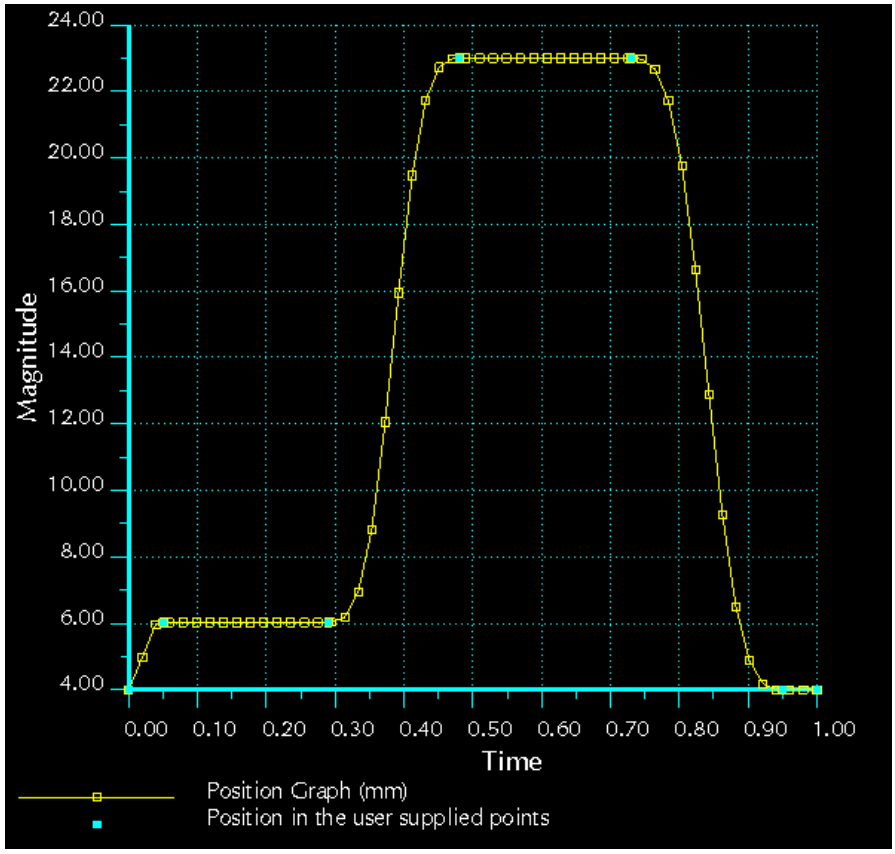

Figure 70: Actuator position as a function of the time cycle

The reciprocal movement between the cam and the actuator is shown in Figure 71. As it can be noticed, there is a first phase, where the actuator puts the strike plate and the latch in reciprocal contact. At this stage, the force is consequently applied by the actuator. Then, the cam makes it possible to retract the latch from the strike plate and, when the latch is completely disengaged, the actuator can reach the final position. At this stage, the cam, working on the handle pin, can return to its initial position, releasing at the same time the latch to its resting position. Finally, the actuator can return to the start position.

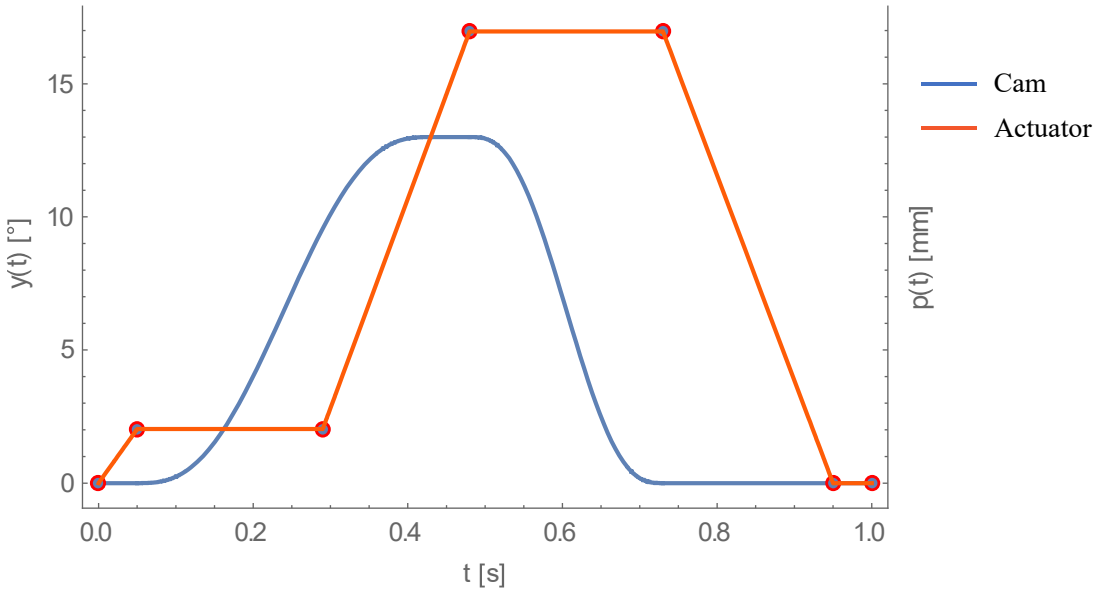

Figure 71: Graph of the reciprocal movement between the cam and the actuator

6.4 Summary of the test bench design

As explained in the first chapter, there are two ways to accelerate the test: increasing the load applied on the device or increasing the speed test. In this chapter a brief presentation of a new testing bench has been presented with the purpose of providing a general idea to be developed.

The standard testing speed, as remarked by the Standard [13], should not exceed 10 cycles/min due to the huge moving masses. Therefore, the idea was to remove the door in the test, and to directly apply the force on the strike plate. This procedure allows, indeed, to reduce the moving masses and to increase the testing speed, as well as the applied force.

In this case too, the latch is initially engaged with the strike plate. The latch movement was controlled by a cam, which was accurately studied, in order to accurately simulate door opening as recommend by the standard.

The actuator movement, as well as the strike plate movement, was then synchronized with the cam, in order to apply the force on the latch, before the latch is retracted. After the latch is disengaged, the strike plate may leave the lock device and, before coming back, the latch must return to its resting position. In this way, when the strike plate comes back, is it possible to accurately simulate the door closing.

7. CONCLUSIONS

Sometimes, the durability tests to be performed on mechanical devices according to the standards can be very time-consuming. During the product development phase (design), indeed, companies need to carry out reliability tests, in order to evaluate the actual service life of the components during the standard use. Moreover, such development process is generally based on trial and error methods that can be very expensive in terms of time and costs. In this case, accelerated life testing can be an interesting option for cutting down both development time and cost.

In the literature, some studies deal with accelerated life testing, but they generally focus on the statistical methods to be applied on it. Almost all of these studies are related to electronic components that, due to their constant failure rate, are simpler to be studied. Just a few studies are related to simple mechanical components (e.g. bearings).

In this study, a general accelerated testing method was developed to be applied to complex mechanical devices, where the combination of fatigue and wear can lead to a nonlinear behavior during the test. Regarding the combination of fatigue and wear mechanisms, some studies were carried out, but they deal with single component standard specimens. In complex components, wear can, for instance, introduce a transition in terms of friction coefficient that can, in turn, increase the stresses on the other components, causing a nonlinear behavior.

In order to accelerate the test on a mechanical device, besides increasing the testing frequency, it is necessary to increase the loads. FEA can be used in order to evaluate the stress field on each component of the device. The experimental tests, then, can provide the mechanical characterization of the materials involved in assembly. Finally, the combination of FEAs and experimental test results can be used to develop an analytical model able to predict the expected life of a component tested in extreme condition.

A locking device has been taken as a demonstrator of the accelerated life testing methodology.

Several FEAs were carried out in order to detect the stress field (in terms of contact pressures and bending stresses) of each component during the accelerated life test at different load condition levels.

Moreover, experimental tests were carried out where no relevant data could be retrieved in the literature.

Particularly, the effect of different coatings on the fatigue behavior of 11 SMnPb 30 free cutting steel was analyzed. Fatigue tests were made on a four-point rotating bending machine. For each sample type 30 specimens were tested in order to obtain the fatigue curve and the fatigue limit of the material. The data were processed by statistical tools ANOVA and F-Test and it was assessed that there is no significant effect of the coating on the fatigue performance. The fatigue limit is 53% of UTS in agreement with the commonly accepted ratios for metallic materials.

Then the effects of coating thickness and contact pressure on the wear rate of a nickel coated zinc alloy was investigated using a sliding on cylinder testing machine. Three different levels for the applied load and three different levels for the coating thickness were analyzed. The sliding distance was set at 500 m, corresponding in the case of study at the overall sliding distance after 200,000 cycles. The experimental results were processed by means of a two-way ANOVA and fisher test. It was assessed that the coating thickness implies no significant differences in terms of wear rate. The contact pressure instead, proved to be highly effective on the wear rate. Focusing on the wear test output, it was assessed that there is a first transition in terms of friction coefficient after 150 m and a second one after 350 m. This outcome suggests that at the first stage the coating is worn out but, in the wear track there is some residue of nickel still that worn out completely at the second stage. Focusing on this result, further experimental tests were carried out at a reduced sliding distance of 150 m. In this case also, the data processed with the aforementioned statistical tools allowed to asses that the wear rate is strongly affected just from the applied load.

Using the experimental and the numerical results an analytical model was developed. Due to the contact pressure, the latch wear introduces a transition of the friction coefficient that increases the stresses on the other components. The FEA allow to evaluate the stress field of each component at different levels of friction coefficient and applied load. The combination of the fatigue data and the Miner's rule made it possible to predict the actual number of cycles up to failure of each component. It was assessed that there is a good correlation between the number of cycles up to failure given by the analytical model and the experimental ones.

REFERENCES

1. Nelson, W. *Accelerated testing : statistical models, test plans and data analyses*; John Wiley & Sons: New York, 1990; ISBN 0-471-52277-5.
2. R. E. Thomas, G. B. Gaines, M.M.E. CONSIDERATIONS FOR VALID ACCELERATED LIFE TESTING. *Conf. Electr. Insul. Dielectr. Phenom. (CEIDP), Annu. Rep.* **1983**, 153–160.
3. Tebbi, O.; Guerin, F.; Dumon, B. Comparative study of accelerated testing models, applications in mechanics. *Proc. IEEE Int. Conf. Syst. Man Cybern.* **2001**, *4*, 2099–2104.
4. Silverman, M. HALT vs. ALT: When to use which technique? *Proc. - Annu. Reliab. Maintainab. Symp.* **2006**, *00*, 310–312.
5. Borgia, O.; De Carlo, F.; Fanciullacci, N.; Tucci, M. Accelerated life tests for new product qualification: A case study in the household appliance. In Proceedings of the IFAC Proceedings Volumes (IFAC-PapersOnline); 2013; Vol. 46, pp. 269–274.
6. Nelson, W. Accelerated Life Testing - Step-Stress Models and Data Analyses. *IEEE Trans. Reliab.* **1980**, *R-29*, 103–108.
7. Schatzoff, M.; Lane, T.P. A general step stress model for accelerated life testing. *Jt. Stat. Meet.* **1987**.
8. Goba, F.A. Bibliography on Thermal Aging of Electrical Insulation. *IEEE Trans. Electr. Insul.* **1969**, *EI-4*, 31–58.
9. Miller, R.; Nelson, W. Optimum Simple Step-Stress Plans for Accelerated Life Testing. *IEEE Trans. Reliab.* **1983**, *R-32*, 59–65.
10. Zhao, W.; Elsayed, E.A. A general accelerated life model for step-stress testing. *IIE Trans. (Institute Ind. Eng.* **2005**, *37*, 1059–1069.
11. Srivastava, P.W.; Shukla, R. A log-logistic step-stress model. *IEEE Trans. Reliab.* **2008**, *57*, 431–434.
12. Zhang, C.; Chuckpaiwong, I.; Liang, S.Y.; Seth, B.B. Mechanical component lifetime estimation based on accelerated life testing with singularity extrapolation. *Mech. Syst. Signal Process.* **2002**, *16*, 705–718.
13. EN 12209 *Building hardware – Mechanically operated locks and locking plates – Requirements and test methods*; European Committee for Standardization: Brussels, 2016;

14. EN 12844 *Zinc and zinc alloys — Casting — Specification*; European Committee for Standardization: Brussels, 1998;
15. ISO 1458 *Metallic coatings — Electrodeposited coatings of nickel*; 2002;
16. EN 10149-1 *Hot rolled flat products made of high yield strength steels for cold forming - Part 1: General technical delivery conditions*; 2013;
17. EN 10087 *Free-cutting steel - Technical delivery conditions for semi-finished products, hot-rolled bars and rods*; 1998;
18. ASTM A959 *Specifying Harmonized Standard Grade Compositions for Wrought Stainless Steels 1*; ASTM International, 2016;
19. EN ISO 10364 : 2018 BSI Standards Publication Structural adhesives – Determination of the pot life (working life) of multi-. **2018**.
20. EN 10149-2 Hot rolled flat products made of high yield strength steels for cold forming. Technical delivery conditions for thermomechanically rolled steels. **2016**.
21. Klemenc, J.; Fajdiga, M. Estimating S-N curves and their scatter using a differential ant-stigmergy algorithm. *Int. J. Fatigue* **2012**, *43*, 90–97.
22. Klemenc, J. Influence of fatigue-life data modelling on the estimated reliability of a structure subjected to a constant-amplitude loading. *Reliab. Eng. Syst. Saf.* **2015**, *142*, 238–247.
23. Croccolo, D.; De Agostinis, M.; Fini, S.; Olmi, G.; Robusto, F. Coating effect on the fatigue strength of a free cutting steel. *Proc. Inst. Mech. Eng. Part C J. Mech. Eng. Sci.* **2019**, *0*, 1–12.
24. Carvalho, A.L.M.; Voorwald, H.J.C. Influence of shot peening and hard chromium electroplating on the fatigue strength of 7050-T7451 aluminum alloy. *Int. J. Fatigue* **2007**, *29*, 1282–1291.
25. Díaz, J.A.; Passarelli, M.; Berríos, J.A.; Puchi-Cabrera, E.S. Fatigue behavior of a 4340 steel coated with an electroless Ni-P deposit. *Surf. Coatings Technol.* **2002**, *149*, 45–56.
26. Mrva, P.; Kottfer, D.; Kaczmarek Effect of shot peening and NiAl coating on fatigue limit of Mg-Al-Zn-Mn alloy. *Arch. Metall. Mater.* **2011**, *56*, 743–748.
27. Kralya, V.O.; Molyar, O.H.; Khimko, A.M.; Puhachevs'kyi, D.O. Fatigue characteristics of VT22 titanium alloy with wear-resistant coatings. *Mater. Sci.* **2006**, *42*, 853–857.
28. Zhang, Y.Z.; Wu, Y.Y.; Yao, M. Effects of electroless deposition and shot peening on fatigue strength of 3OCrMo4 steel. *Mater. Sci. Technol.* **1996**, *12*, 776–779.

29. Ramanujachar, K.; Subramanian, S. V Micromechanisms of tool wear in machining free cutting steels. *Wear* **1996**, *197*, 45–55.
30. Lou, D.; Cui, K.; Jia, Y. Study on the machinability of resulfurized composite free-cutting steels. *J. Mater. Eng. Perform.* **1997**, *6*, 215–218.
31. Ray, K.K.; Das, J.; Dixit, A.; Chakraborty, M.; Chakravorty, S.; Guha, S.N. Effect of cold deformation on the machinability of a free cutting steel. *Mater. Manuf. Process.* **2006**, *21*, 333–340.
32. Chen, S.-C.; Zhu, R.; Xue, L.-Q.; Lin, T.-C.; Li, J.-S.; Lin, Y. Effects of elemental Sn on the properties and inclusions of the free-cutting steel. *Int. J. Miner. Metall. Mater.* **2015**, *22*, 141–148.
33. Suzuki, T.; Li, Y.; Koizumi, Y.; Chiba, A. Quantitative evaluation in hot workability of SUS303 free-cutting steel. *Mater. Sci. Eng. A* **2013**, *563*, 117–124.
34. Naghdy, S.; Akbarzadeh, A. Characterization of dynamic recrystallization parameters for a low carbon resulfurized free - cutting steel. *Mater. Des.* **2014**, *53*, 910–914.
35. Joyot, P.; Rakotomalala, R.; Pantalé, O.; Touratier, M.; Hakem, N. A numerical simulation of steady state metal cutting. *Proc. Inst. Mech. Eng. Part C J. Mech. Eng. Sci.* **1998**, *212*, 331–341.
36. Aggarwal, M.L.; Khan, R.A.; Agrawal, V.P. Optimization of micro welds in leaf springs used in automotive vehicles. *Indian J. Eng. Mater. Sci.* **2006**, *13*, 217–220.
37. *Manuale di trattamenti e finiture*; Tecniche Nuove, Ed.; Milano, 2003;
38. Straffellini, G. *Friction and Wear - Methodologies for Design and Control*; Springer International Publishing, Ed.; Switzerland, 2015;
39. BSI BS ISO 1143 : 2010 BSI Standards Publication Metallic materials — Rotating bar bending fatigue testing. **2010**.
40. International Standard Organization ISO 2081, Metallic and other inorganic coatings - Electroplated coatings of zinc with supplementary tratments on iron or steel. In; 2008 ISBN 5935522004.
41. ISO 1456 *Metallic and other inorganica coatings - Electrodeposited coatings of nickel, nickel plus chromium, copper plus nickel and copper plus nickel plus chromium*;
42. Fini, S.; De Agostinis, M.; Robusto, F.; Olmi, G.; Bogojević, N.; Ćirić Kostić, S.; Croccolo, D.; Vranić, A. Fatigue Response of As-Built DMLS Maraging Steel and Effects of Aging, Machining, and Peening Treatments. *Metals (Basel).* **2018**, *8*,

505.

43. Croccolo, D.; De Agostinis, M.; Fini, S.; Olmi, G.; Vranic, A.; Ciric-Kostic, S. Influence of the build orientation on the fatigue strength of EOS maraging steel produced by additive metal machine. *Fatigue Fract. Eng. Mater. Struct.* **2016**, *39*, 637–647.
44. Croccolo, D.; De Agostinis, M.; Fini, S.; Morri, A.; Olmi, G. Analysis of the influence of fretting on the fatigue life of interference fitted joints. In Proceedings of the ASME International Mechanical Engineering Congress and Exposition, Proceedings (IMECE); 2014; Vol. 2B.
45. Meneghetti, G.; Dengo, C.; Lo Conte, F. Bending fatigue design of case-hardened gears based on test specimens. *Proc. Inst. Mech. Eng. Part C J. Mech. Eng. Sci.* **2018**, *232*, 1953–1969.
46. Atig, A.; Ben Sghaier, R.; Seddik, R.; Fathallah, R. A simple analytical bending stress model of parabolic leaf spring. *Proc. Inst. Mech. Eng. Part C J. Mech. Eng. Sci.* **2018**, *232*, 1838–1850.
47. ISO 12107 *Metallic materials - Fatigue testing - Statistical planning and analysis of data*; 2012;
48. Olmi, G. Low cycle fatigue experiments on turbogenerator steels and a new method for defining confidence bands. *J. Test. Eval.* **2012**, *40*.
49. Croccolo, D.; De Agostinis, M.; Fini, S.; Olmi, G.; Bogojevic, N.; Ciric-Kostic, S. Effects of build orientation and thickness of allowance on the fatigue behaviour of 15–5 PH stainless steel manufactured by DMLS. *Fatigue Fract. Eng. Mater. Struct.* **2018**, *41*, 900–916.
50. De Agostinis, M.; Fini, S.; Olmi, G. The influence of lubrication on the frictional characteristics of threaded joints for planetary gearboxes. *Proc. Inst. Mech. Eng. Part C J. Mech. Eng. Sci.* **2016**, *230*, 2553–2563.
51. Berger, P.D.; Maurer, R.E.; Celli, G.B. *Experimental design: With applications in management, engineering, and the sciences: Second edition*; 2017;
52. Croccolo, D.; De Agostinis, M.; Fini, S.; Olmi, G.; Robusto, F.; Tonelli, L. WEAR BEHAVIOR OF ELECTRODEPOSITED NICKEL COATING ON ZP5 ZINC ALLOY (Under revision). *Proc. Inst. Mech. Eng. Part C J. Mech. Eng. Sci.*
53. Kececioglu, D. *Reliability and Life Testing Handbook*; Prentice-Hall: Englewood Cliffs, 1993;
54. Lu, C.J.; Meeker, W.O. Using degradation measures to estimate a time-to-failure

distribution. *Technometrics* **1993**, *35*, 161–174.

55. Boulanger, M.; Escobar, L.A. Experimental design for a class of accelerated degradation tests. *Technometrics* **1994**, *36*, 260–272.
56. Tseng, S.-T.; Yu, H.-F. A termination rule for degradation experiments. *IEEE Trans. Reliab.* **1997**, *46*, 130–133.
57. Strelec, H. A model for accelerated life testing. *Struct. Saf.* **1993**, *12*, 129–136.
58. Carev, M.B.; Koenig, R.H. Reliability Assessment Based on Accelerated Degradation: A Case Study. *IEEE Trans. Reliab.* **1991**, *40*, 499–506.
59. Jiang, J.; Xiao, G.; Wang, Y.; Liu, Y. Tribological behavior of nano-sized SiCp/7075 composite parts formed by semisolid processing. *Metals (Basel).* **2018**, *8*.
60. Croccolo, D.; De Agostinis, M.; Fini, S.; Olmi, G.; Robusto, F.; Cavalli, O.; Vincenzi, N. The influence of material, hardness, roughness and surface treatment on the frictional characteristics of the underhead contact in socket-head screws. In Proceedings of the American Society of Mechanical Engineers, Pressure Vessels and Piping Division (Publication) PVP; 2018; Vol. 2.
61. Santecchia, E.; Cabibbo, M.; Hamouda, A.M.S.; Musharavati, F.; Popelka, A.; Spigarelli, S. Investigation of the Temperature-Related Wear Performance of Hard Nanostructured Coatings Deposited on a S600 High Speed Steel. *Metals (Basel).* **2019**, *9*, 332.
62. Tocci, M.; Pola, A.; Girelli, L.; Lollio, F.; Montesano, L.; Gelfi, M.; Tocci, M.; Pola, A.; Girelli, L.; Lollio, F.; et al. Wear and Cavitation Erosion Resistance of an AlMgSc Alloy Produced by DMLS. *Metals (Basel).* **2019**, *9*, 308.
63. Gines, M.J.L.; Tuckart, W.; Abraham, S. Dry sliding wear behavior of hard chromium and nickel-based coatings in ball on ring test. In Proceedings of the Proceedings - International Brazilian Conference on Tribology; 2010; pp. 287–298.
64. Ye, Z.; Cheng, H.S.; Chang, N.S. Wear characteristics of nickel/silicon carbide composite coating in lubricated reciprocating contacts. *Tribol. Trans.* **1996**, *39*, 527–536.
65. Zheng, C.; Liu, Y.; Qin, J.; Ji, R.; Zhang, S. Experimental study on the wear behavior of HVOF sprayed nickel-based coating. *J. Mech. Sci. Technol.* **2018**, *32*, 283–290.
66. Khan, M.A.; Sundarrajan, S.; Duraiselvam, M.; Natarajan, S.; Kumar, A.S. Sliding

wear behaviour of plasma sprayed coatings on nickel based superalloy. *Surf. Eng.* **2017**, *33*, 35–41.

67. Kesavan, D.; Kamaraj, M. The microstructure and high temperature wear performance of a nickel base hardfaced coating. *Surf. Coatings Technol.* **2010**, *204*, 4034–4043.
68. Panagopoulos, C.N.; Papachristos, V.D. The corrosive wear of nickel coating on mild steel. *J. Mater. Sci.* **1996**, *31*, 2931–2936.
69. Zishan, C.; Hejun, L.; Qiangang, F. SiC wear resistance coating with added Ni, for carbon/carbon composites. *Surf. Coatings Technol.* **2012**, *213*, 207–215.
70. Pursche, G.; Schmidt, G. Improved wear protection by modified electrodeposited iron layers. *SCHMIERUNGSTECHNIK* **1985**, *16*, 83–86.
71. Schmidt, G.; Steinhäuser, S. Characterization of wear protective coatings. *Tribol. Int.* **1996**, *29*, 207–214.
72. Chen, T.; Wu, F.; Wang, H.; Liu, D. Laser cladding in-situ Ti(C,N) particles reinforced ni-based composite coatings modified with CeO2 nanoparticles. *Metals (Basel).* **2018**, *8*.
73. Tonelli, L.; Martini, C.; Ceschini, L. Improvement of wear resistance of components for hydraulic actuators: Dry sliding tests for coating selection and bench tests for final assessment. *Tribol. Int.* **2017**, *115*, 154–164.
74. ASTM G77 *Standard Test Method for Ranking Resistance of Materials to Sliding Wear Using*; ASTM International;
75. Yang-tao, X.; Yu-jie, D.; Wei, Z.; Tian-dong, X. Microstructure and texture evolution of electrodeposited coatings of nickel in the industrial electrolyte. *Surf. Coatings Technol.* **2017**, *330*, 170–177.
76. K. L., J. *Contact mechanics.pdf*; Cambridge University Press: Cambridge, 1985;
77. ASTM A276/A276M Standard Specification for Stainless Steel Bars and Shapes. *ASTM Int.* **2017**, 1–8.
78. Luo, J.K.; Flewitt, A.J.; Spearing, S.M.; Fleck, N.A.; Milne, W.I. Young's modulus of electroplated Ni thin film for MEMS applications. *Mater. Lett.* **2004**, *58*, 2306–2309.
79. EN 1935 Building hardware — Single-axis hinges — Requirements and test methods. **2002**.